High Fidelity Micromechanics-Based Statistical Analysis of Composite Material Properties

by

Ghulam Mustafa
B.Sc., University of Engineering and Technology Taxila, Pakistan, 2006
M.Sc., Hanyang University, South Korea, 2011

A Dissertation Submitted in Partial Fulfillment
of the Requirements for the Degree of

DOCTOR OF PHILOSOPHY

in the Department of Mechanical Engineering

Supervisory Committee

High Fidelity Micromechanics-Based Statistical Analysis of Composite Material Properties

by

Ghulam Mustafa
B.Sc., University of Engineering and Technology Taxila, Pakistan, 2006
M.Sc., Hanyang University, South Korea, 2011

Supervisory Committee

Dr. Curran Crawford, Department of Mechanical Engineering
Co-Supervisor

Dr. Afzal Suleman, Department of Mechanical Engineering
Co-Supervisor

Prof. Dr. Abbas S. Milani, School of Engineering, Okanagan Campus UBC
External Member

Abstract

Supervisory Committee
Dr. Curran Crawford, Department of Mechanical Engineering
Co-Supervisor
Dr. Afzal Suleman, Department of Mechanical Engineering
Co-Supervisor
Prof. Dr. Abbas S. Milani, School of Engineering, Okanagan Campus UBC
External Member

Composite materials are being widely used in light weight structural applications due to their high specific stiffness and strength properties. However, predicting their mechanical behaviour accurately is a difficult task because of the complicated nature of these heterogeneous materials. This behaviour is not easily modeled with most of existing macro mechanics based models. Designers compensate for the model unknowns in failure predictions by generating overly conservative designs with relatively simple ply stacking sequences, thereby mitigating many of the benefits promised by composites.

The research presented in this dissertation was undertaken with the primary goal of providing efficient methodologies for use in the design of composite structures considering inherent material variability and model shortcomings. A micromechanics based methodology is proposed to simulate stiffness, strength, and fatigue behaviour of composites. The computational micromechanics framework is based on the properties of the constituents of composite materials: the fiber, matrix and fiber/matrix interface. This model helps the designer to understand in-depth the failure modes in these materials and design efficient structures utilizing arbitrary layups with a reduced requirement for supporting experimental testing. The only limiting factor in using a micromechanics model is the challenge in obtaining the constituent properties. The overall novelty of this dissertation is to calibrate these constituent properties by integrating the micromechanics approach with a Bayesian statistical model.

The early research explored the probabilistic aspects of the constituent properties to calculate the stiffness characteristics of a unidirectional lamina. Then these stochastic stiffness properties were considered as an input to analyze the wing box of a wind turbine blade. Results of this study gave a gateway to map constituent uncertainties to the top-

level structure. Next, a stochastic first ply failure load method was developed based on micromechanics and Bayesian inference. Finally, probabilistic SN curves of composite materials were calculated after fatigue model parameter calibration using Bayesian inference.

Throughout this research, extensive experimental data sets from literature have been used to calibrate and evaluate the proposed models. The micromechanics based probabilistic framework formulated here is quite general, and applied on the specific application of a wind turbine blade. The procedure may be easily generalized to deal with other structural applications such as storage tanks, pressure vessels, civil structural cladding, unmanned air vehicles, automotive bodies, etc. which can be explored in future work.

Table of Contents

List of Tables

List of Figures

Acknowledgments

I am greatly indebted to my academic supervisors Dr. Curran Crawford and Dr. Afzal Suleman for their immeasurable help and support throughout the time of my graduate studies. Without their thoughtful guidance through the years, I certainly could not have accomplished my graduate studies successfully.

I wish to express my deep gratitude to Dr. Michael K. McWilliam for his insightful discussions, suggestions and corrections that were invaluable in enhancing the quality of the dissertation.

I owe a huge debt to my parents for their love, especially my mother, for her deep insight to encourage me to study round the globe. I would also like to thank my brothers for their love and encouragement.

Also, I would like to acknowledge the Natural Sciences and Engineering Research Council of Canada (NSERC), Composite Research Network (CRN), and the University of Victoria for a one-year Graduate Award for the financial support of my PhD studies.

Dedication

I would like to dedicate this dissertation to my Mother Miss Raziya Begum who always helps me to become better and stronger and my wife Arsala Awan for her love. Without their unmitigated support in every possible way I would not have been able to accomplish this work. I would also like to thank my family and friends for their loving guidance and support during my study and research life.

Chapter 1 Introduction

Fibre reinforced thermosetting composite materials are widely used in light weight structural applications due to their high specific stiffness and strength properties. However, predicting their mechanical behaviour accurately is a difficult task because of the complicated nature of these heterogeneous materials. This behaviour is not easily modeled with most of the existing macro mechanics based models. Designers compensate for the model unknowns in failure predictions by generating overly conservative designs utilizing overly large safety factors, thereby mitigating many of the benefits promised by composites. The research presented in this dissertation has as its primary goal to provide efficient, high fidelity methodologies for composite material failure predictions for use in the design of structures made up of composite materials.

The methodology developed is based on micromechanics model which has been shown in prior work to more accurately be able to simulate the stiffness, strength, and fatigue behaviour of composites. This is in contract to more typical homogenization based formulas [1, 2] that have difficulties accounting for the various failure modes and matrix-fibre material interactions in composites. The micromechanics model helps the designer to understand in-depth failure modes in these material and design efficient structures. Micromechanics models themselves are not novel in the literature [3, 4, 5, 6], although their use in practise remains relatively rare. A key limiting factor in employing micromechanics models is the unavailability of the constituent properties. In reality, the underling physical properties are subject to uncertainty from material variations. Moreover, in contrast to metallic materials, this uncertainty is compounded by variations layup and curing processes.

The novelty of the work presented in this dissertation is therefore to calibrate these constituent properties by integrating a micromechanics approach with Bayesian statistical models. The outputs of the proposed analysis method are also unique in providing probabilistic metrics of predicted mechanical performance, rather than simply mean or worst case predictions. This aspect can afford the composite designer the ability to use appropriate safety factors and work to desired reliability levels, or alternatively refine materials and production processes to achieve desired levels of reliability. Overall

proposed methodology helps to lower the testing costs, next to its better accuracy in predicting damage modes.

The focus in this research was on continuous fiber reinforced polymer (FRP) composite laminates but could be extended more broadly to other composite materials like textile composites or braided composites where there are more inherent non-linearities in the material response. Throughout this research, extensive experimental data sets from various sources [7, 8, 9, 10] have been used to evaluate the proposed model results. The micromechanics-based probabilistic framework formulated here is quite general; applications are illustrated herein for wind turbine blade composite laminates. The procedure could also be applied to other structural applications such as storage tanks, pressure vessels, civil structural cladding, unmanned air vehicles, automotive bodies.

1.1 Dissertation Outline

The body of this dissertation is comprised of four separate papers that have already been published or submitted to peer-reviewed academic journals and/or presented in international conferences, as indicated at the start of every chapter. The literature review relevant to the specific topics is discussed in the introduction section of each chapter (paper).

Chapter 2 presents a study that aims to bring together a high fidelity micro-model based stiffness calculations of composite materials and probabilistic analysis. The homogenization approach coupled with a Monte Carlo simulation method is used to predict variability in composite material properties. This chapter starts with the concept of Representative Unit Cell (RUC) models and the stiffness properties calculation procedure using Rule of Mixture and homogenization based approaches. Then the concept of the Monte Carlo Simulation along with Latin Hypercube sampling and sensitivity analysis is introduced. Chapter 2 closes with a discussion on the applicability of the presented approach in this chapter to a wind turbine blade analysis.

Chapter 3 focuses on the probabilistic first ply failure (FPF) analysis of composite laminates using a high fidelity multi-scale approach called M-SaF (Micromechanics based approach for Static Failure). For this, square and hexagonal representative unit cells of composites were developed to calculate constituent stresses with the help of

bridging matrix between macro and micro stresses called stress amplification factor. Separate failure criterion was applied to each of the constituents (fiber, matrix, and interface) in order to calculate damage state. The successful implementation of M-SaF requires strength properties of constituents which are most difficult and expensive to characterize experimentally and this limits the use of M-SaF in the early design stages of a structure. This obstruction is overcome by integrating a Bayesian inference approach with M-SaF. Bayesian inference calibrates M-SaF FPF model parameters as posterior distributions from the prior probability density functions drawn from the lamina test data. The posterior statistics were then be used to calculate probabilistic FPF for a range of different laminates.

Chapter 4 is an extension of chapter 3, where the last ply failure (LPF) was calculated using a damage evolution algorithm. The analysis was carried out on a three dimensional representative unit cell of the composite. The predictions from the model were compared with the available test data for E-glass/epoxy in the literature.

In chapter 5, the micromechanics approach was extended from predicting the static behavior of composites to performing fatigue analysis. The primary objective of this work was to estimate the probabilistic fatigue life of laminated composites. A micromechanics model for Fatigue Life Failure (M-LaF) and again a Bayesian inference approach were employed. The proposed framework is applied to various glass fiber reinforced composite lamina and laminates, followed by an application to wind turbine blade.

The workflow in Figure 1.1 shows the connections of all chapters towards end goal of this dissertation which is to perform statistical analysis of composite properties at ply level using micromechanics and then carry out the probabilistic/reliability investigation of structures for robust performance.

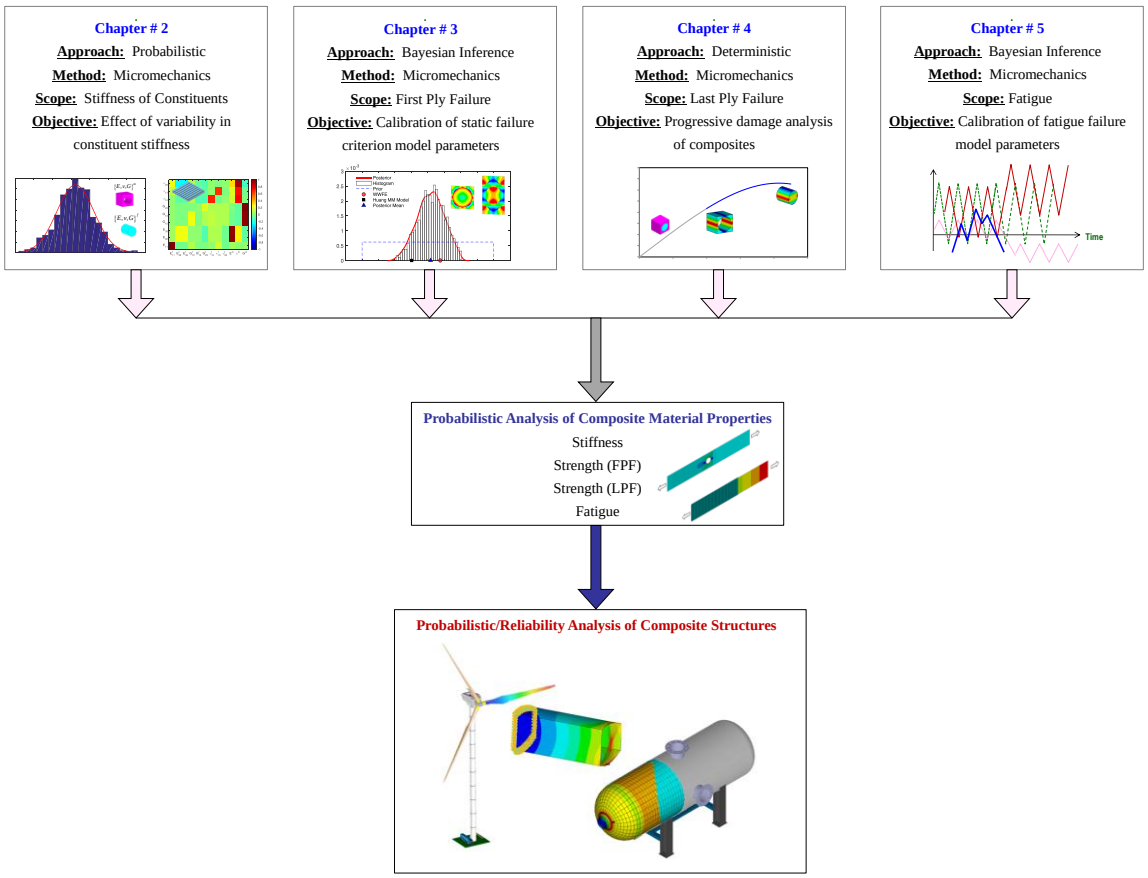

Figure 1.1: Research workflow in this dissertation

Conclusions and recommendations for the future work are offered in chapter 6.

1.2 Research Contributions

In summary, the novel contributions arising from this work are as follows:

a) **Structural probabilistic and sensitivity analysis**: A computational framework is formulated based on micromechanical model along with statistical information of constituent stiffness properties to extract the stochastic models of composite materials at lamina level. These stochastic models were then applied to perform probabilistic and sensitivity analysis of wind turbine blade structure to highlight the key material properties that most influence the structural response (see Chapter 2). This work was published in Composite Structure Journal [11].

b) **Calibration of constituent properties**: A Bayesian inference formulation was employed to combine the test data from physical experiments and predictions using

micromechanical model to calibrate the M-SaF model parameters. With these calibrated parameters, a first ply failure (FPF) probabilistic analysis of a variety of laminates was then performed (see Chapter 3). This paper is submited for publication to the Journal of Composite Materials. The first order statistics of posterior of M-SaF model parameters was used to predict last ply failure (LPF) (see Chapter 4). This work was presented at the 10th Canada-Japan Conference [12].

c) **Probabilistic fatigue analysis of composites**: The hybrid approach using Bayesian and micromechanical model that was developed for static case was extended to perform probabilistic fatigue analysis for various lamina and laminates (see Chapter 5). This paper was published in the special issue of the Composite Structures Journal [13].

Chapter 2 Probabilistic Micromechanical Analysis of Composite Material Stiffness Properties for a Wind Turbine Blade

This paper was published in Composite Structures Journal and published online in August 2015.

Mustafa, Ghulam, Afzal Suleman, and Curran Crawford. "Probabilistic micromechanical analysis of composite material stiffness properties for a wind turbine blade." Composite Structures 131 (2015): pp 905-916.
[http://dx.doi.org/10.1016/j.compstruct.2015.06.070]

This chapter is an initial step towards a bigger picture to analyze the composite structures using micromechanics and statistical models. The scope of this chapter is confined to the stiffness and use of Monte Carlo approach for probabilistic analysis of composite materials. The later chapter covers strength and fatigue of composites using Bayesian inference model.

ABSTRACT

This work presents a coupled approach for stiffness property prediction of composite materials used in wind turbine blades using an advanced micromechanics and reliability-based methodologies. This approach demonstrates how to map the uncertainties in the fiber and matrix properties onto the equivalent stiffness properties of composite laminates. Square and hexagonal unit cells were employed for the estimation of the composite equivalent properties. The finite element formulation of the unit cells were performed in the ANSYS Multiphysics. The results from numerical experimentation conform well with the available test data and to the results from the Modified Rule of Mixture (MROM). A probabilistic analysis using Monte Carlo Simulation with Latin Hypercube Sampling was used to assess the uncertainties in the equivalent properties according to the variability in the basic properties of the constituents. Furthermore, a sensitivity analysis based on the Spearman Rank Order correlation coefficients was carried out to highlight the influence of important properties of the constituents. As an illustration, the above approach is applied to analyze a 5 MW wind turbine blade section under static loading. Results demonstrate the possibility of the coupled approach at macro level (structure) from micro level (unit cell) with the aim to design robust structures.

2.1 Introduction

The size of wind turbines is increasing to capture more energy and this trend will continue into the future [14]. Several multi-MW prototype wind turbines exist for offshore applications [15, 16]. The power of a wind turbine scales as square of the rotor diameter, while the mass of the blade (for similar conceptual designs) scales as the cube of rotor diameter. Considering these scaling laws one might predict that in the end material costs would govern and avert further scaling. The cost of the blade would then also scale as the cube of rotor diameter but advanced structural concepts reduce its scaling exponent to ~2.5 [17]. A polymer-based composite material is a good choice for large structures such as wind turbine blades. The high strength-to-density ratio, high stiffness-to-density ratio, good fracture toughness, fatigue performance and suitability for use in fast production of large structures makes composites a good choice for their use in structural applications. The composite properties provided by the manufacturer are generally the average properties in a particular manufacturing environment. On top of this, manufacturers usually don't mention the number of tests that they performed to obtain the average. This adds risk to structural design, especially for large-scale composite layups such a blades. It is impossible to completely control variation in the composite properties. There are many factors that contribute to that variation including: batch-to-batch production, manufacturing conditions like temperature, pressure, and humidity, curing time, labour skill, along with the property variations in the basic building blocks of the ply (the fiber and the matrix). These variations in the mechanical properties of composite materials are due primarily to variation in the properties of the constituents - the fiber and matrix [18]. This variation in properties establishes a scatter in the response of a structure made up from this material, for example, the deflection of the wind turbine blade. Therefore, it is necessary to consider the variable nature of composite properties at the design stage. Current wind turbine blade design is based on a deterministic approach with a large factor of safety to ensure target static and fatigue limits [19]. It is very expensive experimentally to obtain the design allowables for a composite laminate in a deterministic approach as significant test campaigns for each candidate layup are required.

The micromechanics (MM) based homogenization approach is good alternative to characterize the stiffness properties of composite materials [2, 3]. The Rule of Mixtures (ROM), also known as the Simple Rule of Mixture (SROM), is one of the oldest and simplest forms of micromechanics for calculating mechanical properties of unidirectional plies [2, 20, 21]. Halphin [22] proposed a Modified Rule of Mixture (MROM) as there are shortcomings in calculating the transverse Young's modulus and in-plane shear modulus using SROM. Dong et al. [23] simulate the behaviour of various unit cells using an asymptotic homogenization technique. Other researchers have considered the uncertainty in the basic constituent's properties with the homogenization approach. Kamiński and Kleiber [24] calculated the first two probabilistic moments of the elasticity tensor using the homogenization method of composite structure. However, due to the complicated mathematical formulation, these studies are of limited applicability.

The present study aims at bringing together high fidelity micro-model based stiffness calculations of composite materials and probabilistic analysis. The homogenization approach coupled with a Monte Carlo simulation method is used to predict variability in composite material properties. The paper is organized as follows. Section 2.2 introduces the concept of the Representative Unit Cell (RUC) models and the stiffness properties calculation procedure using Rule of Mixture and homogenization based approaches. Section 2.3 provides details of the Monte Carlo Simulation along with Latin Hypercube sampling and sensitivity analysis. Section 2.4 presents the results. Section 2.5 details the applicability of the method to a wind turbine blade section analysis. Section 2.6 summarizes the most important conclusions drawn from this study.

2.2 Theory

2.2.1 Representative Unit Cell (RUC) Models

The wind turbine blade structure is made up of polymer-based composite laminates, which are in turn made up of plies stacked in a certain sequence. These plies are made up of fibre and matrix constituents. All these levels are divided into two main groups, the macro and micro levels as shown in the Figure 2.1. Customarily, one moves right or left in these levels via localization and homogenization. A homogenization procedure provides the response of a structure given the properties of the structure's constituents.

Conversely, the localization method provides the response of the constituents given the response of the structure.

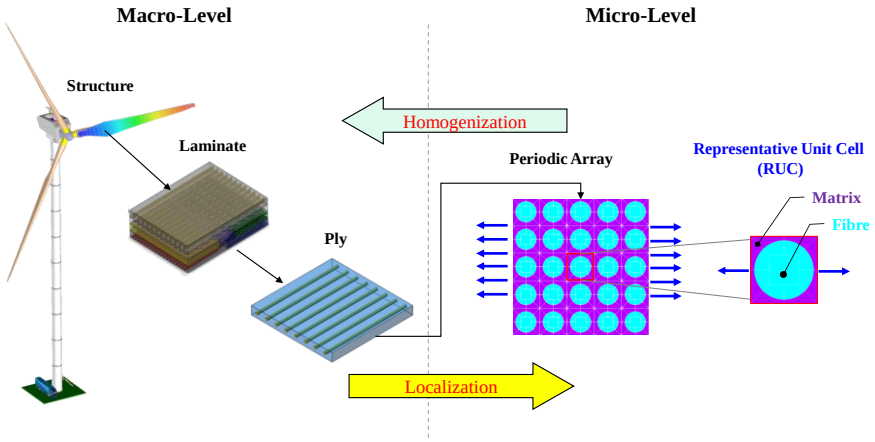

Figure 2.1: Macro and Micro levels structures

The fibres are randomly arranged in the real unidirectional (UD) ply. The far left side of Figure 2.2 shows a cross section of a continuous UD ply [25]. There is no obvious regular pattern in which the fibres are arranged. A true representation of the fibre arrangement is shown in the middle of Figure 2.2. To aid computation, an idealized fibre arrangement is used, as shown in the far right side of the Figure 2.2. In this study, an idealized square (SQR) RUC model is used for probabilistic analysis as shown at the bottom of Figure 2.2. Although it is possible with suitable boundary conditions to represent a hexagonal arrangement with square unit cell. Other choices for the RUC, such as triangular RUC, could be exploring in the future. The implication of assuming fibres packed in regular manner is not predicting well strain hardening behaviour due to assumed elastic/perfectly plastic behaviour as assumed for the matrix. On the other side, this behaviour is quite noticeable for randomly distributed fibers in stress-strain curve. Also, the RUC considered in this work did not consider fiber misalignment and it would have an effect on composite properties like longitudinal compressive strength. This will lead to over predictions and will add weight to the structure considering safety factors. This is obviously beyond the scope of the present paper but it’s worth mentioning to readers.

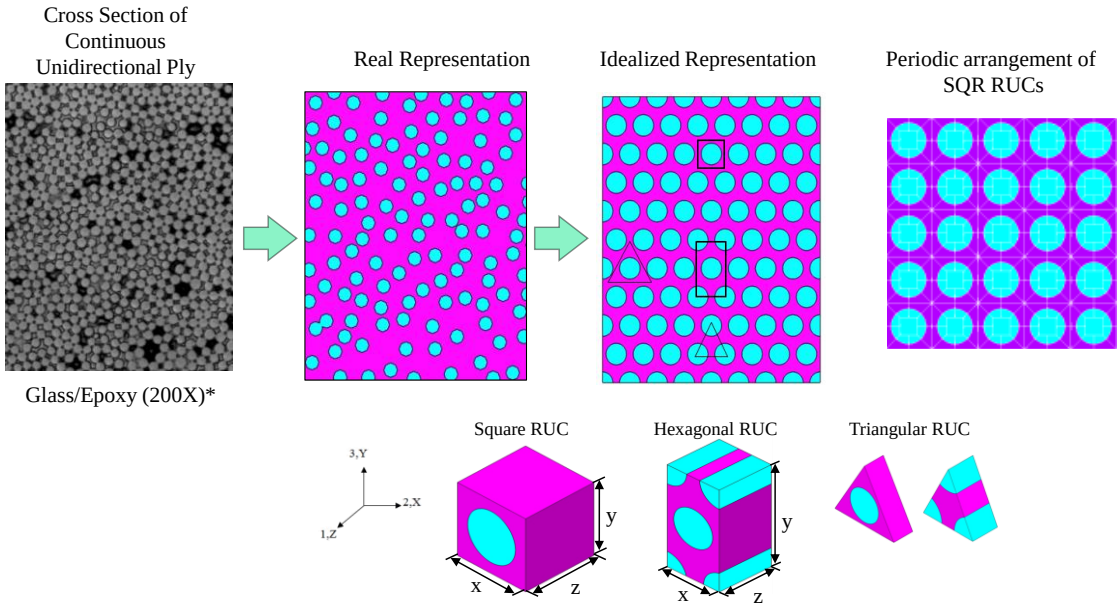

Figure 2.2: Representative Unit cell models for composite analysis

2.2.2 Rule of Mixture (ROM)

Structures made up from composite materials can be designed by tailoring the constituent properties. This requires high fidelity analysis and design of composite materials. Micromechanics is an approach that handles this scenario by establishing a relationship between the constituents and the ply or lamina. Several theoretical models have been proposed for the prediction of composite properties from those of the constituent fiber and matrix. An investigation of the existing micromechanics models has been summarized by Hashin [26]. The Rule of Mixtures (ROM) is one of the oldest and simplest forms of micromechanics for calculating the mechanical properties of unidirectional plies [2, 20, 21]. There is not an accurate prediction for the transverse Young's modulus E_{22} and in-plane shear modulus G_{12} through SROM. This deficiency is overcome by the Modified Rule of Mixture (MROM) as proposed by Halphin [22].

2.2.3 Ply Stiffness Computational Procedure with RUC

It is not easy to determine experimentally the longitudinal and transverse shear moduli of unidirectional composites. It is also difficult to predict these moduli using MROM as they require ply level information [2]. Thus, numerical techniques such as the finite element method (FEM) are needed to facilitate these predictions. The stiffness properties

of a unidirectional (UD) ply are calculated using FEM from the constituent's properties: the fibre and resin (or matrix) properties; fibre volume fraction V_f which controls the geometric parameter of the RUC. For example, in the case of SQR RUC, the radius of the unit cell is given as $r_f^{SQR} = \sqrt{V_f xy/\pi}$, where x and y is lengths of square unit cell as shown in Figure 2.2.

The behaviour (stress and strain fields) of fiber and resin under uniform loading is quite different due to their different material properties. Therefore, special attention must be paid in order to make sure that linear stress-strain relationships can be used to compute the elastic properties of the lamina. In the stiffness properties prediction procedure, it is assumed that in an undamaged state both constituents are perfectly bonded everywhere along the length of the fibre/resin interface. For a fully reversible linear material domain, the constitutive relationship between stress and strain for a UD ply is given in Equation 2.1. For the plane stress case, the stiffness matrix $\bar{\mathrm{C}}$ is invertible to obtain a compliance matrix $\bar{S}$. Their product must produce a unity matrix, i.e. $[\bar{S}] = [\bar{C}]^{-1}$. By definition, ply stiffness properties can be computed from the elements of the $[\bar{S}]$ matrix [25].

$$\begin{bmatrix} \bar{\sigma}_1 \\ \bar{\sigma}_2 \\ \bar{\sigma}_3 \\ \bar{\sigma}_4 \\ \bar{\sigma}_5 \\ \bar{\sigma}_6 \end{bmatrix} = \begin{bmatrix} \bar{C}_{11} & \bar{C}_{12} & \bar{C}_{13} & 0 & 0 & 0 \\ \bar{C}_{21} & \bar{C}_{22} & \bar{C}_{23} & 0 & 0 & 0 \\ \bar{C}_{31} & \bar{C}_{32} & \bar{C}_{33} & 0 & 0 & 0 \\ 0 & 0 & 0 & \bar{C}_{44} & 0 & 0 \\ 0 & 0 & 0 & 0 & \bar{C}_{55} & 0 \\ 0 & 0 & 0 & 0 & 0 & \bar{C}_{66} \end{bmatrix} \begin{bmatrix} \bar{\varepsilon}_1 \\ \bar{\varepsilon}_2 \\ \bar{\varepsilon}_3 \\ \bar{\varepsilon}_4 \\ \bar{\varepsilon}_5 \\ \bar{\varepsilon}_6 \end{bmatrix} \qquad \text{Equation 2.1}$$

2.2.4 Boundary Conditions on RUC

The homogenization approach acts as a bridge between the microscopic and macroscopic scale analyses. Homogenization consists of two steps: 1) calculate local stresses and strains in constituents 2) use homogenization to obtain global stresses and strains for elastic property calculations. The successful implementation of homogenization assumes that the RUC has global repetition or periodicity. There are varieties of homogenization approaches to predict the composite material behaviour [20, 27]. The homogenization technique given by Sun and Vaidya [27] is most widely used because of its relatively low computation cost and this can be achieved by applying

proper boundary conditions (BCs) that are periodic. These periodic BCs give more practical results compared with other boundary conditions such as uniform stress boundary condition or kinematic uniform boundary conditions, and have been validated by various researchers [28, 29]. The periodic boundary conditions satisfy three statements: 1) the deformation should be the same on the opposite surface, 2) the stress vectors acting on opposite surfaces should be opposite in direction in order to have stress continuity across the boundaries of unit cell, and 3) there is no separation or overlap between the neighbouring RUC. The displacement field boundary condition on the boundary Γ of domain Ω of the unit cell is given in Equation 2.2 as stated by Suquet [30]:

$$u_i(x_1, x_2, x_3) = \bar{\varepsilon}_{ik} x_k + u_i^*(x_1, x_2, x_3) \qquad \text{Equation 2.2}$$

In the above, $\bar{\varepsilon}_{ik}$ is the global average strain of the periodic structure and x_k represents a linear distributed displacement field. u_i^* is a periodic part of the displacement from one RUC to another on the boundary surface and, unfortunately, it cannot be directly applied to the boundaries since it is unknown. In order to determine the stiffness matrix $[C]$ of the constitutive Equation 2.1, different displacement boundary conditions are applied on the RUC with appropriate periodicity as determined by Equation 2.2. The graphical explanation of these BCs is given in Figure 2.3.

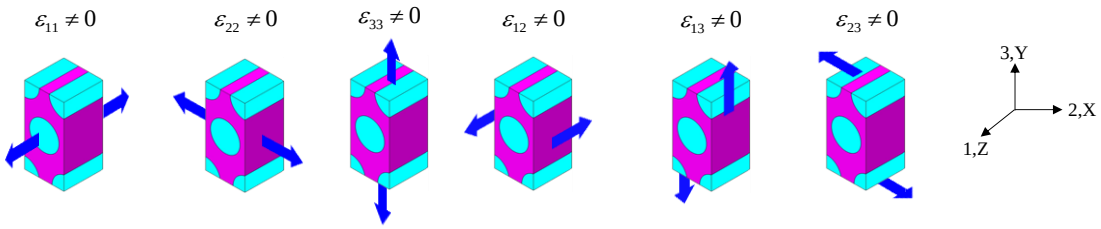

Figure 2.3: Boundary Conditions for Calculation of Effective Material Properties of UD

The constraint equations have been applied in the FEM code ANSYS. To apply constraint equations on the nodes of opposite faces of the RUC, identical mesh schemes were applied on opposite surfaces of the RUC. The degree of freedom (DOF) coupling technique in ANSYS is utilized to apply periodic boundary conditions. The coupling and constraint equations relates the motion of one node to another [31]. For example, in the

case of $\varepsilon_{13} \neq 0$, the constrained equations applied are shown in Figure 2.4. The Von-Mises stress distribution on the RUC under BCs is also given in Figure 2.4. Two important points should be noted from the RUC stress distribution. First, stresses at the same location on opposite sides are the same and this confirms the traction continuity. The second is that the boundary faces are no longer planes.

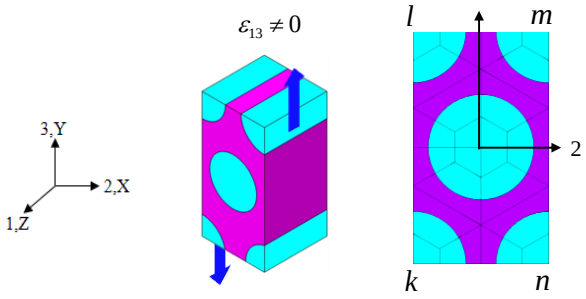

$$\begin{vmatrix} u_x^{1+} - u_x^{1-} = 0 & u_x^{2+} - u_x^{2-} = 0 & u_x^{3+} - u_x^{3-} = 0 \\ u_y^{1+} - u_y^{1-} = 0 & u_y^{2+} - u_y^{2-} = \varepsilon_{12} d_{nk} & u_y^{3+} - u_y^{3-} = 0 \\ u_z^{1+} - u_z^{1-} = 0 & u_z^{2+} - u_z^{2-} = 0 & u_z^{3+} - u_z^{3-} = \varepsilon_{12} d_{mn} \end{vmatrix}$$

Figure 2.4: Shear Boundary Conditions on HEX RUC

2.3 Probabilistic analysis

2.3.1 Monte Carlo Simulation approach and Latin Hypercube Sampling

Most probabilistic techniques require running deterministic models multiple times with different realizations of random input variables. The key difference between various probabilistic techniques is the choice of the realization from the current analysis to the previous one. A probabilistic analysis answers a number of questions: 1) how much scatter induced due to randomness in the input variables; 2) what is the probability the output parameters are no longer fulfilled based on design criterion; 3) which random input variable most affect the output parameters which helps to screen the design variables [31]?. The Monte Carlo Simulation (MCS) approach is one of the most general tools to perform stochastic analysis under uncertainty of input variables [32]. In this work, the second order statistics of the responses are obtained using MCS with the random input variables (RVs) specified by their mean μ and standard deviation σ. The

MCS consists of three steps: 1) generation of realization corresponding to probability distribution function (PDF) – Latin Hypercube Sampling is used for this purpose in this work; 2) a finite element simulation evaluates responses for each realization; 3) statistical analysis of the results yields valuable information concerning the sensitivities of the responses to the stochastic RVs. In the Latin Hypercube Sampling technique the range of all random input variables is divided into n intervals with equal probability and the sample generation process has a memory in the meaning that the sampling points cannot cluster together.

2.3.2 Sensitivity Analysis

Analysis of parameter sensitivity investigates the effect of variability of certain input random variables on the variability of design-relevant response quantities; the sensitivities can be described by coefficients of correlation. One of the most commonly used coefficient of correlation which is calculated by Spearman's rank correlation and is given in Equation 2.3 between two random variables X and Y:

$$r_{X,Y} = 1 - \left[\frac{6 \sum d^2}{n(n^2 - 1)}\right] \qquad \text{Equation 2.3}$$

where d is the difference between rank order of variable 1 and rank order of variable 2 and n is the number of samples in each set.

The flow chart to calculate probabilistic properties of a UD composite based on the constituent's uncertainties in a modular fashion is illustrated in Figure 2.5.

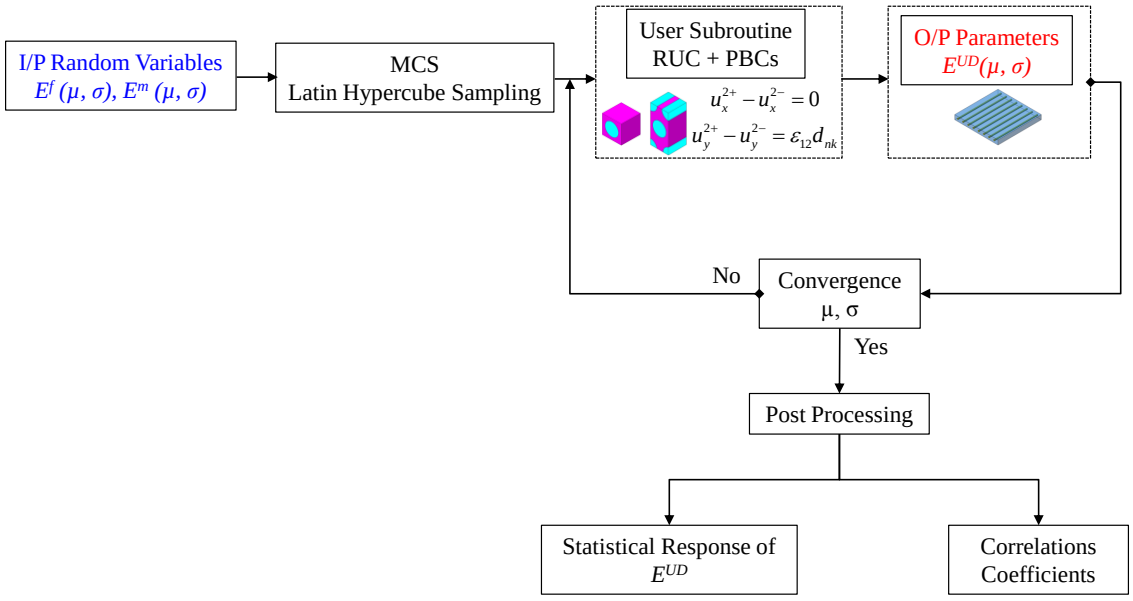

Figure 2.5: Probabilistic analysis flow chart from constituent stiffness properties

2.4 Results and Discussion

2.4.1 Boundary Conditions for 2D Unit Cell

The periodic boundary conditions (BCs) devised by Xia [29] and given in Equation 2.4 are applied to a SQR and HEX unit cell FEM model which insures that the composite has the same deformation mode and there is no separation between unit cells. To verify the BCs, a 2-dimensional unit cell model is considered first. The fiber volume fraction is 50%. The elastic moduli and Poisson's ratio for the fiber and matrix are $E_{11}^f = 72500\ MPa, v_{12}^f = 0.22$ and $E^m = 2600\ MPa, v^m = 0.42$, respectively.

$$u_i^{j+}(x,y,z) - u_i^{j-}(x,y,z) = c_i^j(i,j = x,y,z) \qquad \text{Equation 2.4}$$

In Equation 2.4, u_i^{j+} and u_i^{j-} are displacements of one pair of nodes at opposite boundary faces, with identical coordinates in the other two directions. The constant c_i^j represent the stretch or contraction of the unit cell model under the action of normal forces or shear deformations due to the shear forces. A simple fibre-matrix domain was defined in ANSYS [31] tool as shown in Figure 2.6. The FEM unit cell model and the deformed shape of the unit cell are shown in Figure 2.6. The boundaries do not remain

planes after load application, and shear stresses are uniform in the unit cell. Table 2.1 compares the present results with Xia [29] demonstrating excellent agreement of shear strain, shear stress, and equivalent shear modulus.

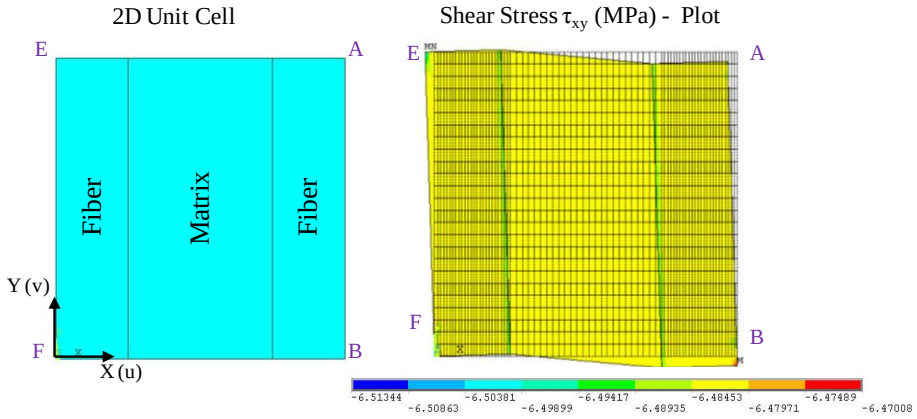

Figure 2.6: 2D unit cell and shear stress distribution

Table 2.1: 2D unit cell model result comparison

Parameter	Xia et al [29]	FEM
Shear Stress, τ_{xy} (MPa)	6.4831	6.4917
Shear Strain, γ_{xy} (-)	0.0036	0.0036
Shear Modulus, G (MPa)	1801	1803

2.4.2 Boundary Conditions for 3D Unit Cell

The next step was to define a finite element model of a square unit cell and repeated array in order to compare the behaviour under identical loadings and boundary conditions. The 3-D structural solid element, SOLID45, is used for the FEM analysis. The material properties of Silenka E-Glass 1200 tex and MY750 Epoxy are given in Table 2.2.

Table 2.2: Material Properties of Fiber and Matrix

Properties	E-glass Fiber	Properties	MY750 Epoxy
E_{11}^f (GPa)	74.0	E^m (GPa)	3.35
E_{22}^f, E_{33}^f (GPa)	74.0	v^m (-)	0.35
G_{12}^f, G_{13}^f (GPa)	30.8		
v_{12}^f (-)	0.2		

The responses of the multi-cell array and the unit cell model were compared for different loading conditions with proper periodic boundary conditions. As an example, the comparison of the SQR and HEX multi-cell array and the unit cell models under shear load is shown in Figure 2.7. From Figure 2.7, it is clear that the stress distributions in the multi-cell model and the unit cell are identical. There is no boundary separation, which verifies the boundary conditions. The rest of the boundary conditions were verified in a similar manner.

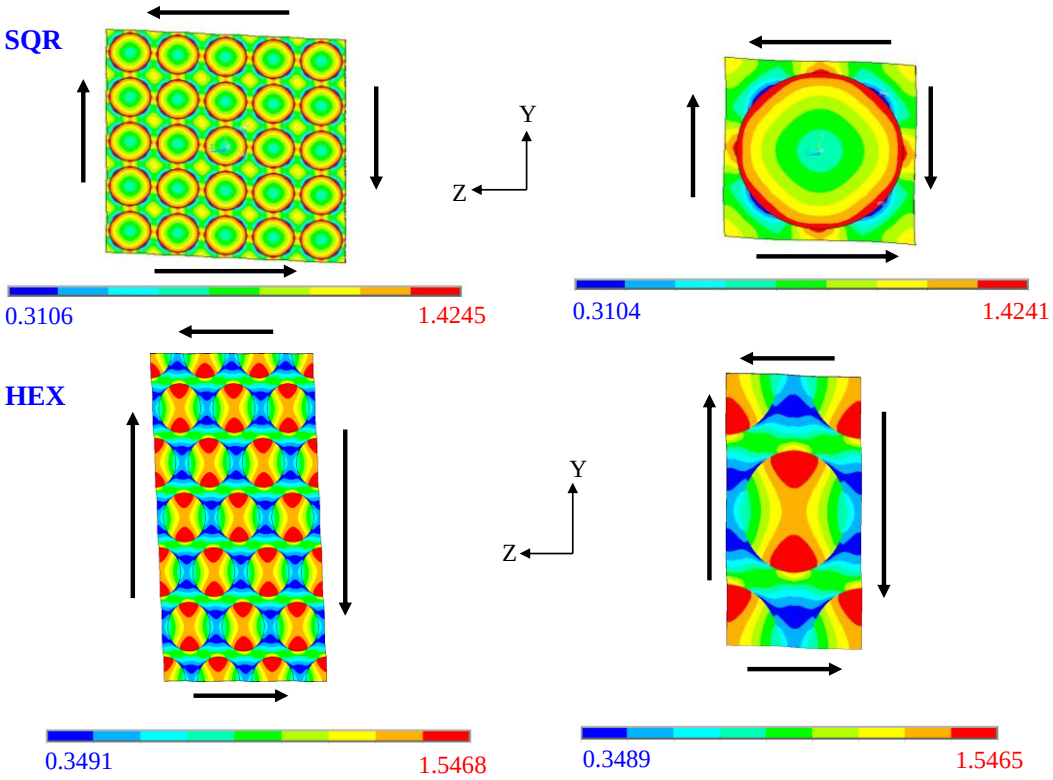

Figure 2.7: Comparison of Shear Stress (N/m2) distribution in Multi-Cell & Unit Cell Model

2.4.3 UD Ply Stiffness Properties

To verify the homogenization technique, the stiffness properties were determined with the SQR and HEX unit cell first and compared with test data [7] as well as predictions from SROM and MROM. The same E-glass fibre and MY750 epoxy was used for this analysis. The stiffness properties were calculated in the linear elastic region. The comparisons were made using 60% fiber volume fraction. The predictions were compared with test data [7] and were found to be in good agreement, as shown in Figure 2.8.

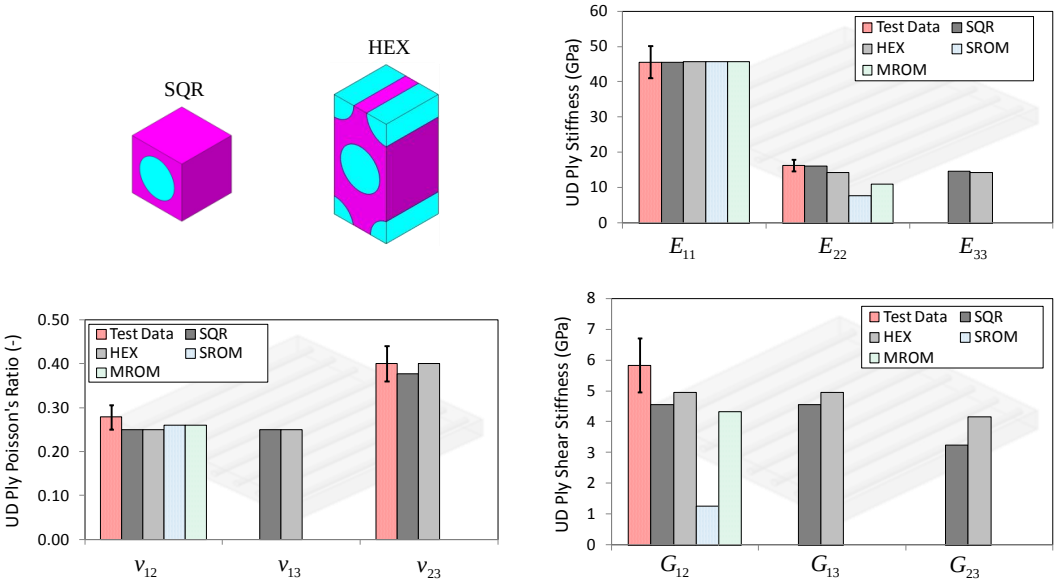

Figure 2.8: Comparison of Stiffness Properties from RUC with test data

2.4.4 Statistical Model Description and Monte Carlo Simulation

In this section, the Monte Carlo Simulation approach is coupled with a homogenization based stiffness calculation procedure to access the uncertainty of the stiffness properties of UD due to variation in the constituent's properties. This coupling is achieved in three steps: 1) generation of realizations according to the Latin Hypercube Sampling technique of random variables, i.e. the fiber and the matrix; 2) using the RUC and homogenization approach to simulate UD properties against each set of realizations; 3) post-processing the results to calculate statistical response and sensitivities of the output response parameters. Steps 1 and 2 were implemented in the finite element tool

ANSYS PDS and ANSYS Multiphysics respectively by user defined subroutines. Step 3 is performed partially in ANSYS PDS and in MATLAB. The generation of the realizations is based on the probability distribution; a Gaussian distribution is used for fiber and matrix property random variables. Note that an alternate choice of the distribution type would not modify the overall methodology. The Gaussian probability density function (PDF) is given in Equation 2.5. The mean μ_X and standard deviation σ_X are the two parameters describing the Gaussian PDF for each random variable X.

$$f_X = \frac{1}{\sqrt{2\pi\sigma_X}} exp\left[-\frac{(x-\mu_X)^2}{2\sigma_X^2}\right] \qquad \text{Equation 2.5}$$

The details of the constituent random variables are given in the Table 2.3. The properties of the constituents (E-glass fiber and MY750 matrix) were taken from [7]. A 5% standard deviation is considered where data was missing for a particular quantity. The response parameters include: longitudinal modulus (E_{11}), transverse modulus (E_{22}) and (E_{33}), in-plane shear modulus (G_{12}) and (G_{13}), transverse shear modulus (G_{23}), major Poisson's ratio (v_{12}), and minor Poisson's ratio (v_{13}) and (v_{23}).

Table 2.3: Input Random Variables for Calculation of UD Properties

Material	Random Variable	Symbols	Mean	Std dev
Fiber	Longitudinal modulus (GPa)	E_{11}^f	74.00	18.50
	Transverse modulus (GPa)	E_{22}^f	74.00	14.80
	Transverse modulus (GPa)	E_{33}^f	74.00	14.80
	In-plane shear modulus (GPa)	G_{12}^f	30.80	7.70
	Transverse shear modulus (GPa)	G_{13}^f	30.80	6.16
	Transverse shear modulus (GPa)	G_{23}^f	30.80	6.16
	Major Poisson's ratio (-)	v_{12}^f	0.20	0.01
	Minor Poisson's ratio (-)	v_{13}^f	0.23	0.01
	Minor Poisson's ratio (-)	v_{23}^f	0.23	0.01
Matrix	Elastic Modulus (GPa)	E^m	3.35	0.84
	Poisson's ratio (-)	v^m	0.35	0.02
	Shear modulus (GPa)	G^m	1.24	0.25

A common question is the required number of iterations to be performed with the Monte Carlo method. Equation 2.6 [33] can be used to estimate the required number of runs by the standard error of the mean of the distribution relation:

$$error = \frac{z\sigma_X}{\sqrt{n}} \qquad \text{Equation 2.6}$$

where z is a confidence multiplier and its value is 2 for 95% confidence level, σ_X is standard deviation and n is the is the number of runs or simulations performed in the Monte Carlo simulation. The percentage error of the mean becomes:

$$E = \frac{100z\sigma_X}{\mu_X\sqrt{n}} \qquad \text{Equation 2.7}$$

For the estimation of runs n, the Equation 2.7 becomes:

$$n = \left[\frac{100z\sigma_X}{\mu_X E}\right]^2 \qquad \text{Equation 2.8}$$

For example, using UD longitudinal stiffness (E_{11}) from test data, $\mu_{E_{11}} = 45.6\ GPa$ and $\sigma_{E_{11}} = 9.12\ GPa$, for a 95% confidence level $z = 2$ and $E = 2$, the required number of Monte Carlo simulations is 400.

The results of the probabilistic analysis after post-processing in MATLAB are given in Figure 2.9. The μ, σ, κ represents the mean, standard deviation, and kurtosis of each parameter respectively. The response parameters are presented as histograms along with the PDFs fit to the data; Gaussian was found to be a good fit for the UD properties. The higher standard deviation in the stiffness property of the fiber is reflected in the UD longitudinal property response parameter. The probability that the UD longitudinal stiffness E_{11} is smaller than 35 GPa is 0.16677 with a 95% confidence level. The lower stiffness of E-glass/epoxy composites will cause more deflection in the blade. Therefore, it is important to calculate this probability. The standard deviation in UD transverse

stiffness is 3.00 GPa. The standard deviations in shear modulii and Poisson's ratio are given in the Figure 2.9.

The evaluation of the probabilistic sensitivities is based on the correlation coefficients between all random input variables and a particular random output parameter. The sensitivity analysis was performed using the Spearman rank coefficient of correlation approach to investigate correlation between input design variables and output response parameters. The results of this analysis are shown in the Figure 2.10. These correlations explain the strength of the relationship between the stochastic quantities and range from -1 to +1. A correlation of -1 describes perfect negative relation and +1 a strong positive relation. A correlation close to 0 indicates no or weak relation. It can be clearly seen from Figure 2.10 that UD longitudinal stiffness E_{11} has a strong relation with fiber longitudinal modulus. Likewise, E_{22} has a strong positive relation (close to 1) with matrix modulus E^m. The shear properties of composites are also very impotent, particularly in wind turbine blade shear webs [34]. The sensitivity analysis shows that matrix shear modulus G^m correlates very highly with UD lamina shear molulii, i.e. G_{12}, G_{13}, G_{23} but G^m has only a minor sensitivity to the UD lamina Poisson's ratio. This sensitivity analysis aids in improving the material according to design requirements as well as screening out unnecessary design variables for optimization purposes.

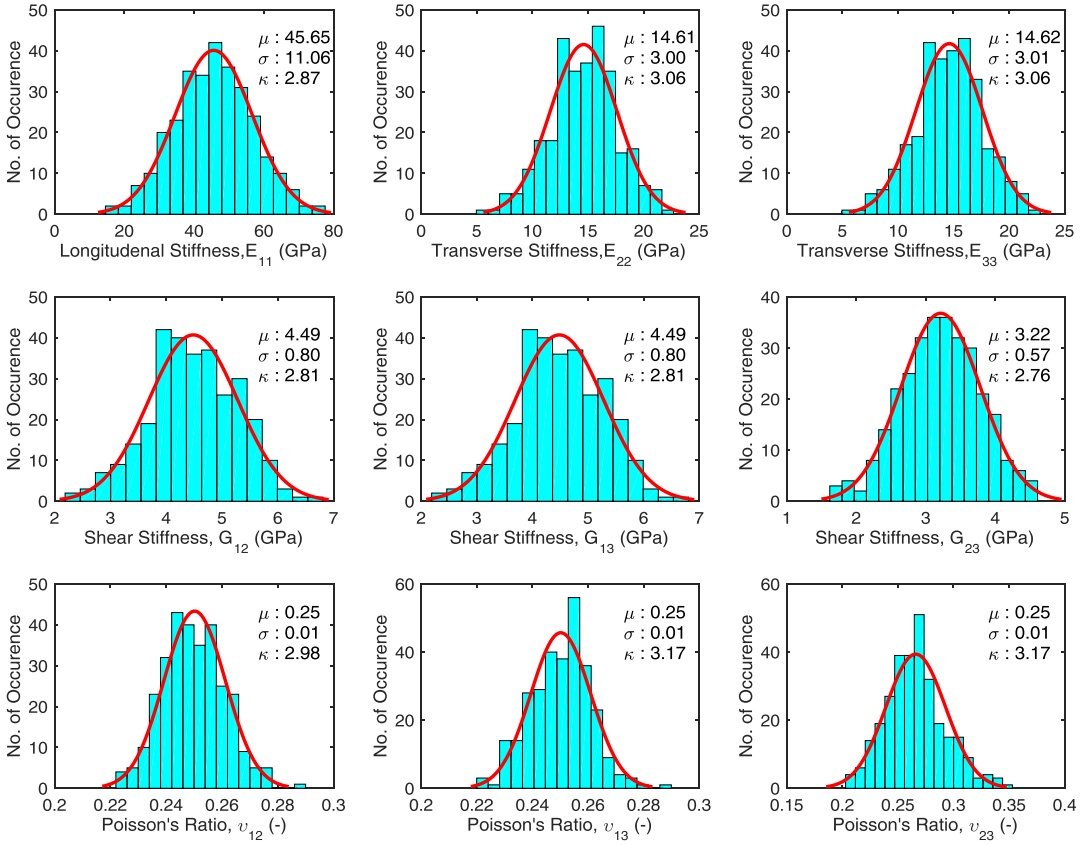

Figure 2.9: Histograms & PDFs of Output Parameters: Top row represents longitudinal and transverse stiffness, middle row for shear stiffness, and bottom row for Poisson's ratio

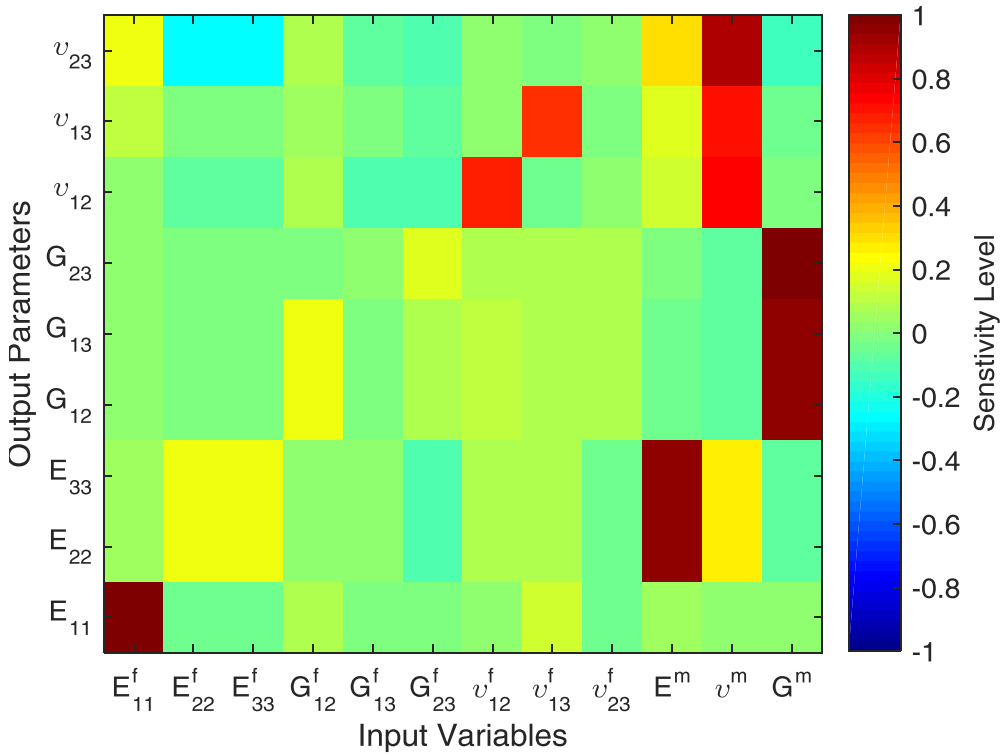

Figure 2.10: Spearman Rank Order Correlation Coefficients

The statistical interdependence between the output response parameters was also calculated by a Spearman rank order correlation coefficients approach. Figure 2.11 shows the sensitivity plot of the response parameters, i.e. UD stiffness properties. It can be seen from this Figure 2.11, some properties are strongly correlated with others and some are in a week manner. This is important information for further analysis of the wind turbine blade. At the time of declaring the stochastic properties of UD for the analysis of blade, a threshold criterion will be applied between correlations in UD properties. This will not only accelerate the overall simulation time but also give more insight into structural response dependency on the input variables as explained in the following section.

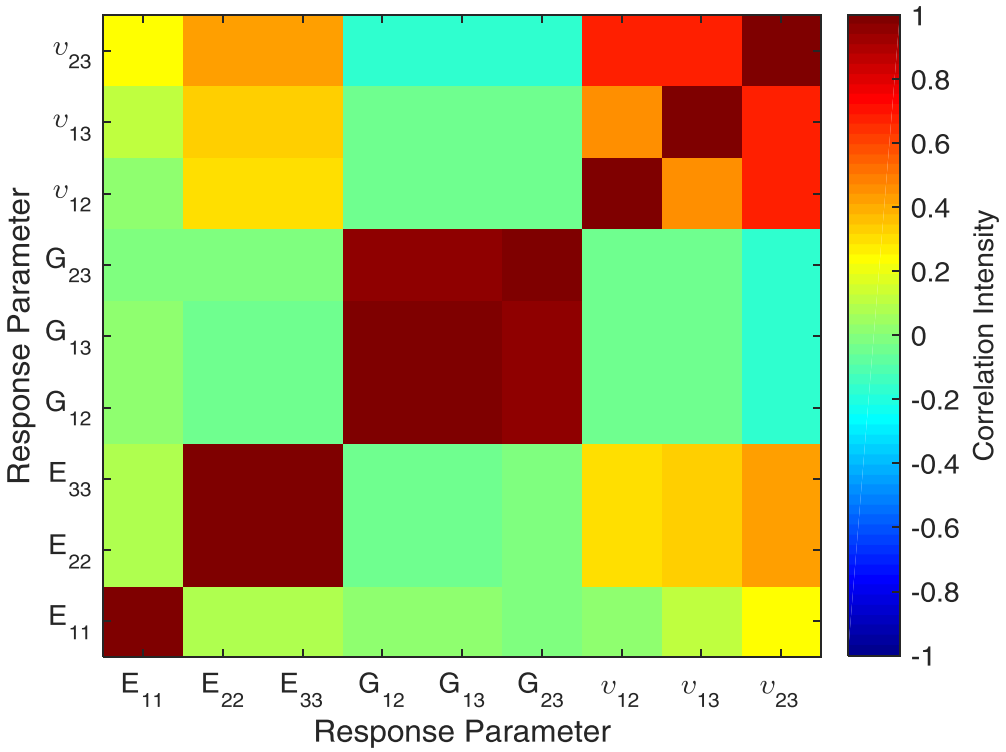

Figure 2.11: Spearman Rank Order Correlation Coefficient Matrix between Output Parameters

2.5 Application to Wind Turbine Blade Section

A case study was carried out to highlight the implications of micromechanics-based probabilistic analysis for realistic application to a composite wind turbine blade structure. Wind turbine blades can be analyzed as beam-like structures, as is done by current design codes [19, 35]. In this section though, the analysed blade is modeled in more detail as a shell structure. The investigated blade has shell and spar/web type internal structural layout. The aerodynamic outer shell is obvious as it is providing required aerodynamic characteristics to the blade. The internal blade structure consists of spar caps and shear webs. The spar caps carry the bending and axial loads. The shear webs carry the shear stress and provide airfoil shape stability. The classic embodiment of this concept is similar to the steel I-beam except that there are shells around the outside that form the aerodynamic shape. The geometry and other specifications of the rotor blade considered in this research is based on the NREL 5MW baseline wind turbine described in [36]. A 61 m blade is attached to a hub with a radius of 2 m, which gives the total rotor radius of 63 m. Although the blade is composed of several airfoil types, in this work the airfoil

used is the NREL-S818 [37] from maximum chord to the tip of the blade. The first portion of the wind blade is a cylindrical in shape. Further away from the root the cylinder is smoothly blended into a NREL-S818 airfoil at maximum chord. The power curve and other environmental parameters are given in Figure 2.12.

A part of the blade is considered for simplicity of computation. The details of the blade wing box and the composite layup sequence are given in the Figure 2.13. The investigated blade consists of three different types of E-glass/epoxy composites: unidirectional (UD) plies, BX $[\pm 45°]_s$, and TX $[0°/\pm 45°]_s$. The UD and TX are used in the shell structure along with a PVC core. The BX and PVC core [38] is used in shear webs to provide shear resistance. The properties of the materials used in the wing box analysis were calculated from the probabilistic analysis on RUC as described in the previous section.

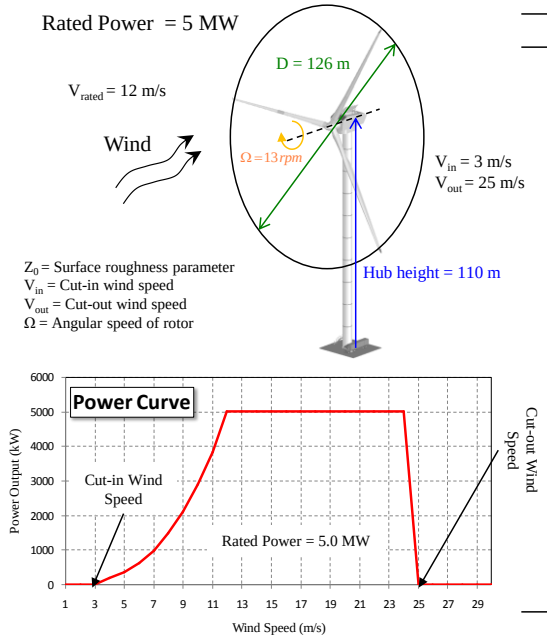

Parameter	Units	NREL-5M
Rated Power	MW	5
IEC Class	(-)	1A
Number of blades	(-)	3
Rated wind speed	m/s	12
Cut-in wind speed	m/s	3
Cut-out wind speed	m/s	25
Blade Tip Speed	m/s	81.7
Rated Rotor Speed	rpm	13
Tip Speed Ratio	(-)	6.81
Diameter	m	126
Blade Length	m	63
Hub Height	m	110
Maximum Chord	m	4
Maximum Twist	deg	14
Precone	deg	2.5
Direction	(-)	Clockwise
Orientattion	(-)	Upwind

Figure 2.12: NREL-5MW baseline wind turbine specifications

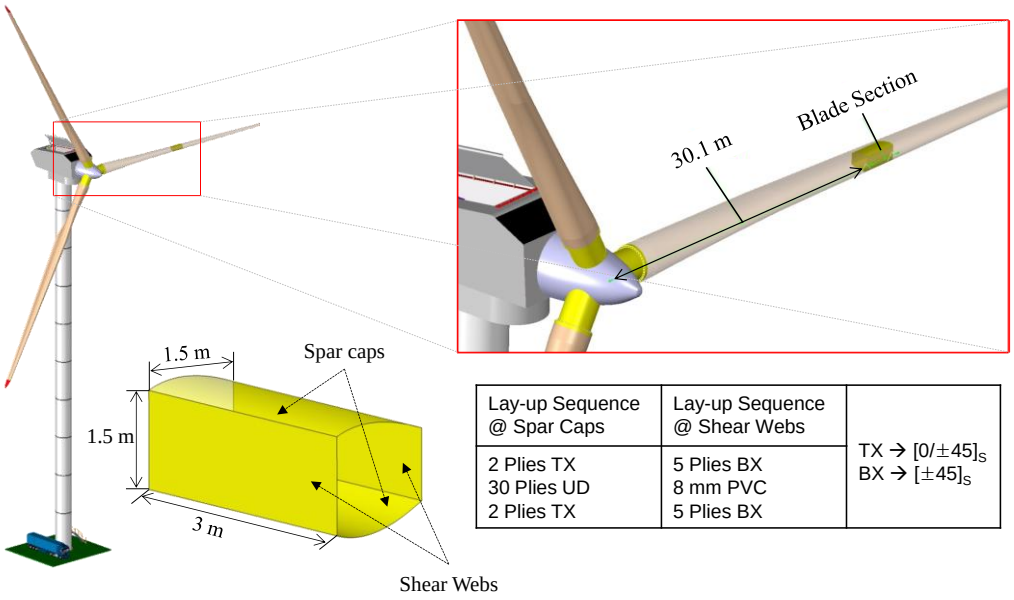

Figure 2.13: Blade Wing Box and typical stacking sequence

The finite element model of the wing box is shown in the Figure 2.14. This model was generated in the ANSYS Multiphysics module. The wing box was modelled using the SHELL181 ANSYS element type [31]. Two types of loads were applied: flapwise and edgewise loads. These loads were calculated using an aeroelastic computer-aided engineering tool for horizontal axis wind turbines, FAST [39]. Figure 2.14 shows the boundary conditions applied to the wing box section. The quasi-static analysis were performed according to IEC-DLC 6.1 load case [19]. In this load scenario, the rotor of a parked wind turbine is either in standstill or idling condition. For an annual average wind of 12m/s, the 50-year extreme wind is 70m/s which is the maximum of the 3s average. The left side of Figure 2.14 shows the FEM results under one set of input realizations and the maximum deflection calculated with this set of realizations was 195.1 mm.

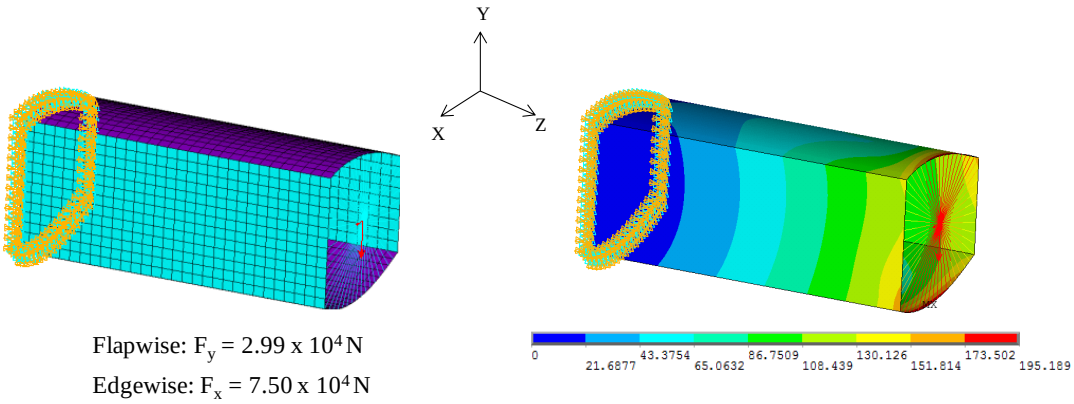

Flapwise: $F_y = 2.99 \times 10^4$ N

Edgewise: $F_x = 7.50 \times 10^4$ N

Figure 2.14: Boundary conditions & FEM modelling of wing box

Figure 2.15 illustrates the procedure used to calculate the probabilistic response of the wing box caused by uncertainties in the UD properties in a modular manner. These modules consist of: 1) selection of input design variables and description of their mean and standard deviation along with distribution type; 2) realization generation using efficient Latin Hypercube Sampling (LHS) approach; 3) user subroutine is used to calculate stiffness properties of UD with micro model and periodic boundary conditions (PBCs); 4) post processing of data performed once convergence criteria on mean values and standard deviations is met; 5) filters are applied with a threshold of 35% on the correlations given in Figure 2.11 to screen the unimportant design variables. This value is subjective at the moment but can be better decided using null hypothesis testing and will be incorporated in future work; 6) probabilistic finite element analysis were performed on the wing box with filtered correlation matrix and stochastic properties of UD. The results of step 6 were then post-processed to calculate the overall probabilistic response of the wing box.

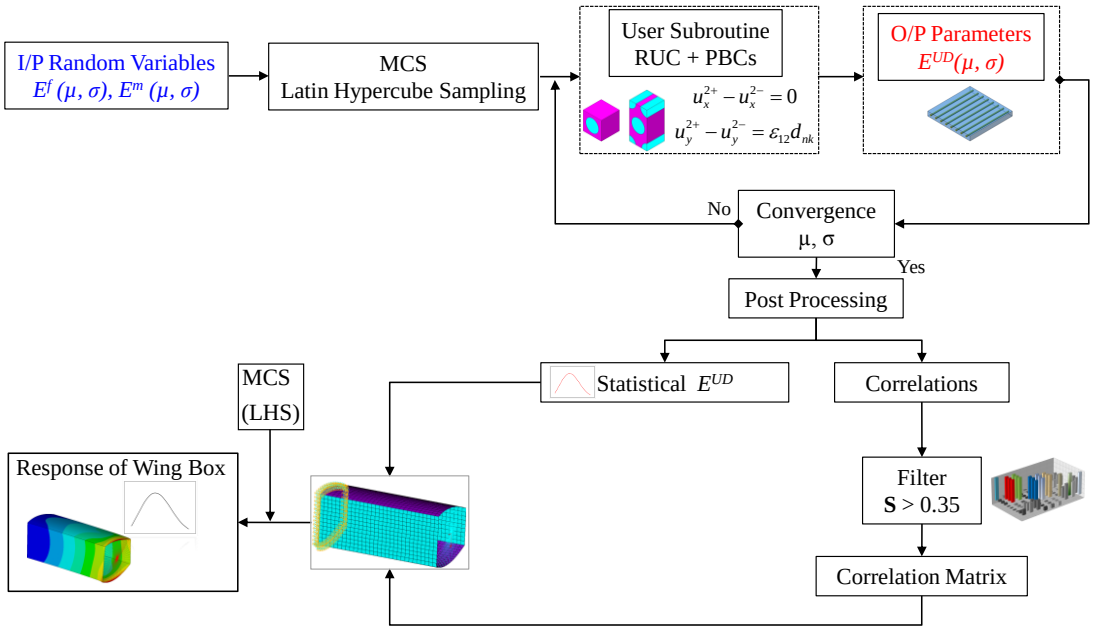

Figure 2.15: Flow chart for probabilistic deflection analysis of wing box

A summary of the stochastic response of the wing box deflection is shown in the Figure 2.16 with and without considering correlation and the fitted PDF on the right side of the Figure 2.16. The PDF fit to the data is a Weibull distribution, even though the distributions of inputs were Gaussian. The 2-parameter Weibull model used to fit the data.

$$f_X = \frac{\beta}{\alpha} exp\left(\frac{x}{\alpha}\right)^{\beta-1} e^{-(x/\alpha)^{\beta}} \qquad \text{Equation 2.9}$$

One of the Weibull model parameter α controls the scale and the second one β controls shape. Several methods have been devised to estimate the parameters that will fit the particular data distribution. Some available parameter estimation methods include probability plotting, rank regression, and maximum likelihood estimation (MLE) [40, 41]. The MLE approach in MATLAB was used to estimate the Weibull parameters. The Weibull parameters are given in the Figure 2.16. The MCS applied in this work used 500 realizations for probabilistic analysis of the blade section, without the use of a MCS convergence criterion. In order to have a fair comparison between results with and without including correlations, the same seed number was used to generate the random

realizations. As can be seen from the histogram on the left side and the fit PDF on the right side of Figure 2.16, the correlations have little effect on the maximum displacement of the wing box. However, inclusion of the correlation coefficients highlighted in detail the important factors on the deflection of wing box, as shown in Figure 2.17 which shows the sensitivities on output response parameter with a 95% significance level. Based on these results, ignoring correlations suppressed the sensitivities of input variables on the response parameters. The consideration of correlations helps to screen some of the unimportant factors such as $E_{22}, E_{33}, \nu_{12}, E_{13}$ with a threshold of 20%. These parameters can therefore be treated as deterministic in the future reliability analysis. Also, from the sensitivity analysis, one can conclude that E_{11} and G_{12} are the two key input variables that controls the deflection and these variables are related to the output deflection response in a strong negative manner, which means with the increase of these variables, the deflection response will be lower. Overall, these analyses illustrate the capability of the coupled approach for structural robust analysis by indicating the variables to change in order to achieve a given reliability level.

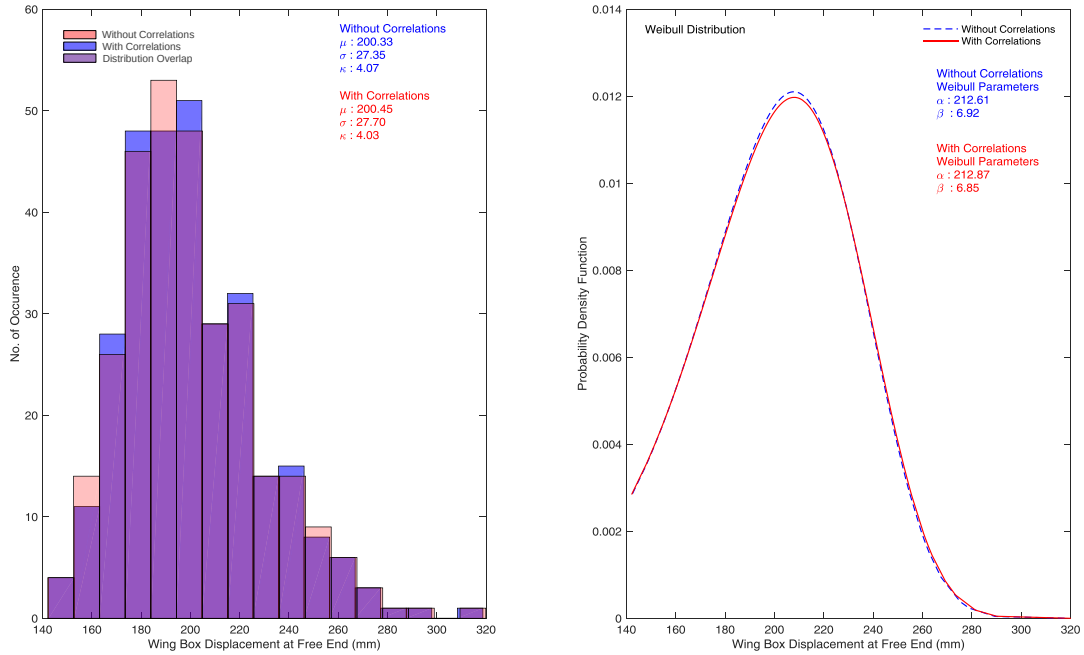

Figure 2.16: Wing box deflection with and without correlation

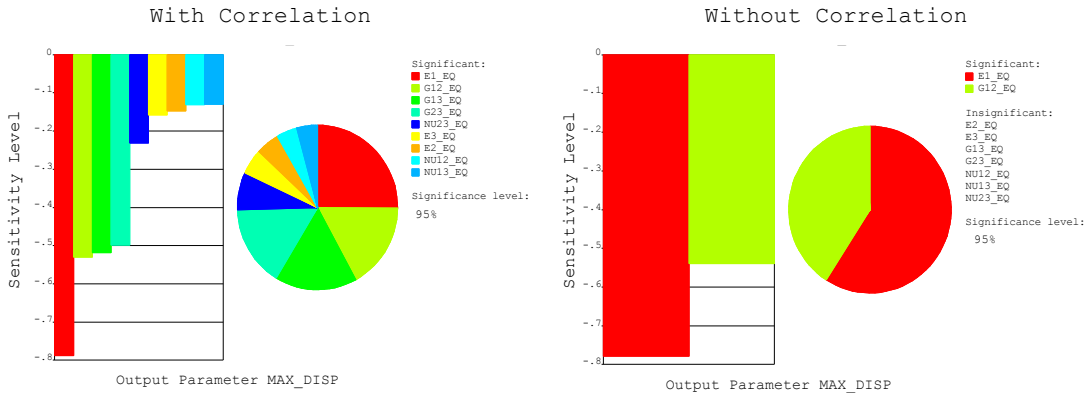

Figure 2.17: Wing box deflection sensitivities with and without correlation

2.6 Conclusion

This work aimed to develop a coupled approach for stiffness property prediction of composite materials used in wind turbine blades using advanced micromechanics and reliability-based methodologies. The homogenization approach was used with a unit cell to estimate composite material stiffness properties. The predicted results were compared with SROM and MROM along with the test data and found to be in good agreement with test data and MROM. The work was then extended to perform the probabilistic analysis with Monte Carlo Simulation to incorporate uncertainties in the constituent's properties. Latin Hypercube Sampling was employed to cover most of the input variable design space. From the probabilistic analysis, it was found that the equivalent properties of UD followed the Gaussian distribution and these properties were affected by variations in fiber and matrix properties. The Spearman Rank Order sensitivity analysis gave insights into important constituent's properties and found that the modulus of fiber and matrix has more influence on composite properties. In addition, correlations were calculated between UD properties which were then used in blade analysis. This probabilistic micromechanical approach for composite materials provides a useful tool for performing preliminary material design for finalizing material for structural application.

From a practical point of view, the method was then applied to a 5MW wind turbine blade structural analysis. A section of the blade was considered for demonstration purposes. The stochastic finite element analysis was performed in ANSYS/Multiphysics

using a user subroutine in order to simulate probabilistic response of wing box section. Two analyses were simulated with and without correlations between UD properties. There was no significant difference between PDFs but ignoring correlations suppressed the sensitivities of input variables on the response of wing box. Also, it was found that longitudinal modulus and in-plane shear modulus of the composite are the most critical material properties that influence deflection of the blade box. Besides this, sensitivity analysis screens out unimportant input variables which can be treated as deterministic in the further analysis. Furthermore, sensitivity analysis highlights the key material properties that most influence the response of the structure and this will eliminate/reduce unnecessary time consuming and expensive full testing campaign. In future work, the proposed probabilistic analysis can help determine constraints for use in structural optimization. The next step in this research is to expand micromechanics based probabilistic analysis to estimate strength and fatigue life of composites using Bayesian Inference approach.

Chapter 3 Probabilistic First Ply Failure Prediction of Composite Laminates using a multi-scale M-SaF and Bayesian Inference Approach

This paper is submitted for publication to the Journal of Composite Materials.

This chapter is a next step to analyze the composite structures using micromechanics and statistical models. The prime goal of this chapter is to focus on the strength prediction of composite materials using Bayesian inference statistical method. The scope is limited to first ply failure prediction of composites in this chapter.

ABSTRACT

This paper presents a probabilistic first ply failure (FPF) analysis of composite laminates using a high fidelity multi-scale approach called M-SaF (Micromechanics based approach for Static Failure). For this, square and hexagonal representative unit cells of composites are developed to calculate constituent stresses with the help of a bridging matrix between macro and micro stresses referred to as the stress amplification factor matrix. Separate failure criteria are applied to each of the constituents (fiber, matrix, and interface) in order to calculate the damage state. The successful implementation of M-SaF requires strength properties of the constituents which are the most difficult and expensive to characterize experimentally, limiting the use of M-SaF in the early design stages of a structure. This obstacle is overcome by integrating a Bayesian Inference approach with M-SaF. An academic sample problem of a cantilever beam is used to first demonstrate the calibration procedure. Bayesian Inference calibrates the M-SaF FPF model parameters as posterior distributions from the prior probability density functions drawn from lamina test data. The posterior statistics were then be used to calculate probabilistic FPF for a range of different laminates.

3.1 Introduction

Composite materials fail in a more obscure manner than metals under various mechanical and environmental loads such as thermal/ice and moisture effects. The complicated nature of composite failure arises from various factors such as delimitation, matrix cracking, fiber rupture, imperfections and voids from composite manufacturing process, de-bonding between interfaces, and interlaminar damage. These failure modes must be fully accounted for in the design and analysis phase of the structure. Therefore, a predictive methodology needs to capture most the relevant failure modes in composites.

The different approaches available for failure analysis of composite materials can broadly be divided into two main categories: macro level and micro level approaches [42]. In macro level approaches, a ply or lamina is treated as the main building block in which properties of the constituents, i.e. the fiber and the matrix, are smeared to generate homogeneous characteristics for the composite structural member. The work by Azzi and Tasi [1] focused on the analysis of thin plies and proposed an interaction-based formulation. Later, Tsai and Wu [43] provided interaction-based quadratic failure criterion for laminates using on-axis stresses at ply level as failure contributors. This failure criterion is by far the most widely used in industry currently due to its ease of use. The different failure modes, fibre or matrix failure, were identified specifically in the failure criterion given by Hashin and Rotem [9]. Hart-Smith used isotropic failure criteria to cover orthotropic cases [44]. He used a strain to characterize the failure rather than stress. Puck [45] used Mohr-Coulomb effective stresses to calculate fracture conditions. Puck proposed an analytical form for the case of plane stress that shows matrix failure to occur in compression. All these criteria are macroscopic formulations that work at a ply level but do not directly take into account the constituent's failure modes. Also, a large number of mechanical properties are required to use these models for structural analysis, properties that are unique to each layup/lamina. For example, even with the same base constituent materials, composites differing only in their fiber volume fractions require separate test campaigns to determine their respective properties. Furthermore, it is difficult to relate macro level failure theories to consider time dependent environmental loads such as those that induce creep effects.

As an alternative to macro level theories, there is another way to look at the problem, namely at the micro level. Micro level failure theories conduct the damage assessment at the micro level of the fibre and matrix constituents. The fibre and matrix properties are homogeneous within their own volume, and therefore no homogenization of properties is necessary. This eliminates the need for interaction parameters. Micro level analyses have been made of reinforced composites by employing representative unit cells. There are several typical packing arrangements available for unit cells to represent the true unordered composite fibers, including square, hexagonal, and diamond unit cells [46]. These are referred to called Unit Cells (UC), Representative Unit Cells (RUC), or Representative Volume Elements (RVE). A UC is defined as a representative sample of material on the micro structural level.

The micro level approach hasn't received as much attention in the past due to the unavailability of constituents' properties for analysis. Aboudi [47] proposed a micromechanics model, known as the "Method of Cells" (MOC). It is based on a unit cell with fibres having a square shape of a composite that are arranged in a periodic fashion in matrix. The damage algorithm used by Aboudi is catastrophic in nature, which means that the composite is predicted to have failed when either of the constituents is damaged. This is an overly simplistic and conservative model, especially considering matrix cracking found commonly in experiments but which is not necessarily catastrophic.

Advancements in computational capabilities has spurred the evolution of the MOC into the Generalized Method of Cells (GMC) [48]. In the GMC approach, the unit cell can be discretized into an arbitrary number of sub-cells; this helps to model complex unit cell shapes. The drawback with GMC is the lack of normal-shear coupling in the analysis. That means the application of macroscopic normal stress to GMC model produces only normal sub cell stresses even though the unit cell is orthotropic. This lack of coupling has major inferences for predicting the behavior of such materials. Another micromechanics-based approach developed by Kwon and Berner [49] consists of a periodic unit cell geometry the same as Aboudi [47]. Their failure criterion assumed the sudden death of the constituents once failure was detected. The work by González and LLorca [50] shows the micromechanical analyses on representative volume elements (RVE) using the elasto-plastic constitutive model. The multi-continuum theory (MCT) is a micromechanics

based theory proposed by Mayes and Hansen [51] in which phase averaging of stresses at the micro-level are applied to each constituent, i.e. the fiber, the matrix and the interface.

Huang [52] proposed a micromechanics-based bridging model to analyze the strength of composite laminates in World Wide Failure Exercise (WWFE) [53]. Notably, Huang also used different constituent properties than provided by WWFE organizer; these properties differ from as small as 4% to as large as 33%. The only reason to use different properties is to predict test data as closely as possible. Some researchers back-calculated constituent properties from lamina properties using a simple rule of mixture [3]. Others calibrated material properties in a deterministic fashion with the aid of genetic algorithm and gradient-based techniques [54, 55]. These calibrated values were the mean parameters and do not reflect any uncertainty due to the material's natural variability. Therefore, the predictive capability of these micro models hinges on the availability of constituents properties.

In contrast to deterministic approaches to analysis, the Bayesian theorem provides measures of conditional probability [56, 57]. Bayesian methods are presently becoming popular in science and engineering as a mean of probabilistic inference [58]. In these methods, the expert opinion or quantitative previous information is reflected in prior distributions which basically cover a wide range of possible values of the parameters to be estimated. These values are then updated using likelihood functions by utilizing test data to determine posterior distributions. This process can be iterated as additional test data becomes available, to refine the parameter estimates. It is also an advantageous approach as determinist analysis incorporating conservative safety factors can be replaced with probabilistic and robustness metrics to define acceptable performance.

There are two objectives of the work presented here. Firstly, a first ply failure (FPF) prediction method for laminated composites using a micromecahnics approach is developed, resulting in a Micromechanics for Static Failure (M-SaF) method. Secondly, a unified framework for the representation and quantification of uncertainty present in the fiber and matrix properties is developed through the use of a Bayesian Inference approach, in order to calculate probabilistic composite failure using M-SaF. The proposed framework is applied to glass fiber reinforced composite laminates. The remainder of the paper is organized as follows. In section 3.2, M-SaF is explained, in

particular an explanation of the constituent failure criterion. A comprehensive explanation of the Bayesian Inference technique is summarized in section 3.3. Section 3.4 details the computational implementation of M-SaF combined with the Bayesian Inference approach. Section 3.5 provides an illustrative example of a cantilever beam analysis to demonstrate the overall Bayesian approach. Results for a range of composite test cases are presented in section 3.6, followed by conclusions offered in section 3.7.

3.2 M-SaF Methodology

3.2.1 Representative Unit Cell (RUC) Models

Composite structures such as wind turbine blades are made up of polymer-based composite laminates, which are in turn made up of plies stacked in a prescribed sequence and orientation. These plies are made up of fibre and matrix constituent materials. All these levels are divided into two main groups, the macro and micro levels as shown in the Figure 3.1. Customarily, one moves right or left in these levels via localization and homogenization. A homogenization procedure provides the response of a structure given the properties of the structure's constituents. Conversely, the localization method provides the response of the constituents given the response of the structure.

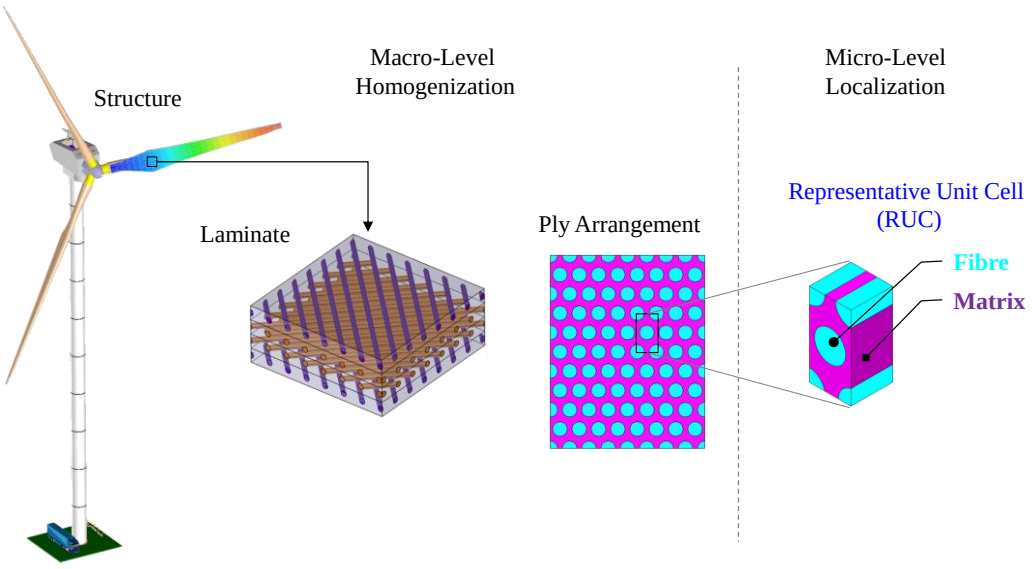

Figure 3.1: Macro and Micro levels of composite structure

The fibres are randomly arranged in the real unidirectional (UD) ply. The top of Figure 3.2 shows a cross section of a continuous UD ply [25]. There is no obvious regular pattern in which the fibres are arranged. A true representation of the fibre arrangement is shown in the middle of Figure 3.2. To aid computation, an idealized fibre arrangement is used, as shown in the bottom of the Figure 3.2. In this study, an idealized square (SQR) RUC model is used for probabilistic analysis as shown at the bottom of Figure 3.2. Although it is possible with suitable boundary conditions to represent a hexagonal arrangement with square unit cell. Other choices for the RUC, such as triangular RUC, could be exploring in the future. The modelling and mesh generation of the RUC were performed within the ANSYS Multiphysics finite element environment [31].

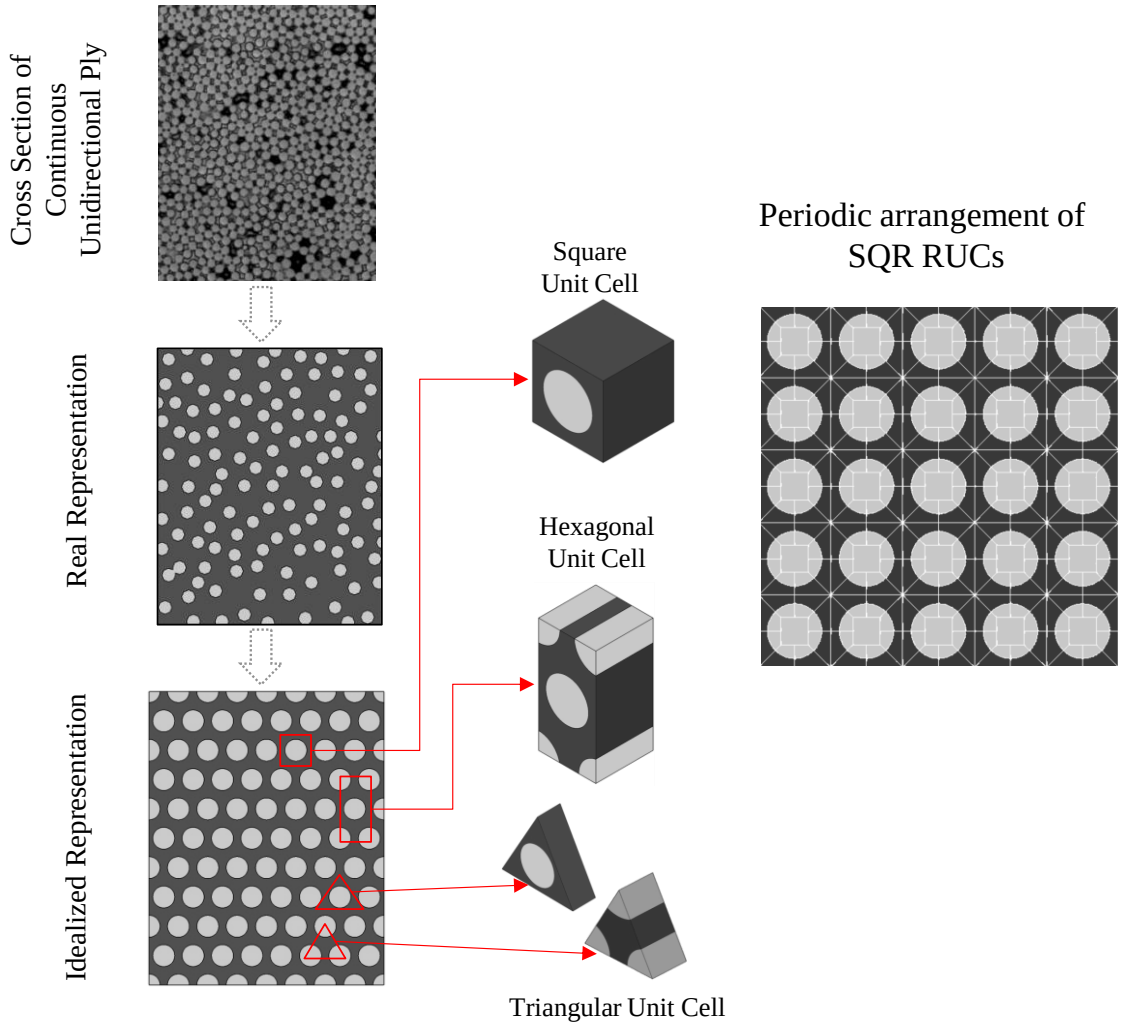

Figure 3.2: Representative unit cell models for unidirectional ply

3.2.2 Boundary Conditions on RUC

The homogenization approach acts as a bridge between the microscopic and macroscopic scale analyses. Homogenization consists of two steps: 1) calculating local stresses and strains in the constituents 2) using homogenization to obtain global stresses and strains for elastic property calculations. The successful implementation of homogenization assumes that the RUC has global repetition or periodicity. There are a variety of homogenization approaches to predict composite material behaviour [20, 27]. The homogenization technique given by Sun and Vaidya [27] is the most widely used because of its relatively low computational cost and can be implemented by applying proper boundary conditions (BCs) that are periodic. These periodic BCs give more practical results compared with other boundary conditions, such as uniform stress boundary conditions or kinematic uniform boundary conditions, and have been validated by various researchers [28, 29]. The periodic boundary conditions satisfy three statements: 1) the deformation should be the same on the opposite surface, 2) the stress vectors acting on opposite surfaces should be opposite in direction in order to have stress continuity across the boundaries of unit cell, and 3) there is no separation or overlap between the neighbouring RUCs. The displacement field boundary condition on the boundary Γ of domain Ω of the unit cell is given in Equation 3.1 as stated by Suquet [30]:

$$u_i(x_1, x_2, x_3) = \bar{\varepsilon}_{ik} x_k + u_i^*(x_1, x_2, x_3) \qquad \text{Equation 3.1}$$

where $\bar{\varepsilon}_{ik}$ is the global average strain of the periodic structure and x_k represents a linear distributed displacement field. u_i^* is a periodic part of the displacement from one RUC to another on the boundary surface and, unfortunately, it cannot be directly applied to the boundaries since it is unknown. For a RUC with parallel opposite surfaces (such as SQR and HEX) the displacements on a parallel opposite boundaries Γ^{j+} and Γ^{j-} are expressed in Equation 3.2 and Equation 3.3:

$$u_i^{j+} = \bar{\varepsilon}_{ik} x_k^{j+} + u_i^* \qquad \text{Equation 3.2}$$

$$u_i^{j-} = \bar{\varepsilon}_{ik} x_k^{j-} + u_i^* \qquad \text{Equation 3.3}$$

where u_i^* is the same on the two parallel boundaries due to periodicity. The difference between Equation 3.2 and Equation 3.3 is given as:

$$u_i^{j+} - u_i^{j-} = \bar{\varepsilon}_{ik}(x_k^{j+} - x_k^{j-}) = \bar{\varepsilon}_{ik}\Delta x_k^j \qquad \text{Equation 3.4}$$

where Δx_k^j is constant with the known $\bar{\varepsilon}_{ik}$ making the right hand side of the equation constant. These displacement constraint equations can be implemented in a finite element code like ANSYS [31]. Additional constraints must be enforced in order to avoid rigid body motion of the unit cell. For example, a displacement constraint applied at arbitrary point $(\hat{x}_1, \hat{x}_2, \hat{x}_3)$ of the RUC is:

$$u_i(\hat{x}_1, \hat{x}_2, \hat{x}_3) = 0 \qquad \text{Equation 3.5}$$

A composite ply is considered as a homogenous orthotropic material with effective stiffness properties in Classical Laminate Theory (CLT). These material properties are, in fact, 'average' material properties of the composite. In order to describe this homogeneity at a macro level, we need to take volumetric averages of the stress and strain tensor over the RUC as:

$$\bar{\sigma}_{ij} = \frac{1}{V}\int_V \sigma_{ij}(x, y, z)dV \qquad \text{Equation 3.6}$$

$$\bar{\varepsilon}_{ij} = \frac{1}{V}\int_V \varepsilon_{ij}(x, y, z)dV \qquad \text{Equation 3.7}$$

The concept behind Sun's approach [27] is that the strain energy stored in the homogenous unit cell is equal to that in a heterogeneous unit cell provided that perfect bonding occurs at the fiber-matrix interface under appropriate boundary displacements u_i that would produce uniform stress $\bar{\sigma}_{ij}$ and strain $\bar{\varepsilon}_{ij}$. The strain energy stored in the

homogenous material of volume V is given in Equation 3.8 and in the heterogeneous volume V in Equation 3.9.

$$U = \frac{1}{2}\int_V \bar{\sigma}_{ij}\bar{\varepsilon}_{ij}dV \qquad \text{Equation 3.8}$$

$$U' = \frac{1}{2}\int_V \sigma_{ij}\varepsilon_{ij}dV \qquad \text{Equation 3.9}$$

$$U' = \frac{1}{2}\int_V \sigma_{ij}(\varepsilon_{ij} - \bar{\varepsilon}_{ij} + \bar{\varepsilon}_{ij})dV \qquad \text{Equation 3.10}$$

$$U' = \frac{1}{2}\int_V \sigma_{ij}(\varepsilon_{ij} - \bar{\varepsilon}_{ij})dV + \frac{1}{2}\bar{\varepsilon}_{ij}\int_V \sigma_{ij}dV \qquad \text{Equation 3.11}$$

$$U' = \frac{1}{2}\int_V \sigma_{ij}\left(\frac{\partial u_i}{\partial x_i} - \frac{\partial \bar{u}_i}{\partial x_i}\right)dV + \frac{1}{2}\bar{\sigma}_{ij}\bar{\varepsilon}_{ij}\,V \qquad \text{Equation 3.12}$$

Taking the difference between the stored strain energies in the heterogeneous and homogenous volumes yields:

$$U' - U = \frac{1}{2}\int_V \sigma_{ij}\left(\frac{\partial u_i}{\partial x_i} - \frac{\partial \bar{u}_i}{\partial x_i}\right)dV \qquad \text{Equation 3.13}$$

With the use of the equilibrium condition $\partial\sigma_i/\partial x_i = 0$, Equation 3.13 can be written as:

$$U' - U = \frac{1}{2}\int_V \frac{\partial}{\partial x_i}\left[\sigma_{ij}(u_i - \bar{u}_i)\right]dV \qquad \text{Equation 3.14}$$

With the use of Gauss's theorem:

$$U' - U = \frac{1}{2}\int_S \sigma_{ij}(u_i - \bar{u}_i)n_j dV \qquad \text{Equation 3.15}$$

where S is the surface of the RUC over which this integration is applied, and n represents the outward unit normal vector. On the surface S: $u_i = \bar{u}_i$, leading to the final result that:

$$U = U' \qquad \text{Equation 3.16}$$

The average stress and strain quantities ensure equivalence between strain energy from the homogenous RUC with that from heterogeneous one. In order to determine the stiffness matrix, different displacement boundary conditions are applied on the RUC with appropriate periodicity as determined by Equation 3.1. The graphical explanation of these BCs is given in Figure 3.3.

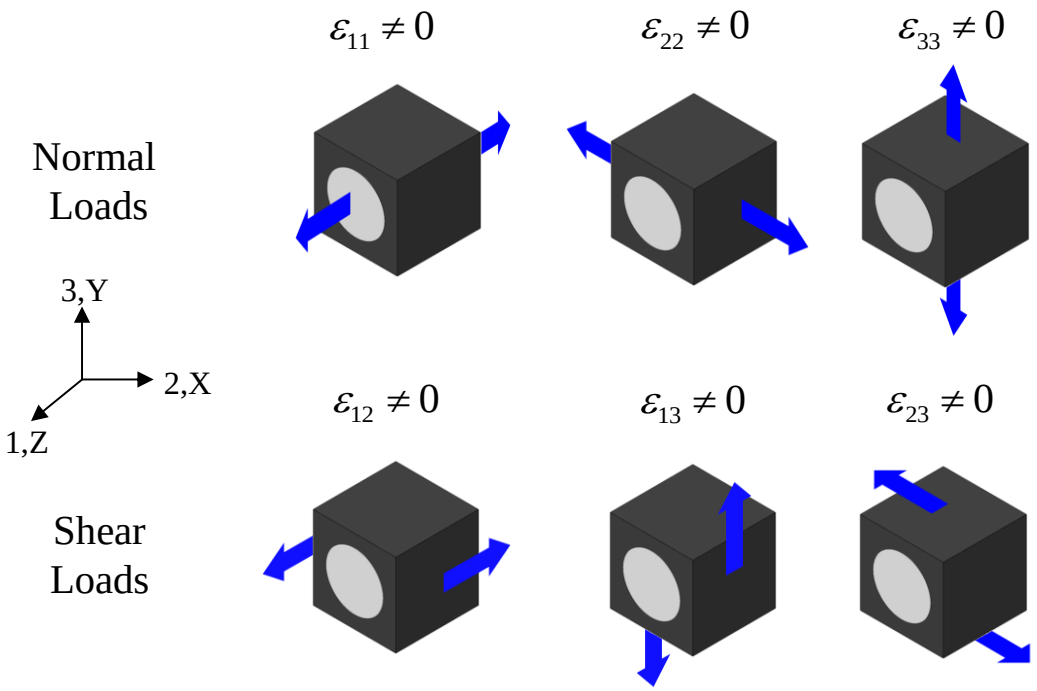

Figure 3.3: Boundary conditions for calculation of effective material properties of UD

The constraint equations have been applied in the FEM code ANSYS. To apply constraint equations on the nodes of opposite faces of the RUC, identical mesh schemes were applied on opposite surfaces of the RUC. The degree of freedom (DOF) coupling technique in ANSYS is utilized to apply periodic boundary conditions. The coupling and constraint equations relate the motion of one node to another [31]. For example, in the

case of $\varepsilon_{13} \neq 0$, the constrained equations applied are shown in Figure 3.4. The Von-Mises stress distribution on the RUC under the BCs is also given in Figure 3.4. Two important points should be noted from the RUC stress distribution. First, stresses at the same location on opposite sides are the same confirming the traction continuity condition. The second is that the boundary faces are no longer planes.

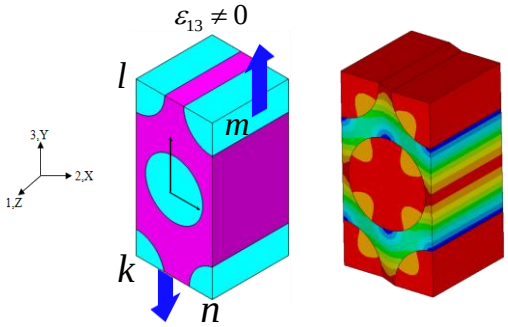

$$\begin{vmatrix} u_x^{1+} - u_x^{1-} = 0 & u_x^{2+} - u_x^{2-} = 0 & u_x^{3+} - u_x^{3-} = 0 \\ u_y^{1+} - u_y^{1-} = 0 & u_y^{2+} - u_y^{2-} = \varepsilon_{12} d_{nk} & u_y^{3+} - u_y^{3-} = 0 \\ u_z^{1+} - u_z^{1-} = 0 & u_z^{2+} - u_z^{2-} = 0 & u_z^{3+} - u_z^{3-} = \varepsilon_{12} d_{mn} \end{vmatrix}$$

Figure 3.4: Shear boundary conditions on RUC

3.2.3 Stress Amplification Factor (SAF)

The matrix and fiber materials possess different mechanical properties. For example, a glass or carbon fiber has a higher modulus of elasticity than the epoxy matrix. This stiffness disparity will be reflected in the dissimilar stresses in the two constituents under load. An illustration of this is shown in Figure 3.5 which shows stress distribution in SQR and HEX RUCs under an applied unit load $\bar{\sigma}_2 = 1$. The stress $\bar{\sigma}_2$ is referred to as a macro stress. It can be seen from the Figure 3.5 that the stresses within the RUCs are no longer unitary. The stress distribution in the RUC is called a micro stresses. From Figure 3.5, the maximum stress concentration, both in the SQR and HEX RUC, occurs at the fiber-matrix interface in the direction of the applied macro load, whereas the stress concentration is at its lowest value in the matrix region near interface which is perpendicular to the applied macro load.

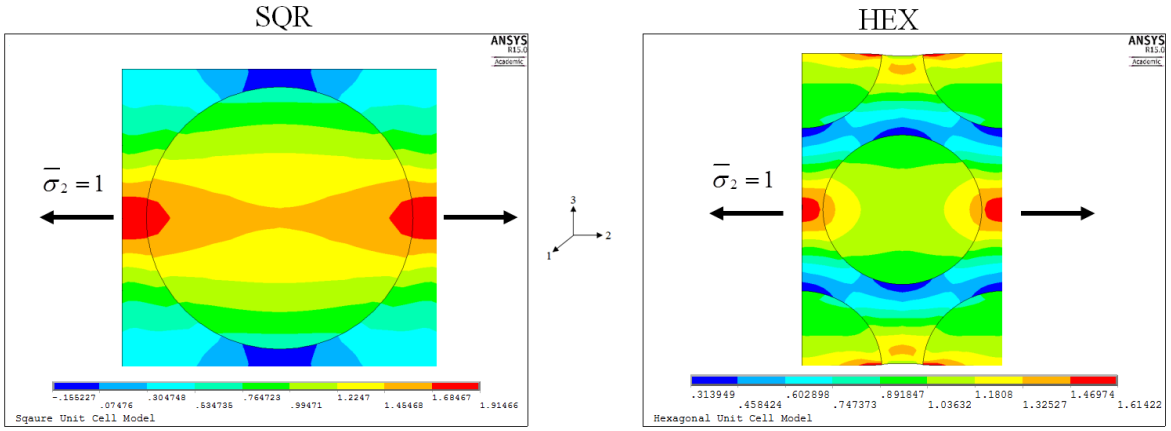

Figure 3.5: Stress (MPa) distribution in RUC subjected to a unit load

Below the elastic limit, the macro stresses under mechanical and thermal loads are related to the micro stresses via the following relationship [3, 6, 59, 60]:

$$\{\sigma\} = [A^M]\{\bar{\sigma}\} + [A^T]\Delta T \qquad \text{Equation 3.17}$$

where matrices $[A^M]$ and $[A^T]$ denote Stress Amplification Factors (SAFs) for macro mechanical stresses and for the macro temperature increment, respectively. Another name for these matrices found in literature is Stress Magnification Factor [3, 6]. Also, $\{\sigma\}$ and $\{\bar{\sigma}\}$ represent the tensor form of the micro and macro stresses respectively. This work considers only mechanical stresses, so the last term on the right hand side of Equation 3.17 is excluded; the superscript M denoting mechanical stresses is also omitted for the sake of simplicity. Based on Equation 3.17, the micro stresses in the fiber and matrix are related to the macro stresses as:

$$\{\sigma\}^f = [A]^f\{\bar{\sigma}\} \qquad \text{Equation 3.18}$$

where $[A]^f$ and $[A]^m$ represent SAF for fiber phase and matrix phase respectively under mechanical loading. These matrices are determined by the finite element method for a particular fiber volume fraction and specific fiber-matrix mixture. It is necessary to apply proper boundary conditions (BC) to obtain the SAF. These BC include: (i) nodes at the boundaries of RUC having the same displacements and (ii) the free faces must remain flat

as proposed by [6, 29]. The SAFs constitute a 6 x 6 matrix. For all stresses in a Cartesian coordinate system XYZ (or 123), Equation 3.18 can be expanded into Equation 3.19 [59, 60]. The superscript j represents either the fiber or the matrix phase.

$$\begin{bmatrix}\sigma_1\\ \sigma_2\\ \sigma_3\\ \sigma_4\\ \sigma_5\\ \sigma_6\end{bmatrix}^{(j)} = \begin{bmatrix}A_{11} & A_{12} & A_{13} & A_{14} & A_{15} & A_{16}\\ A_{22} & A_{21} & A_{23} & A_{24} & A_{25} & A_{26}\\ A_{31} & A_{32} & A_{33} & A_{34} & A_{35} & A_{36}\\ A_{41} & A_{42} & A_{43} & A_{44} & A_{45} & A_{46}\\ A_{51} & A_{52} & A_{53} & A_{54} & A_{55} & A_{56}\\ A_{61} & A_{62} & A_{63} & A_{64} & A_{65} & A_{66}\end{bmatrix}^{(j)} \begin{bmatrix}\bar{\sigma}_1\\ \bar{\sigma}_2\\ \bar{\sigma}_3\\ \bar{\sigma}_4\\ \bar{\sigma}_5\\ \bar{\sigma}_6\end{bmatrix} \qquad \text{Equation 3.19}$$

The elements of the SAF are determined by applying unit macro mechanical loads of vector $\{\bar{\sigma}\}$ to the model one at a time. For example, with the application of a unit mechanical load $\bar{\sigma}_2 = 1$, Equation 3.19 can be simplifies to Equation 3.20 as:

$$\begin{bmatrix}\sigma_1\\ \sigma_2\\ \sigma_3\\ \sigma_4\\ \sigma_5\\ \sigma_6\end{bmatrix}^{(j)} = \begin{bmatrix}A_{11} & A_{12} & A_{13} & A_{14} & A_{15} & A_{16}\\ A_{22} & A_{21} & A_{23} & A_{24} & A_{25} & A_{26}\\ A_{31} & A_{32} & A_{33} & A_{34} & A_{35} & A_{36}\\ A_{41} & A_{42} & A_{43} & A_{44} & A_{45} & A_{46}\\ A_{51} & A_{52} & A_{53} & A_{54} & A_{55} & A_{56}\\ A_{61} & A_{62} & A_{63} & A_{64} & A_{65} & A_{66}\end{bmatrix}^{(j)} \begin{bmatrix}0\\ 1\\ 0\\ 0\\ 0\\ 0\end{bmatrix} \qquad \text{Equation 3.20}$$

Solving a linear system of equations leads to:

$$\begin{bmatrix}\sigma_1\\ \sigma_2\\ \sigma_3\\ \sigma_4\\ \sigma_5\\ \sigma_6\end{bmatrix}^{(j)} = \begin{bmatrix}A_{12}\\ A_{22}\\ A_{32}\\ A_{42}\\ A_{52}\\ A_{62}\end{bmatrix}^{(j)} \qquad \text{Equation 3.21}$$

The elements of the SAF in Equation 3.21 are the micro stresses as a result of macro stress $\bar{\sigma}_2 = 1$. The stress contours (in N/m^2) of A_{12}, A_{22}, and A_{42} of Equation 3.21 for SQR and HEX RUC with 60% fiber volume fraction are presented in Figure 3.6.

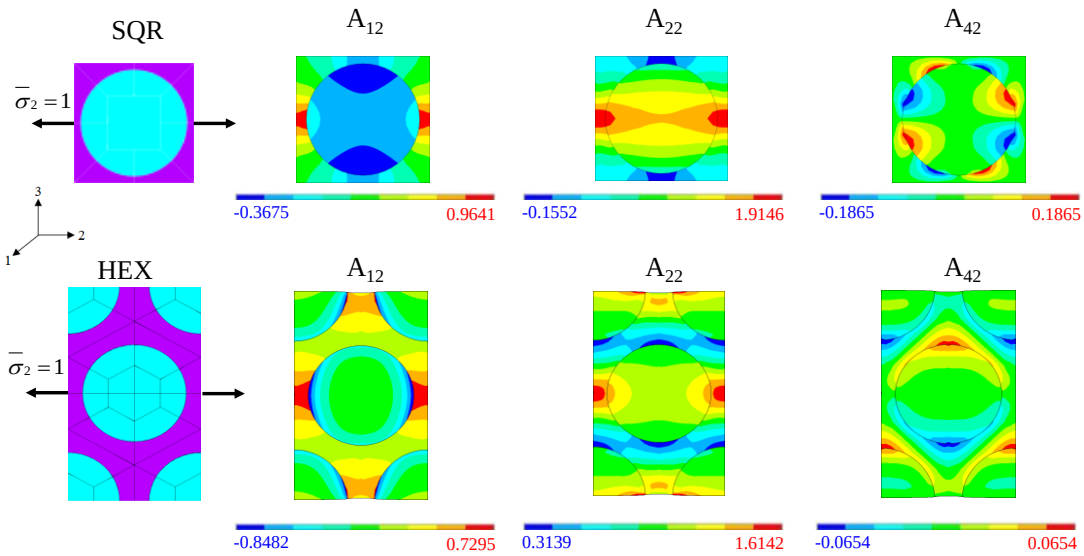

Figure 3.6: SAF distribution in RUC under macro stress

As can be seen from Figure 3.6, the the micro stress distributions vary over the RUCs. It is not feasible computationally to consider SAF at all points in the RUC; it is therefore necessary to define specific positions in the fiber, matrix and fiber-matrix interface in each RUC at which to compute SAF values [59, 60, 61]. The SAFs are extracted within one unit cell, i.e. RUC, inside the multi cell array. The chosen locations for the SAF computations in a single SQR and single HEX RUC is shown in Figure 3.7. Twenty one points in each of RUC are then chosen for the extraction of SAFs. Thirteen points are located at the fiber-matrix interface represented by a solid circle in Figure 3.7. Three points, represented by star in Figure 3.7, consider the fiber region. Three points are located at inter-fiber position and represented by solid squares in Figure 3.7. An inter-fiber location is defined as a place in the RUC where fibers are closest to each other. The two locations marked with solid triangles represent interstitial locations. The interstitial is a location where the fibers are farthest from each other or in other words it is a matrix dominant region. For given constituent properties of the composite and specific fiber volume fractions, the SAF at each of these locations in the RUC is separately calculated independent of the actual macro stresses in the structure. This means that for multiple macro loading cases, and indeed different layup schedules, the SAF must only be calculated once for a given fibre/matrix combination and given fibre volume fraction.

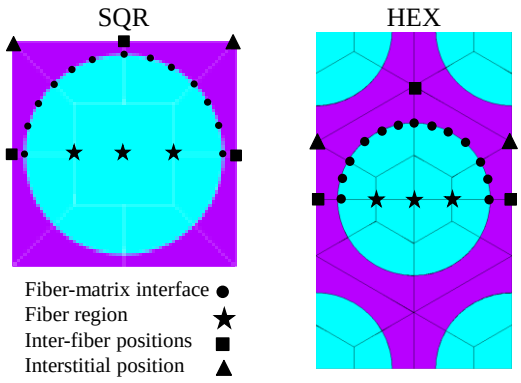

Figure 3.7: SAF locations in SQR and HEX RUC

Once the stress amplification factors are calculated for the RUC, the macro stresses computed in the aggregate structure are amplified with these SAFs to calculate actual micro stresses. Failure criteria are then applied and compared with the critical values as shown in Figure 3.8. In-plane loads in composite laminates, for example in the case of a wind turbine blade, are calculated using the finite element method under particular loading conditions. On-axis ply stresses are then calculated from in-plane loads, either using finite element method output directly or via Classical Laminate Theory (CLT) [2, 3, 43]. These on-axis ply stresses are then multiplied with SAFs to obtain micro stresses.

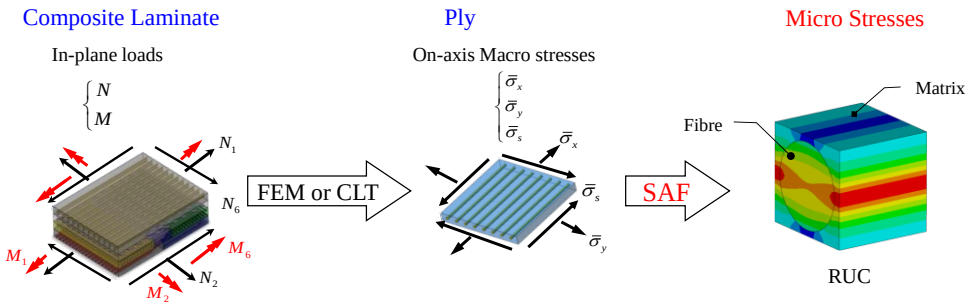

Figure 3.8: Micro stresses calculation procedure

3.2.4 Failure Criterion for the Composite Material Constituents

Three constituent regions exist in composite materials: the fiber, the matrix and the interface. All posses distinct material behaviours and behave differently under the same load [3], so it is rational to apply appropriate failure criteria to each constituent individually. In M-SaF (Micromechanics based Failure analysis under Static loading),

three different models are employed to treat each constituent of the ply differently. The inputs to each of the constituent failure models in M-SaF are the micro stresses which are based on the macro stresses in the structure and the constituent material parameters, mainly the strength properties of the constituents.

For the matrix material, a modified Von-Misses failure criterion proposed by Ragava et al [62] was used in this work. Even though the matrix behaves isotropically, it has different tensile and compressive strengths. The modified version of the Von-Misses criterion considers this aspect of the material. The original form of the modified Von-Misses failure criterion [62] is:

$$(\sigma_1^m - \sigma_2^m)^2 + (\sigma_2^m - \sigma_3^m)^2 + (\sigma_3^m - \sigma_1^m)^2 + 2(C^m - T^m)(\sigma_1^m + \sigma_2^m + \sigma_3^m) = 2C^m T^m \quad \text{Equation 3.22}$$

where T^m and C^m are tensile and compressive strengths of the matrix and superscript m is for matrix material. With $T^m = C^m$, Equation 3.22 becomes the standard Von-Misses criterion. Equation 3.22 can be expressed as a failure criteria:

$$\frac{\sigma_{VM}^{m2}}{C^m T^m} + \left(\frac{1}{C^m} - \frac{1}{T^m}\right) I_1^m \geq 1 \quad \text{Equation 3.23}$$

where σ_{VM}^m is the Von-Missses stress and $I_1^m = \sigma_1^m + \sigma_2^m + \sigma_3^m$ is first stress invariant calculated from the micro stress σ^m in the matrix region of RUC with following relations:

$$\sigma_{VM}^m = \sqrt{\frac{1}{2}[(\sigma_1^m - \sigma_2^m)^2 + (\sigma_2^m - \sigma_3^m)^2 + (\sigma_3^m - \sigma_1^m)^2 + 3(\sigma_4^{m2} + \sigma_5^{m2} + \sigma_6^{m2})]} \quad \text{Equation 3.24}$$

where $\sigma_1^m, \sigma_2^m, \sigma_3^m$ are the normal micro stresses and $\sigma_4^m, \sigma_5^m, \sigma_6^m$ are the shear micro stresses in the matrix. Once the equivalent stress reaches the tensile strength of the matrix, the criterion in Equation 3.23 takes the form in Equation 3.25 and this equivalent stress is called Stassi Equivalent stress model [63, 64, 65].

$$\sigma_{eq}^m = \frac{(\beta - 1) + \sqrt{(\beta - 1)^2 I_1^{m2} + 4\beta\sigma_{VM}^{m2}}}{2\beta} \quad \text{Equation 3.25}$$

where β is a ratio of compressive matrix strength C^m and tensile matrix strength T^m.

The Tsai-Wu quadratic criterion was used for fiber failure because it takes into account the orthotropic behavior of the fiber [3, 25, 43, 64]. It takes the following form in terms of fiber stresses and fiber strength parameters:

$$\sum_{j=1}^{6}\sum_{i=1}^{6} F_{ij}\sigma_i^f\,\sigma_j^f + \sum_{i=1}^{6} F_i\sigma_i^f \geq 1 \qquad \text{Equation 3.26}$$

where F_{ij} and F_i are coefficients that depends on the strengths of the fiber and the superscript f is for the fiber material. The expanded form of Equation 3.26 is:

$$F_{11}\sigma_1^{f2}+F_{22}\left(\sigma_2^{f2}+\sigma_3^{f2}+2\sigma_2^f\sigma_3^f\right)+2F_{12}\left(\sigma_1^f\sigma_3^f+\sigma_1^f\sigma_2^f\right)+F_{66}\left(\sigma_{31}^{f2}+\sigma 12f2+F44\sigma 23f2-\sigma 2f\sigma 3f+F2\sigma 2f+\sigma 3f+F1\sigma 1f\geq 1\right. \qquad \text{Equation 3.27}$$

where $\sigma_1^f, \sigma_2^f, \sigma_3^f$ are the micro stresses normal to the fiber and $\sigma_{12}^m, \sigma_{23}^m, \sigma_{31}^m$ are shear micro stresses in the fiber. The full definition of the coefficients of the quadratic criterion in Equation 3.26 or Equation 3.27 in terms of fiber strengths are given below:

$$F_{11}=\frac{1}{X^fX^{f\prime}};\quad F_{22}=\frac{1}{Y^fY^{f\prime}};\quad F_{12}=\frac{1}{2}\sqrt{\frac{1}{X^fX^{f\prime}Y^fY^{f\prime}}}$$
$$F_{66}=\frac{1}{S_6^{f2}};\quad F_{44}=\frac{1}{S_4^{f2}};\quad F_1=\frac{1}{X^f}-\frac{1}{X^{f\prime}};\quad F_2=\frac{1}{Y}-\frac{1}{Y^{f\prime}} \qquad \text{Equation 3.28}$$

where X^f and $X^{f\prime}$ are the longitudinal tension and compression strengths of the fiber. Y^f and $Y^{f\prime}$ are the transverse tension and compressive strengths of fiber. S_4^f and S_6^f are through-thickness shear and in-plane shear strengths of the fiber. Other researchers [60, 63, 66] used the Maximum Stress Criteria [25] for fibre failure for simplicity. This is expressed in Equation 3.29. Failure is deemed to have occurred once σ_1^f reaches either X^f in case of tensile loading or $X^{f\prime}$ in case of compression loading.

$$\sigma_{eq}^f \geq \left|\sigma_1^f\right| \qquad \text{Equation 3.29}$$

The failure criterion adopted for matrix and fiber assumed that a composite fails when either fiber or matrix fails. However, this can be to some extent subjective. Thus, the M-SaF is rather predicting initial failure. This hypothesis appears to be very restrictive, but the failure of a RUC is a representative of all multiple RUCs with the same stress states. Also, current failure criterion is homogeneous in each constituent, meaning that the entire ply damages upon failure and this might leads to under predictions of composite failure.

The interface between the matrix and fibre plays an important role in ply strengths, such as transverse tensile and shear strengths [67]. Perfect bonding between matrix & fiber is assumed here for typical fibres coated with appropriate sizing to match the employed matrix system. Thus the interface will not enter in the current analysis but could be added in future work.

3.3 Bayesian Inference Methodology for Uncertainty Quantification

3.3.1 Uncertainties

The widespread application of composite materials is accompanied by a widespread concern about quantifying the uncertainties prevailing in their properties. This uncertainty has always been a major concern in the use of composite materials in structural applications. The sources of uncertainty in the design and analysis of composite structures are broadly classified into two categories [68]. The first category is aleatoric uncertainty which is due to the presence of physical variation and inherent randomness in nature. For example, if the outcome of a physical test differs each time the experiment is run under controlled conditions, then this is an example of aleatory uncertainty. This type of uncertainty is irreducible. The second category is referred to as an epistemic uncertainty. This uncertainty is due to the lack of information regarding a particular quantity and/or a physical phenomenon. It arises from errors in measuring that particular quantity [69]. This form of uncertainty can be decreased (and sometimes eliminated) if new information is available. The nature of uncertainties and methods of dealing with them has been a subject of discussion by statisticians, engineers, scientists, and other specialists for extensive time period [70, 71, 72]. In engineering practice, safety factors have been used to practically but crudely handle uncertainty. In the past few decades however, increasing attention is being paid to methods for directly accounting for and

dealing with uncertainty in engineering applications to improve design through reducing the safety factors required for safe operation.

3.3.2 Uncertainty Quantification

In intricate engineered systems, full-scale testing may not be feasible for predicting the structural performance under real operational conditions. Therefore, mathematical models are often used to predict the full-scale structural response under those conditions as accurately as possible. For example, M-SaF helps to accelerate the product design cycle as it only requires constituent's material properties, i.e. stiffness and strength of the fiber and matrix. As aleatoric uncertainty cannot be avoided in the constituent material's properties, it must be quantified and calibrated to inform design decisions.

In general terms, the quantity y_{model} is simulated from a computational mathematical model M with controlled input variables x and unknown (or known to some extent) parameters θ. The basic outline of the model M-SaF in this terminology is given in Figure 3.9. The controlled inputs x to M-SaF are the on-axis stresses which comes directly from the FEM of a structure, RUC, and the fiber and matrix stiffness properties. The parameters θ in the M-SaF model are strength properties of the fiber and matrix phase.

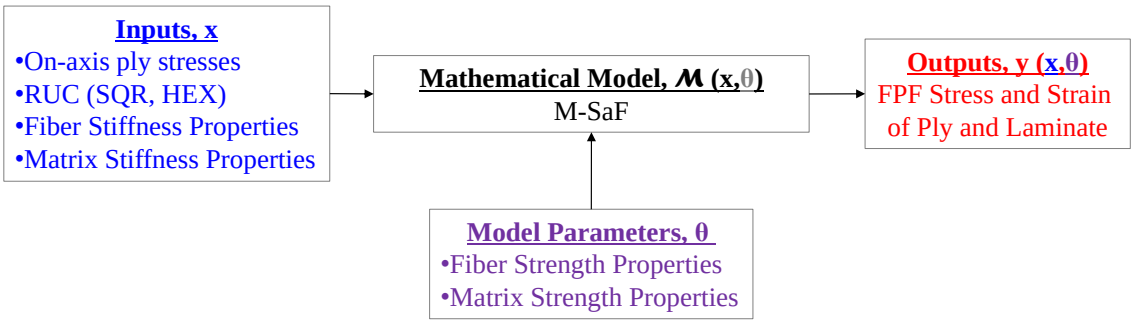

Figure 3.9: Sources of uncertainty in model prediction

There are some model parameters that are easily directly measurable, e.g. matrix tensile strength, however many are not, e.g. fiber strength properties. In general, the availability of measurements is influenced by the availability of the required instrumentation and/or standard testing guidelines. The computational mathematical

model M might be used in two different types of problem formulations: forward and inverse [73]. In the forward problem, the parameters are known and y_{model} must be computed. A simple Monte Carlo simulation (MCS) is an example of forward formulation. The parameters that cannot be measured directly need to be estimated through the inverse problem formulation. In this approach, the final output test data is given and one needs to estimate the parameters θ. The parameter estimation is sometimes referred to as model calibration or model updating by researchers [73].

One of the most basic of such methods is the least-squares technique [74]. In this method, the sum of the squares of the differences between the experimental measurements and the simulated responses of the system is minimized. The Bayesian Inference method (BIM) [75] is considered in this work to tackle the statistical inverse problem. The key objective of this work is to develop a unified framework for the representation and quantification of aleatoric uncertainty present in the fiber and matrix properties through the use of the Bayesian Inference approach. Figure 3.10 depicts the statistical forward and inverse problem. In the case of the statistical forward problem (figure (a) of Figure 3.10) the inputs are the random values of θ that goes to the function (or model) $q(\theta)$ that depends on θ. The typical output is represented by histogram. For the statistical inverse problem (figure (b) of Figure 3.10) the inputs are the distribution of parameters θ defined by the prior and a test data y_{test}. Note that the physical tests are performed without knowing the exact value of θ and are independent of any model of the physical process. The output is represented by tuned probability distribution function (PDF) for parameter θ.

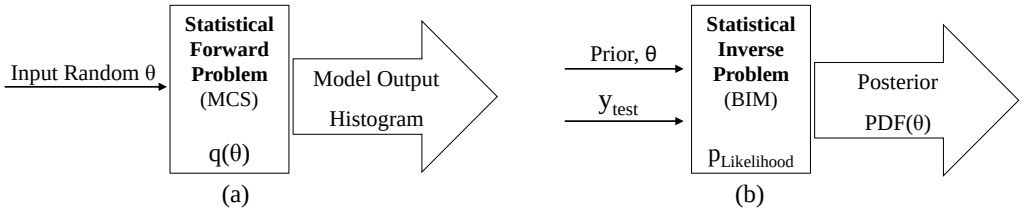

Figure 3.10: The representation of (a) statistical forward problem and (b) statistical inverse problem

3.3.3 Bayesian Inference Methodology

In this section, the Bayesian Inference methodology is explained with a view to calibrating M-SaF mechanical model parameters using available test data. Bayes' theorem, which lies at the heart of the Bayesian method, is presented in its general form, followed by a specific expressions for the likelihood and posterior functions used for calibrating the composite constituent properties. In the Bayesian method, the data are observed from a realized sample, and the parameters are unknown and described probabilistically. In contrast, in the frequentist approach the data are a sample from a random process in which the underlying parameters remain constant during the repeatable sampling process. Described another way, frequentist statistics estimate uncertainty in model outputs from inherently random processes, whereas the Bayesian approach provides estimates of the degree of certainty in an underlying model to explain observed data.

3.3.3.1 Bayes' Theorem

Bayes' theorem estimates the degree of belief in a hypothesis based on the evidence available by using the definition of conditional probability [56]:

$$P(X \cap Y) = P(X|Y)P(Y) = P(Y|X)P(X) \qquad \text{Equation 3.30}$$

where the term $P(X|Y)$ is a conditional probability of X when Y is given. The conditional probability in Equation 3.30 can be re-written as:

$$P(X|Y) = \frac{P(Y|X)P(X)}{P(Y)} \qquad \text{Equation 3.31}$$

In the scenario of estimating the M-SaF model parameters, the conditional probability of parameter θ when a set of test is available can be written as:

$$p(\theta|y_{test}) = \frac{p(y_{test}|\theta)p(\theta)}{\int p(y_{test}|\theta)p(\theta)d\theta} \qquad \text{Equation 3.32}$$

Bayes' theorem in Equation 3.32 is written as a probability density function (PDF) rather than a probability distribution, as this is a more appropriate form for use in the present work. The Bayesian updating formula in Equation 3.32 can be re-written as:

$$f(\theta|y_{test}) = \frac{L(\theta)f(\theta)}{f(y_{test})} \qquad \text{Equation 3.33}$$

where $f(\theta|y_{test})$ is the posterior PDF representing the updated knowledge about the model parameters θ, $f(\theta)$ is the prior distribution about the model parameters θ before the test data was observed (from an initial guess or previous iterations). $L(\theta) = f(y_{test}|\theta)$ represents the likelihood function which is the conditional probability of observing the given test data given the parameter θ. The term $f(y_{test}) = \int L(\theta)f(\theta)d\theta$ is a normalizing constant that makes Equation 3.33 a PDF and ensures that the area under the posterior PDF is equal to unity. In order to apply the Bayesian methodology, the prior distribution $f(\theta)$ and the likelihood function $L(\theta)$ must be specified. These terms are discussed in the following sections. To reiterate, the Bayesian method takes as its input a set of data y_{test} and a prior assumption about the distribution of parameters $f(\theta)$, and produces an updated estimate of $f(\theta)$, the posterior $f(\theta|y_{test})$. In this process, the likelihood function must be evaluated which involved model evaluations combined with use of the test data.

3.3.3.2 Mathematical Model

The computational mathematical model $M(x, \theta)$ represents the set of procedures to simulate values of $y_{model}(x, \theta)$. For example, in the case of M-SaF, the elements of y_{model} are first ply failure stress and first ply failure strain, as well as critical plies and associated failure modes. The predictive model with known input variables x and unknown parameters θ is written as:

$$y_{model}(x, \theta) = M(x, \theta) \qquad \text{Equation 3.34}$$

For M-SaF, the set of variables x are on-axis ply stresses, the RUC model constants, and the stiffness properties of the fiber and matrix materials. The parameters θ are a vector of strength properties of the fiber and matrix materials, i.e.

$[X^f, X^{f'}, Y^f, Y^{f'}, S_4^f, S_6^f, T^m, C^m]$. The superscript f is for fiber and m for matrix. As the mathematical model provides an approximate solution of physical phenomenon, the true value of the model output y_{true} accounting for various sources of uncertainty is given as:

$$y_{test} = y_{model}(x, \theta) + \epsilon_m \quad \text{Equation 3.35}$$

where ϵ_m denote the error which could arise from a measurement or numerical errors, sometimes referred to as the model discrepancy term [76, 77]. In order to predict the mean of y_{model}, the mean of ϵ_m, i.e. μ_{ϵ_m}, is set to zero for unbiased model analysis. This assumption assumes that the measurement process is well calibrated [78, 79] which should be true generally in material testing campaigns given efforts to reduce epistemic sources of error.

3.3.3.3 Likelihood Function Formulation

The first key element of the Bayesian method is to formulate the likelihood function of the observed test data as the conditional probability of the observations given the parameter values. The likelihood function computes the probability that the current θ estimate is representative of the true θ given a set of observed dataset y_{test}. The higher the likelihood, the more likely it is that the best estimates of the parameters have been obtained. Suppose that a random output variable has probability density function $f(y|\theta)$. Given an observed value y of y_{test}, the likelihood of θ for one test data point is defined by [75, 80]:

$$L(\theta) = f(y_{test}|\theta) \quad \text{Equation 3.36}$$

Thus we are considering the likelihood function density as a function of θ, for a fixed y function input. The independent and identical distribution (iid) of a random variable sample is defined so that it has the same probability distribution as other random samples and all samples are mutually independent. For example, if $X_1, X_2, \ldots$ designate the result of the 1st, 2nd, and so on toss of a coin (where X_i=1 means the i-th toss is heads and X_i=0 tails), you have that $X_1, X_2, \ldots$ are iid. They are independent since every time a coin is flipped, the previous result doesn't influence the current one. They are identically

distributed, since every time you flip a coin, the chances of getting head (or tail) are identical, no matter if it's the 1st or the 100th toss (probability distribution is identical over time).

In the case of multiple observations, $y = (y_1, \ldots, y_n)$ is a vector of observed values and unless otherwise stated it is assumed here that $y_1, \ldots, y_n$ are iid. In this case $(y_1, \ldots, y_n|\theta)$ is the product of the marginals. Equation 3.36 for multiple test samples then becomes:

$$L(\theta) = f\left(y_{test}^{(1)}, y_{test}^{(2)}, \ldots\ldots, y_{test}^{(n)}|\theta\right) = \prod_{i=1}^{n} f\left(y_{test}^{(i)}|\theta\right) \qquad \text{Equation 3.37}$$

where $y_{test}^{(i)}$ is i^{th} test data observation and n is the number of test data points available. For iid error ϵ_m which is typically Gaussian distributed with mean $\mu_{\epsilon_m} = 0$ and variance $\sigma_{\epsilon_m}^2$, $N(\mu_{\epsilon_m} = 0, \sigma_{\epsilon_m}^2)$, the likelihood function follows the form:

$$L(\theta) = f(y_{test}|\theta) = \prod_{i=1}^{n} f\left(\left\{y^{(i)}\right\}|\theta_i\right)$$
$$L(\theta) = f(y_{test}|\theta) = \prod_{i=1}^{n}\left[\frac{1}{\sqrt{2\pi\sigma_{\epsilon_m}^2}} exp\left\{-\frac{1}{2\sigma_{\epsilon_m}^2}\left(y_{test}^{(i)} - y_{model}^{(i)}(x, \theta_i)\right)^2\right\}\right] \qquad \text{Equation 3.38}$$

Rearranging, Equation 3.38 becomes:

$$L(\theta) = f(y_{test}|\theta) = \left(2\pi\sigma_{\epsilon_m}\right)^{-n/2} exp\left\{-\frac{1}{2\sigma_{\epsilon_m}^2}\sum_{i=1}^{n}\left(y_{test}^{(i)} - y_{model}^{(i)}(x, \theta_i)\right)^2\right\} \qquad \text{Equation 3.39}$$

where $y_{test}^{(i)}$ is a vector of test data and $y_{model}^{(i)}(x, \theta_i)$ is a vector of mathematical computational model results, computed in this work using M-SaF.

3.3.3.4 Prior Distribution of Parameters

The prior PDF $f(\theta)$ encodes the previous knowledge or user's judgment of the parameter values θ that is independent of the test data and that was determined before observing the test data. Many researchers have addressed the issue of specifying the

priors [81, 82, 83]. There are broadly two categories for the prior: conjugate priors and non-conjugate priors [84]. A prior is said to be conjugate to a class of likelihood functions if the resulting posterior distributions are in the same family as the prior distribution, otherwise, it is non-conjugate prior [80]. There are two typical prior distributions commonly used for material property parameters as shown in Figure 3.11. Both flat (uniform) as well as Gaussian priors will be used in this work. These are non-conjugate priors because posterior distribution dose not fall in the same class as of prior. If little or no information is available, it is appropriate to choose a non-informative prior which is uniform because it is providing the inferential information but gives answers that are only inspired by the shape of the likelihood function [85].

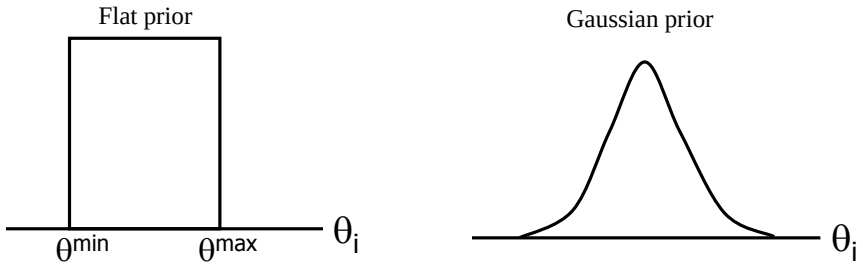

Figure 3.11: Typical priors for Bayesian analysis

3.3.3.5 Posterior of Parameters

The posterior PDF $f(\theta|y_{test})$ represents the updated state of knowledge, after observing the test data, about the parameter that was specified in the prior PDF. Following Bayes' theorem, the likelihood function, when combined with the prior distribution of the unknowns, leads to the posterior distribution. Bayes' theorem in Equation 3.33 can be re-written without the denominator constant $f(y_{test})$ as a proportionality in Equation 3.40. The constant $f(y_{test})$ is a function of the data y_{test} which are fixed for the problem at hand yielding the proportionality assumption.

$$f(\theta|y_{test}) \propto L(\theta)f(\theta) \qquad \text{Equation 3.40}$$

$$f(\theta|y_{test}) \propto \left(2\pi\sigma_{\epsilon_m}\right)^{-n/2} exp\left\{-\frac{1}{2\sigma_{\epsilon_m}^2}\sum_{i=1}^{n}\left(y_{test}^{(i)} - y_{model}^{(i)}(x,\theta_i)\right)^2\right\}.f(\theta_i) \qquad \text{Equation 3.41}$$

Equation 3.41 represents the joint posterior distribution of the parameters once the test data is observed. For a complex computational mathematical model such as M-SaF, analytical solution of the posterior distribution is not possible. Therefore, a numerical method to approximately calculate the posterior is employed. For this purpose, a Markov Chain Monte Carlo (MCMC) technique, specifically the Metropolis-Hastings Algorithm, is used to calibrate the parameters and quantify their uncertainty.

3.3.3.6 Joint Posterior Sampling by Random Walk Metropolis-Hastings Algorithm

One major difficulty in the practical application of the Bayesian approach is that it requires the evaluation of multi-dimensional integrals in the denominator of Equation 3.33:

$$f(y_{test}) = \int L(\theta) f(\theta) d\theta$$

$$f(y_{test}) = \int \left(2\pi\sigma_{\epsilon_m}\right)^{-n/2} exp\left\{-\frac{1}{2\sigma_{\epsilon_m}^2}\sum_{i=1}^{n}\left(y_{test}^{(i)} - y_{model}^{(i)}(x,\theta_i)\right)^2\right\} f(\theta_i) d\theta \qquad \text{Equation 3.42}$$

Generally, the estimation of the Bayesian integral cannot be done analytically. Therefore, stochastic simulation methods in which samples are generated from the joint posterior PDF $f(\theta|y_{test})$ are commonly used. The Bayesian integral may be computed by the Monte Carlo simulation technique [86] or by the importance sampling method [87]. These methods add computational cost and are very expensive in cases where for example sampling requires running FEM analyses. Fortunately, specific methods have been proposed recently for directly computing the posterior PDF $f(\theta|y_{test})$. These are so-called Markov Chain Monte Carlo (MCMC) methods [84]. The MCMC is more efficient than importance sampling as it needs relatively fewer samples to reconstruct a posterior probability density function. Also, MCMC methods don't require directly solving the Bayesian integral in Equation 3.33.

MCMC methods require sampling from the posterior distribution based on the construction of a Markov chain. A Markov chain is a series of randomly generated variables that possess the Markov property defined by the next state only depending on the present state and not on any historical states in the chain. The aim of MCMC methods is to sample the parameter from the posterior as accurately and efficiently as possible, by

directly converging the posterior estimate rather than computing individual terms in Bayes' formula. A broad review of MCMC methods can be found in [88]. Two well-known methods in the literature fall into this category. One is the Random Walk Metropolis-Hastings (M-H) (Metropolis et al. [89]; Hastings et al. [90]) MCMC sampling method; the other is the Gibbs MCMC sampling method [80, 84]. Gibbs sampling [84] is a special case of the Metropolis-Hastings algorithm, where all proposed random walk samples are drawn from a target distribution (the posterior PDF) and the acceptance probability is always unitary. The more general random walk Metropolis-Hastings algorithm draws samples from the posterior distribution of unknown parameters. It is the preferred choice here due to its characteristic of posing an acceptance criterion, Step # 7 below, which limits unnecessary y_{model} runs. Without acceptance criterion, as in Gibbs sampling, comparatively more y_{model} evaluations would be required adding computational cost. The Metropolis-Hastings algorithm ([89, 90]) works as follows:

Step # 1: Set the initial value of the parameter θ, $| \, p(\theta) \neq 0$

Step # 2: Calculate the posterior using Equation 3.41. This step involves running the mechanical model, M-SaF.

j = 2 to N (where N is the maximum number of iterations of the algorithm)

Step # 3-a: Randomly generate a sample parameter input (or realization) θ^* from the prior distribution

Step # 3-b: Calculate $p(\theta^*)$ from prior

Step # 4: Calculate the Posterior $f(\theta^*|y_{test})$ using Equation 3.41. This step involves running the mechanical model y_{model} based on θ^*.So, basically the Equation 3.41 provides an updated information about parameter based on the test data y_{test}.

Step # 5: Calculate the Acceptance Ratio (A_{ratio})

$$A_{ratio} = min\left\{1, \frac{f(\theta^*|y_{test})}{f(\theta^{(j-1)}|y_{test})}\right\} \qquad \text{Equation 3.43}$$

Step # 6: Generate a random value u from a uniform distribution with bounds 0 and 1 $U(0,1)$

Step # 7: Compare A_{ratio} with u

$$\begin{array}{ll} If & u \leq A_{ratio} \\ \text{then} & \theta^{j} = \theta^{*} \\ \text{else} & \theta^{j} = \theta^{j-1} \\ \text{end if} & \end{array} \qquad \text{Equation 3.44}$$

Step # 8: Increment *j* and go back to Step # 3. This loop continues until a sufficient number of samples are obtained so that the posterior distribution stops evolving, or in other words the Markov chain converges. The multiple runs n in Equation 3.41 depend on the number of the test data points available.

The Markov chain takes some iterations at the beginning of the MCMC run to converge to a stationary position. These iterations are called burn-in iterations and are usually discarded from generated samples in order to compose the final posterior PDF and to calculate statistical moments of the posterior. In the end, the posterior distribution is constructed using Kernel Density Estimation (KDE) [91].

3.4 Computational Implementation

3.4.1 Flow chart for First Ply Failure (FPF) analysis using M-SaF

The section explains the overall procedure to calculate first ply failure (FPF) analysis of composite materials using M-SaF in a sequential fashion as illustrated in Figure 3.12. First, global scale FEM analysis is performed on the complete composite structure, such as a wind turbine blade under a particular load condition. From the FEM results, the in-plane loads and stresses are calculated. Then, ply on-axis stresses are computed from the in-plane loads either using FEM or Classical Laminate Theory (CLT); these are the macro stresses. Stress amplification factors (SAF) are calculated from constituent material stiffness properties with chosen RUC and proper boundary conditions under unit loads, for each different fibre/matrix and fibre volume fraction used in the structure. Again note that these computations are independent of the number of load cases considered to compute the macro stresses. Macro stresses are then multiplied with SAFs to obtain the micro stresses. These micro stresses are different in each of the constituent materials. A failure index is determined in the fiber and matrix regions as per the appropriate failure criterion for each constituent. The critical failure index is then used to

compute first ply failure stress and strain. The critical failure index also identifies the critical ply in the laminate and the failure mode. The later information is very helpful during initial design stages and in optimization of the composite structure.

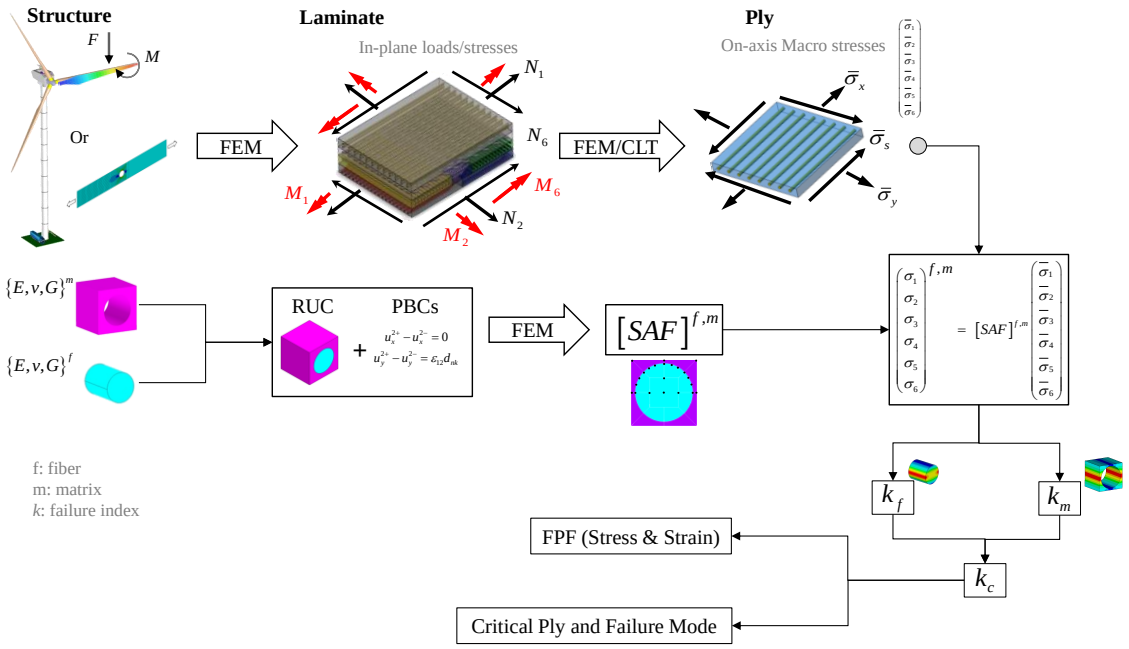

Figure 3.12: Flow chart for First Ply Failure (FPF) analysis using M-SaF

3.4.2 M-SaF with Bayesian Inference Approach

The workflow for M-SaF model parameter estimation using the Bayesian inference approach is shown in Figure 3.13. The inputs to and outputs from M-SaF are given in Figure 3.12. In order to calculate failure indices in the constituents, the strength properties of the fiber and matrix materials, i.e. $X^f, X^{f'}, Y^f, Y^{f'}, S_4^f, S_6^f, T^m, C^m$ are required. This comprises a vector of unknown parameters which has to be calibrated using the Bayesian inference approach. As all the elements of the calibration vector are physical properties, their values have to be positive due to the physical nature of the problem. The test data used for calibration in this work are taken from the OptiDAT data base [8] and the World Wide Failure Exercise (WWFE) [53]. The test data considered for calibration consist of ply or lamina level strengths in the form of either first ply failure load or a stress-strain curve. The model $y_{model}(x, \theta)$ is M-SaF with the x are the known inputs and θ are the unknown parameters. The Bayesian approach uses the test data y_{test} on the model outputs – here the first ply failure (FPF) load – to update the PDF for the

parameters. This is done by applying Bayes' theorem: $f(\theta|y_{test}) = L(\theta)f(\theta)/f(y_{test})$, where $f(\theta|y_{test})$ is the posterior distribution for θ given the y_{test}, $f(\theta)$ is the prior distribution about parameter θ, $L(\theta)$ is the likelihood of the test data given model output using parameters θ and $f(y_{test})$ is a normalization constant. The test data are only used in the calculation of the likelihood. The prior is then combined with the likelihood to provide posterior distribution. The posterior will be narrower and more sharply peaked than the prior indicating that parameter θ is calibrated and the parameter uncertainty is reduced. So, in this way Bayesian inference calibration reduces the uncertainty about the parameter values which are the strength properties of the constituents in this work.

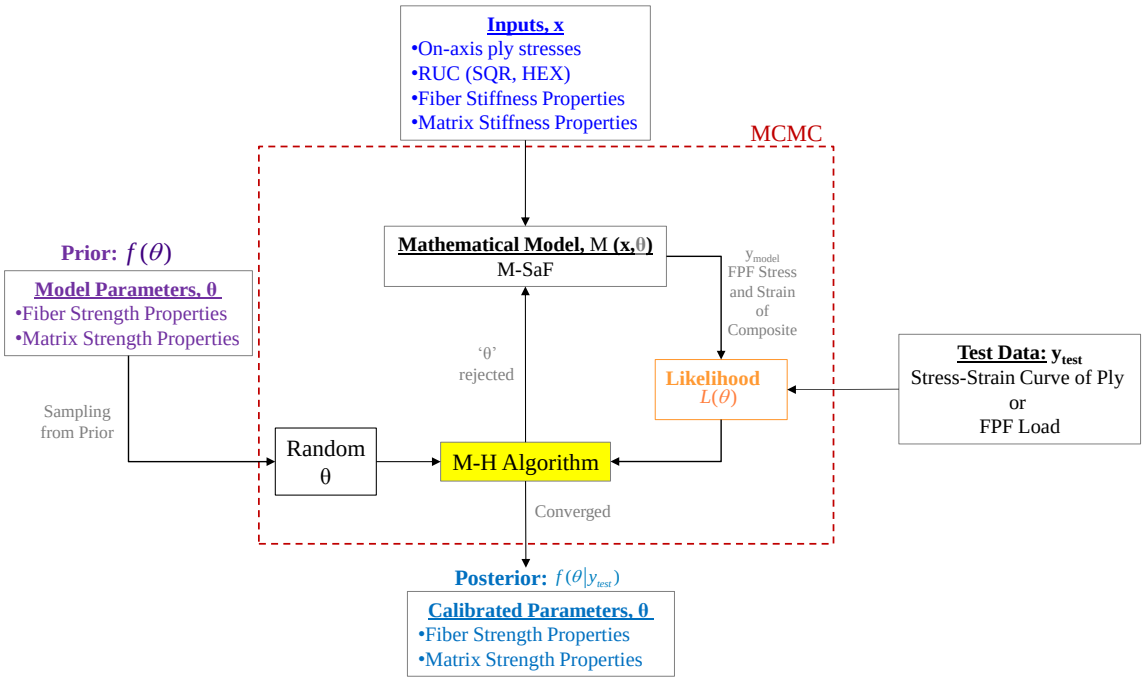

Figure 3.13: Workflow for model parameters estimation using Bayesian

3.4.3 Design and Analysis Application

With the quantified uncertainty in the parameters θ, the posterior distributions will then be used by designers to make probabilistic predictions in first ply failure (FPF) load for a variety of composite laminas and laminates using M-SaF model. The procedure is explained in Figure 3.14. At this stage for the model $M(x, \theta)$: the x are the known inputs and θ are the calibrated PDFs of parameters. The output is probabilistic FPF load and this

information will then be used to calculate the probabilistic response and optimization of the composite structures.

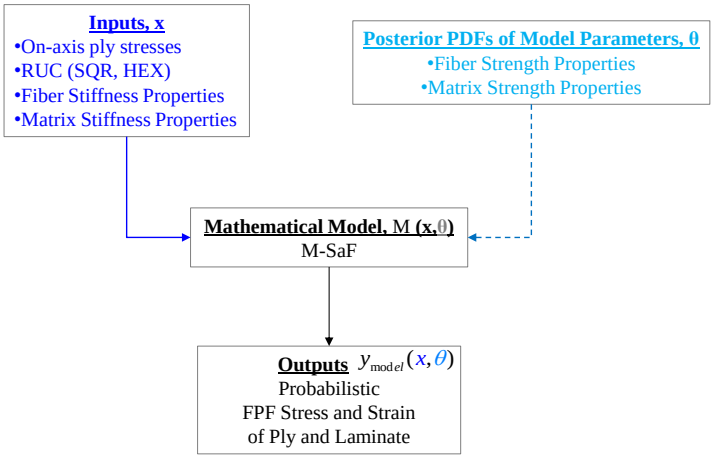

Figure 3.14: Flow chart for probabilistic analysis after Bayesian calibration

3.5 Illustrative Example: Cantilever Beam under Point Load

The basics of the Bayesian methodology framework is demonstrated using a set of cantilever beams $i = 1, 2, \dots, n$ that are subjected to a point load F_y at the free end. The Young's modulus E is constant along the beam span as it is made up of isotropic material, i.e. aluminum that exhibits an aleatory variability in E. The value of E is unknown and the aim is to calibrate it using randomly generated synthetic test data. The test data consists of deflection measurements of cantilever beams at the free end under load F_y. The beam lengths L_i, widths W_i, heights H_i, thicknesses T_i, and the applied load F_y are precisely known, with no epistemological uncertainty and are treated as deterministic values in the analysis. The beam dimensions are $L_i = 3000\,mm$, $W_i = H_i = 300\,mm$, $T_i = 5\,mm$, and $F_y = 500\,N$. For each beam i, the maximum displacement y_{model} at the free end is given by an analytical model $y_{model} = F_y L^3/3E_i$, where I is area moment of inertia, i.e. $I = f(W, H, T)$. This analytic model will also constitute the forward model for each individual beam i with unknown E_i. The schematic of the beam is shown in Figure 3.15 along with a description of mechanical model M inputs and outputs. M has an analytical form in this beam example problem. The flow

chart for calibration of model parameter E is given in Figure 3.16. The bar chart in the lower right of Figure 3.16 represents a typical histogram of the test data.

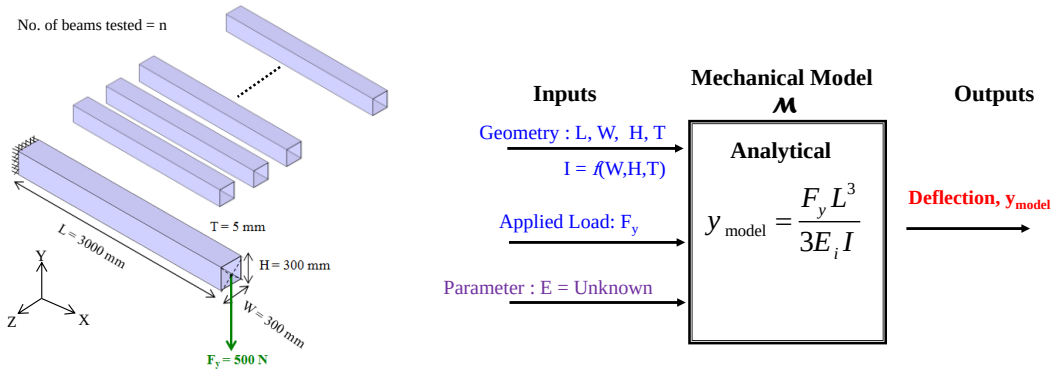

Figure 3.15: Cantilever beam specifications and mechanical model inputs and outputs

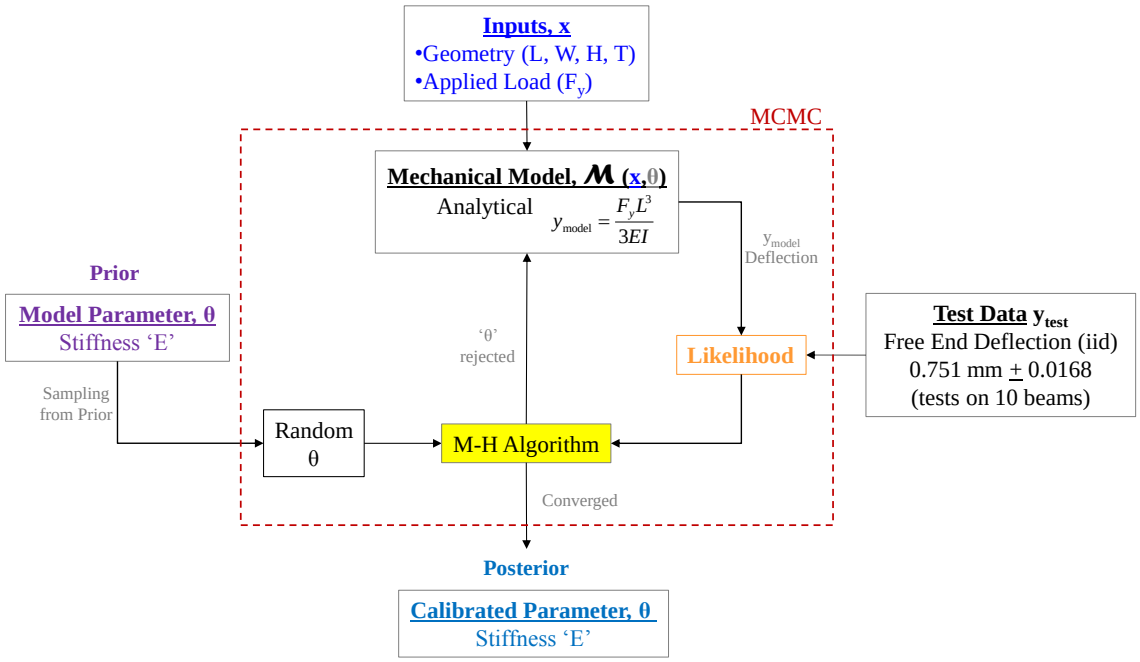

Figure 3.16: Flow chart for cantilever beam model parameter estimation using Bayesian inference

Two test cases are formulated to demonstrate the applicability of the Bayesian inference method. These are listed in Table 3.1. The "test data" is the deflection at the free end of the cantilever beam. The two different types of prior are considered: 1) uniform prior U(min, max); 2) normal prior N(mean, standard deviation). The priors used in each test case are also listed in the Table 3.1. The objective is not only to estimate E from prior but also to see the effect of different priors on the posterior estimates.

Table 3.1: Description of test cases of cantilever beam sample problem

Test Case	Description	Prior for E [GPa]
1	Parameter E is estimated from 100 synthetic pseudo test data generated from $E \sim N(70,5)$	U (50,85)
2		N (65,20)

The MCMC sample size was set to 10^4 after performing convergence studies on various sample sizes. The trace plot of parameter with burn-in period shown in Figure 3.17. This smoother plot of the raw sample traces is helpful in checking for convergence and can make it easier to identify and understand any non-stationarity as well as it provides the subjectively selection of the burn-in period length.

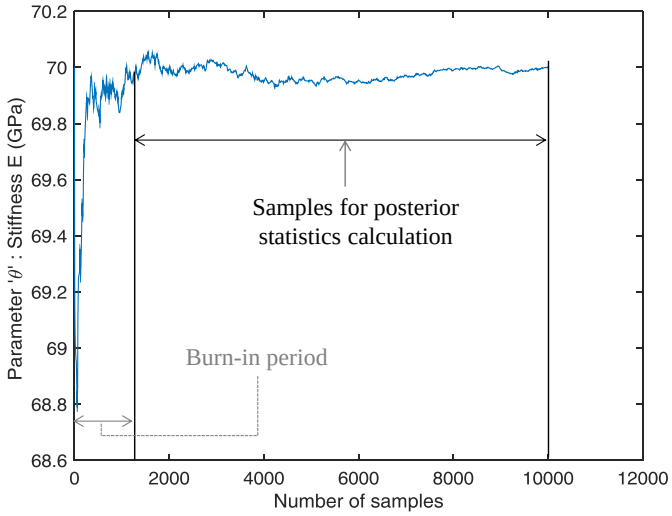

Figure 3.17: Convergence check of the parameter

The Markov chain was initiated at the mean value of the respective prior in each test case. This choice fulfills the required condition of the first step of Metropolis-Hastings random walk algorithm. For these test cases, the trace plots of the Markov chain parameter E along with a moving average of the parameter E is given on the left hand

side of Figure 3.18. The posterior of parameter E is shown on the right of Figure 3.18 along with the prior distribution and true normal distribution in the same figure. The true value is defined as the mean value of the generated samples of E from $N(70, 5)$ in each test case. The algorithm for this simple example performs quite well because the statistics of E that are used to produce the synthetic pseudo test data have been recovered as shown in Table 3.2. The percent difference is less the 2% for the mean. The percent difference in case of the standard deviations is 15%. The normal distribution prior provides better results in terms of mean values.

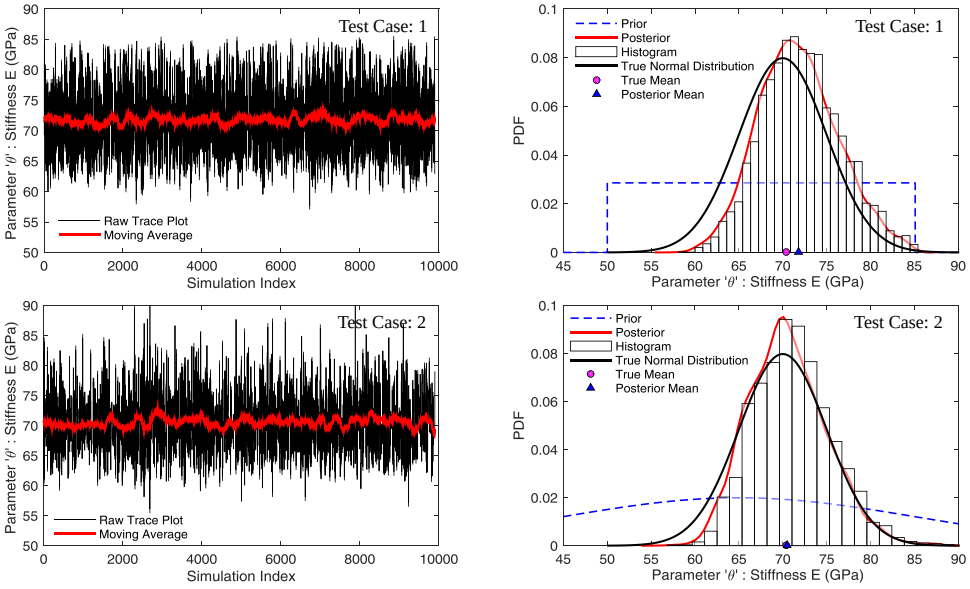

Figure 3.18: The posterior distribution of E in the cantilever beam example (Test case 1 and 2)

Table 3.2: Cantilever beam result comparisons for Test case 1 and 2

Parameter	Test Case 1	Test Case 2
True Mean [GPa]	70.42	70.42
Posterior Mean [GPa]	71.73	70.52
% Difference [-]	1.31	0.10
True Standard Deviation [GPa]	5.31	5.31
Posterior Standard Deviation [GPa]	4.55	4.47
% Difference [-]	15.25	15.82

There is no direct and easy answer to the choice for the range of priors. The analyses from the sensitivity study for various prior ranges shows that there is not much effect on the mean value but there is considerable difference on the standard deviations if the prior range is very narrower. This can be seen in Figure 3.19. The uniform prior was considered for this sensitivity analysis as this is appropriate choice for most of material properties if little or no information is available and, also, this provides the freedom to select any range of values.

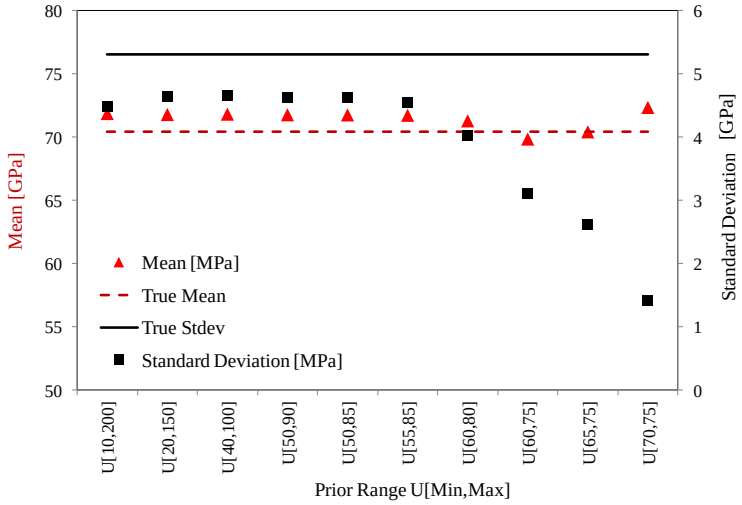

Figure 3.19: Sensitivity study for choice of the prior

3.6 Results and Discussion

3.6.1 Boundary Conditions for 3D Unit Cell

Finite element models of a single unit cell and a repeated array were defined in order to compare behaviours under identical loadings and boundary conditions. The 3-D structural solid element, SOLID45, is used for the FEM analysis. The material properties of Silenka E-Glass 1200 tex and MY750 Epoxy are given in Table 3.3 [53].

Table 3.3: Material properties of Fiber and Matrix

Properties	E-glass Fiber	Properties	MY750 Epoxy
E_{11}(GPa)	74.0	E_m (GPa)	3.35
E_{22}, E_{33}(GPa)	74.0	ν_m (-)	0.35

G_{12}, G_{13} (GPa)	30.8
ν_{12} (-)	0.2

The responses of the multi-cell array and the unit cell model were compared for different loading conditions with proper periodic boundary conditions. As an example, the comparison of the SQR multi-cell array and the SQR unit cell model under shear load is shown in Figure 3.20; the HEX multi-cell array and unit cell models under shear load is shown in Figure 3.21. From Figure 3.20 and Figure 3.21, it is clear that the stress distributions in the multi-cell model and the unit cell are identical. There is no boundary separation, which verifies the boundary conditions. The rest of the boundary conditions were verified in a similar manner.

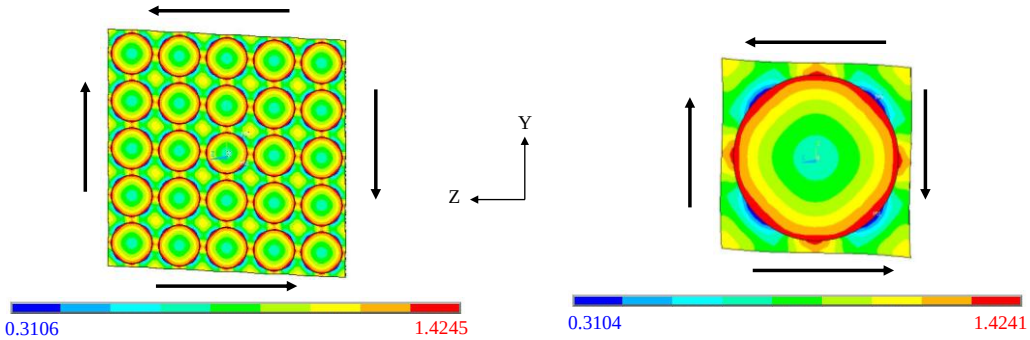

Figure 3.20: Comparison of shear stress (N/m^2) distribution in Multi-Cell & SQR unit cell model

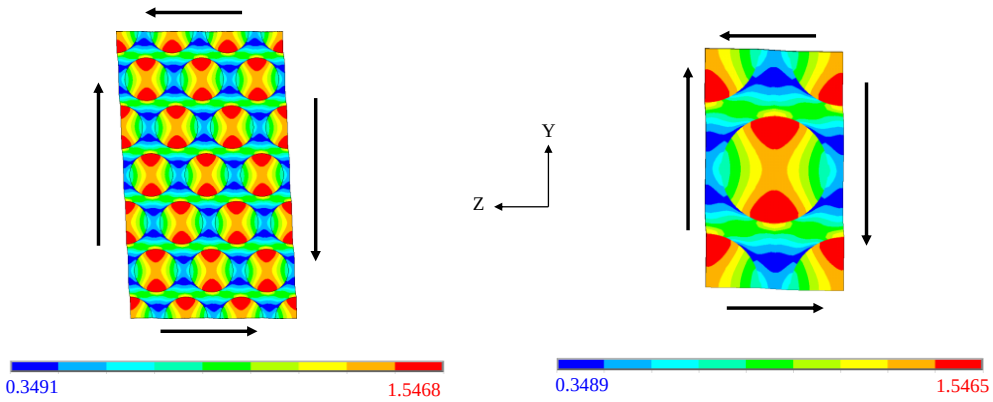

Figure 3.21: Comparison of shear stress (N/m^2) distribution in Multi-Cell & HEX unit cell model

3.6.2 FPF Index and Load of Ply under Tensile Load using Tsai-Wu and M-SaF

An attempt was made to compare the FPF index and load using Tsai-Wu failure criteria [43] and M-SaF methodology. The material system used is E glass fiber and

MY750 epoxy. The ply angle considered varies from 0^o to 90^o. A unit tensile load is applied at the ends. The predicted results from Tsai-Wu and M-SaF with SQR RUC are given in Figure 3.22. There is little deviation in the region where the influence of fiber is greater, but overall a good correlation between the predictions is shown.

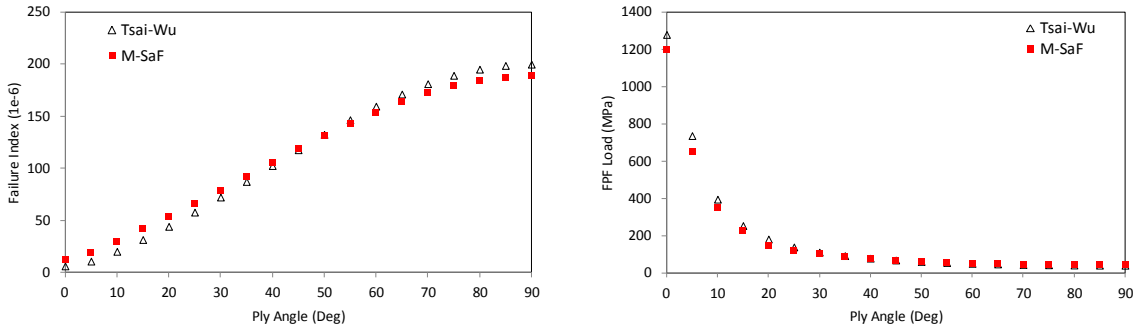

Figure 3.22: Prediction of FPF index and load of ply under tensile loading

3.6.3 Statistical Inverse Problem Results

The proposed Bayesian inference method with the M-SaF framework was employed to calibrate the model parameters and quantify the uncertainties of constituent strength material parameters. The test data used was from the OptiDaT data base [8] and the World Wide Failure Exercise (WWFE) [53]. The ply material used is constructed of the same type of e-glass/epoxy material system as given in Table 3.3. The ultimate longitudinal tensile strength, X, of a ply was used in calibrating the longitudinal tensile strength of the fiber X^f. It is believed that fibers are the main load bearing constituent in this load condition. The laminate UD1 was used for this purpose and there are 10 test data values available in OptiDaT data base. The ultimate transverse tensile strength Y of a ply was used in calibrating the tensile strength of the matrix T^m. It is believed that the matrix is the main load bearing constituent in this load condition. The details of the test data used for these parameters are given in Table 3.4. The prior distribution of X^f is taken as uniform U[1200, 2800] MPa and of T^m also used a uniform prior U[20, 150] MPa.

Table 3.4: Details of the test data used for $\boldsymbol{X^f}$ and $\boldsymbol{T^m}$

Calibration Parameter	Test data information						
	Specimen name	Test type	Test data reference	Specimen lay-up	Number of tests	Test data statistics: Mean [MPa]	Test data statistics: Standard Deviation [MPa]
X^f	UD1	Tension	Ref. [8]	$[0^o]_5$	10	839.88	37.18
T^m	UDT	Tension	Ref. [92]	$[90^o]_{2T}$	5	35.1	2.85

The distributions of these parameters were calibrated using MCMC sampling with the Metropolis-Hastings algorithm. A random value was sampled from the parameter prior distribution in each MCMC iteration. The likelihood function was then calculated from observing test data and the outputs from M-SaF. This step requires running finite element analyses on the RUC. MCMC simulations were carried out for five thousand samples from the prior distribution. The resulting calibrated parameters (X^f, T^m) are shown in Figure 3.23. The top row of Figure 3.23 shows results for X^f and the bottom row is for T^m. The trace plots of both parameters are given as well and appear to be well mixed. The posterior mean of X^f was used in order to calculate the T^m distribution. Similarly, the other parameters were calibrated using posterior mean of rest of the parameters. The first 500 samples were discarded as burn-in samples and were not considered in calculating the statistics of the parameters. In the second column of Figure 3.23, the posterior distribution as a parameter's histograms can be seen along with the prior distributions. The posterior histogram was then fitted with a smoothing curve using the kernel density estimate function in MATLAB. The kernel density estimate returns a probability density estimate for the generated posterior vector. The posterior mean value is plotted as a blue triangular. The circular red dot shows the fiber longitudinal tensile strength provided by WWFE [7]. The square black dot is the value of X^f used by Huang [52] in order to predict test data. As it can seen clearly that the posterior mean is closer to the WWFE value, however the WWFE just provides a single point value. Evidently the

value used by Huang was far from WWFE and the posterior mean. A similar pattern can be found for the parameter T^m. In this case, the posterior mean is closer to the WWFE provided value. The calibration accuracy could be further improved further by utilizing more test data. From the trace plots, the calibrated posterior parameters do exhibit good convergence.

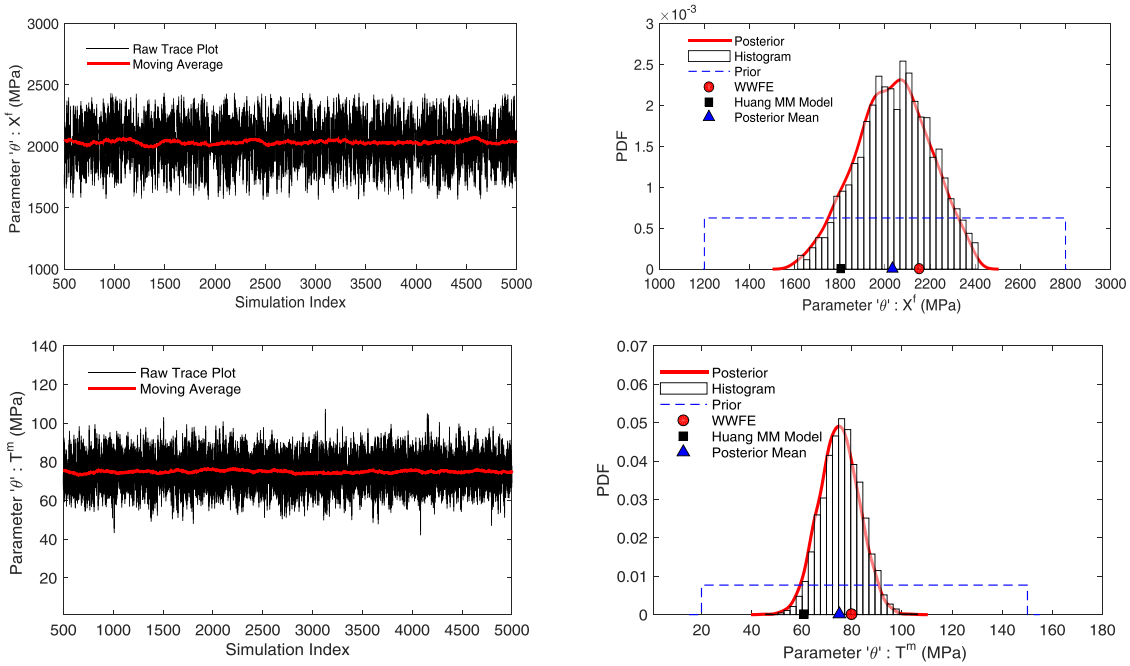

Figure 3.23: The posterior distribution of $\boldsymbol{X^f}$ and $\boldsymbol{T^m}$

In the high fidelity micromechanics and Bayesian coupled framework, it is difficult to assess how much the prior affects the posterior. Specifying the prior distribution is substantially harder when there is little to no information available. From the prior sensitivity analysis given in Figure 3.19, a wider range for the prior (e.g. U[10, 200]) provided posterior statistics that are close to the mid-range prior (e.g. U[55, 85]) and with the conservative prior (e.g. U[65, 75] or U[70, 75]), the posterior statistics deviate significantly, especially for the standard deviation compared with true values. Based on these analyses, priors were selected for constituent material properties. Mid-range priors were selected where there is some information is available in literature. For example, in the case of X^f and T^m priors, there is test data information available in WWFE. The same is true for C^m and $X^{f\prime}$, but in the case of Y^f and $Y^{f\prime}$ wider prior ranges were selected

because no information was available and these wider priors cover a minimum value as close to zero and maximum as high as it is realistic.

Similar procedures were implemented to calibrate the other M-SaF model parameters. The calibrated posteriors were computed for the following parameters: matrix compressive strength C^m; fiber longitudinal compressive strength $X^{f'}$; fiber transverse compressive strength $Y^{f'}$; fiber transverse tensile strength Y^f. For C^m and $Y^{f'}$, the test data is from the WWFE consists of UD ply with [90^o] layup under compressive load. As there is no test data available for the failure mode dominated by fibre transverse compressive failure, this leads the assumption of using this test data for $Y^{f'}$ calibration. The test data for a [90^o] ply under tensile load from WWFE was used for Y^f parameter calibration. A 20% standard deviation is used in case of test data where there are no statistics available. The details of the test data used for these parameters are given in Table 3.5.

Table 3.5: Details of the test data used for other parameters

Calibration Parameter	Test type	Test data reference	Specimen lay-up	Number of tests	Test data statistics	
					Mean [MPa]	Standard Deviation [MPa]
$C^m, Y^{f'}$	Compression	Ref. [53]	$[90^o]_T$	-	144.7	-
$X^{f'}$	Compression	Ref. [8]	$[0^o]_T$	10	800	60.67
Y^f	Tension	Ref. [53]	$[90^o]$	-	40	-

The prior and posterior estimates of all parameters are shown in Figure 3.24. Each parameter was calibrated one at a time in order to reduce the computational time. These distributions show the narrower band of parameter values from the prior distributions. No values of $Y^{f'}$ and Y^f were provided by WWFE, but, with the help of the Bayesian approach, these parameters could non-the-less be calibrated. Little information is available in the literature about the constituent strength properties, which motivated the use of a uniform prior distribution on the basis of perception about respective strength

properties. Five thousand simulations runs were carried out for obtaining posterior distribution of these parameters. Most of the calibrated parameters attained a well-defined peak in the posterior distribution, except C^m. This is a sign that the test data used was insufficient, a situation that could be improved by having additional test data. Overall, the Bayesian inference approach successfully quantified the uncertainties inherent in the constituent strength properties.

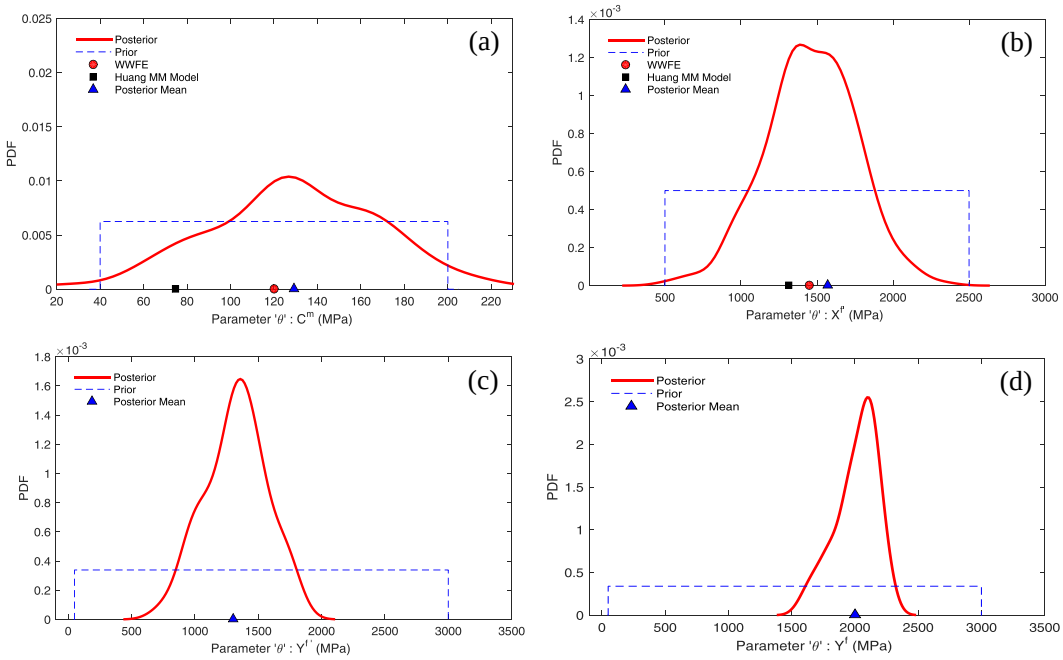

Figure 3.24: The posterior distribution of M-SaF model parameters: (a) matrix compressive strength; (b) fiber longitudinal compressive strength; (c) fiber transverse compressive strength; (d) fiber transverse tensile strength

3.6.4 Statistical Forward Problem Results

This section focuses on analyzing the probabilistic effect of constituent strength properties on the first ply failure (FPF) of composites within stochastic framework. As uncertainties are inherent in the composite materials which is a combined effect of material's natural behaviour and manufacturing process and, therefore, it is necessary for a deterministic M-SaF model to implement the stochastic methodology to account for these uncertainties. For this, all the calibrated parameters with their distributions in the previous section were used to predict the probabilistic FPF of a variety of laminates with

different fiber volume fractions using M-SaF model. The Monte Carlo Simulation (MCS) approach is one of the most general tools to perform stochastic analysis under uncertainty of input variables [32]. The MCS consists of three steps: 1) generation of realization corresponding to probability distribution function (PDF) – which is the posterior prediction from the previous section; 2) a finite element simulation evaluates the responses for each realization; 3) statistical analysis of the results yields valuable information concerning the sensitivities of the responses to the stochastic inputs. A normal distribution with 20% standard deviation of the posterior distribution along with posterior mean was used for the cases where the posterior was calculated with only one test data point. This assumption can be eliminated if the researchers report the detailed statistics of the test data in the literature. The test used for comparison purposes were taken from OptiDAT public database [8] and WWFE [7]. The lamina named "UD1" has five layers with fiber volume fraction is 55%, total laminate thickness is 4.4 mm and represented as $[0^o]_5$ in OptiDAT data set. Two cases are considered and the details for these are given in Table 3.6. These cases help to identify the effect of calibrated posterior PDFs on FPF predictions on UD1.

Table 3.6: Test cases for UD1 probabilistic analysis

Case Number	Case Description
UD1-a	Using posterior PDFs (calibrated) of all constituents
UD1-b	Using only X^f posterior PDF and 1st statistical moment of rest of the calibrated posteriors parameters ($X^{f'}, Y^f, Y^{f'}, T^m, C^m$)

In case UD1-a; the calibrated posterior PDFs of all constituents were considered and for the case UD1-b; the posterior PDF of calibrated X^f is considered only along with the 1st statistical moment of rest of the calibrated posteriors parameters ($X^{f'}, Y^f, Y^{f'}, T^m, C^m$). Figure 3.25 shows the probabilistic analysis of UD1 after post-processing in MATLAB. It is seen that the peak of the curve for the UD1-b case falls right on the test data mean value which is 840 MPa and the PDF of UD1-b case is very close to the OptiDAT test data uncertainty curve, which means by using only X^f posterior

distribution, the test data uncertainty will be recovered because this test data was used to calibrate X^f as expected. In the case of UD1-a, the output PDF has very large standard deviation because of the use of the posterior distributions of all parameters for which many had insufficient test data available to properly converge the posterior estimates for the individual parameters.

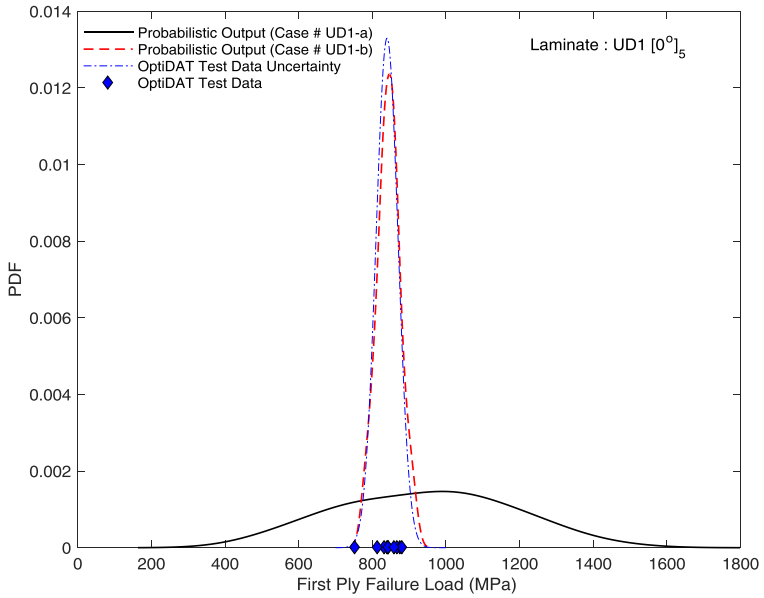

Figure 3.25: Probabilistic FPF of lamina UD1

Next we considered the shear laminate $[\pm 45^o]_S$ with fiber volume fraction of 50%. The source for test data in this case is OptiDAT report [93] and data provided by ETS (École de technologie supérieure, Québec Canada) [94]. The base material in both test data is e-glass/epoxy. In this case, the peak of the posterior distribution matches the test data, as shown in Figure 3.26.

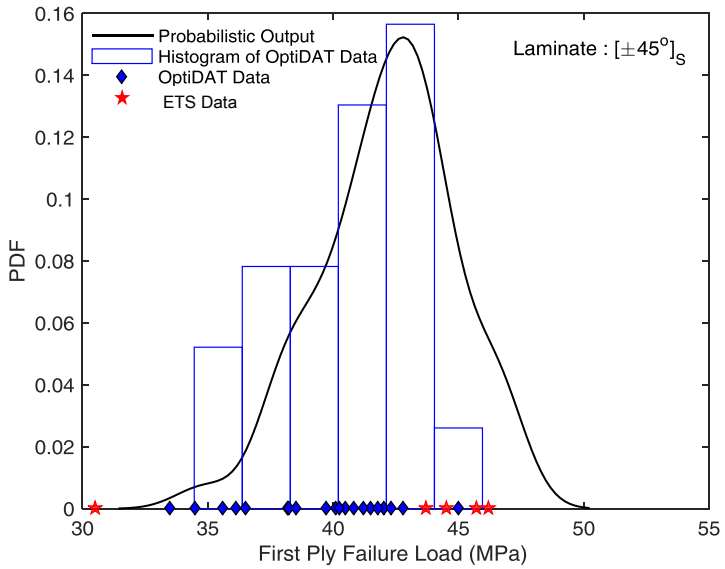

Figure 3.26: Probabilistic FPF of shear laminate

If the experimental mean of FPF from OptiDAT or ETS is assumed to be true, then how significantly different is this from numerically simulated mean using M-SaF? To answer this question, t-tests at 95% significance level are used to determine significant differences between mechanical testing and simulations [95]. The hypothesis to check is the mean from mechanical testing data significantly different from the numerical simulation data? The t-test is performed by calculating the T-value given by the following relation [96]:

t-test statistic model:

$$T = \frac{y_{sim} - y_{test}}{\sqrt{\frac{\sigma_{sim}^2}{n_{sim}} + \frac{\sigma_{test}^2}{n_{test}}}} \qquad \text{Equation 3.45}$$

where *sim* represents simulation and *test* is for test data. y is mean value, σ^2 is variance, and n is sample size. Table 3.7 lists these parameters.

Table 3.7: t-test model parameters

		n	Mean (MPa)	Standard Devotion (MPa)
Test Data	OptiDAT	23	40.88	3.05
	ETS	5	42.13	6.56
Simulation	Numerical Simulation	4500	42.15	6.08

Two assumptions have to be checked before applying t-test. The first: are these independent samples? Yes, since each sample is collected from different source. The second: are these a normal population? This is checked by plotting the data in normality plots. The intention of probability plots is to graphically assess whether the data either from physical tests or numerical simulation could come from a normal distribution. As the plots shown in Figure 3.27 are linear and this shows that the data is normal.

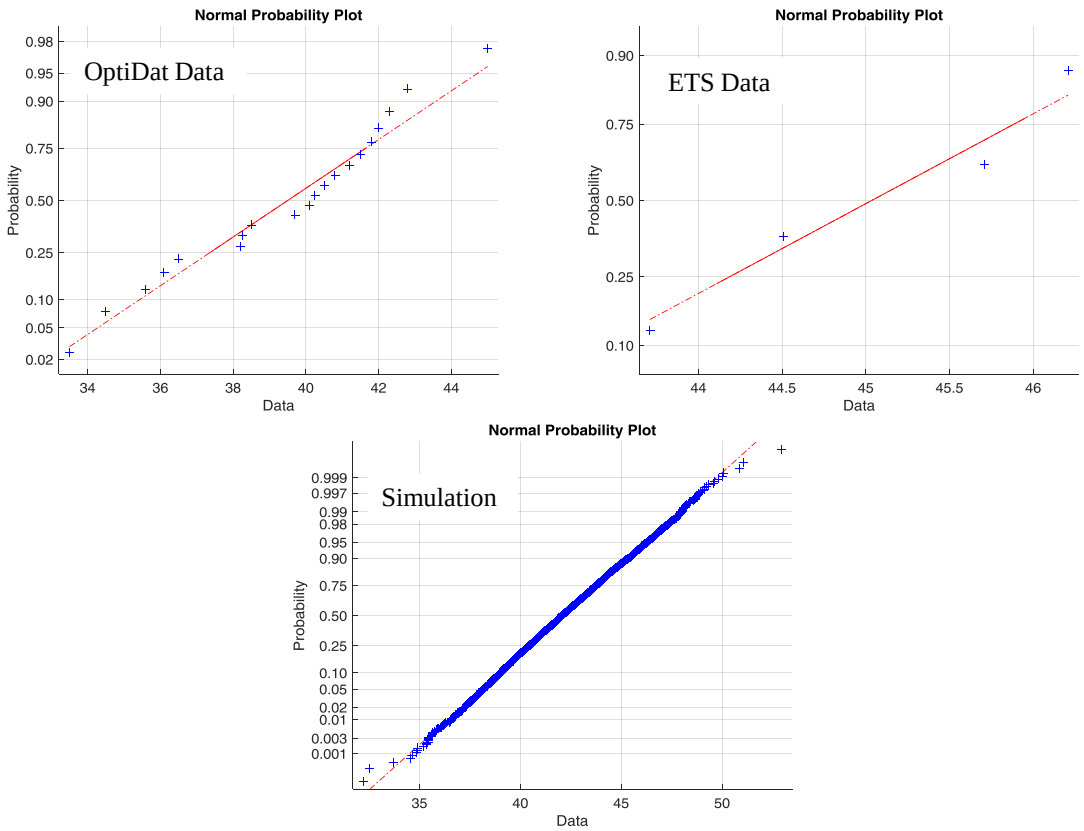

Figure 3.27: Normal probability plots of test data and simulations

The t-test results are shown in Table 3.8. Since $|T|$ is less than $t_{critical}$ in both cases, we conclude that the hypothesis is rejected, and there is statistically evidence to conclude that the numerical mean is not significantly different from the experimental mean.

Table 3.8: t-test statistic results for shear laminate

	OptiDAT	ETS
$\|T\|$	1.994	0.007
$t_{critical}$	2.0686	2.571

The probabilistic FPF predictions for angle ply laminates, i.e., $[+30^o/-60^o]_S$ and $[+15^o/-75^o]_S$ and cross-ply laminate $[0^o/90^o]_T$ are shown in Figure 3.28. The load acts in the longitudinal tensile direction. These consist of fibreglass and epoxy material with 60% fiber volume fraction. The test data was taken from [97] for angle ply laminates and from the WWFE in case of cross-ply laminate [7]. There is good correlation found in the case of cross-ply laminates between predictions and test data, although clearly more test data is required for a definite comparison, however this is not available in literature.

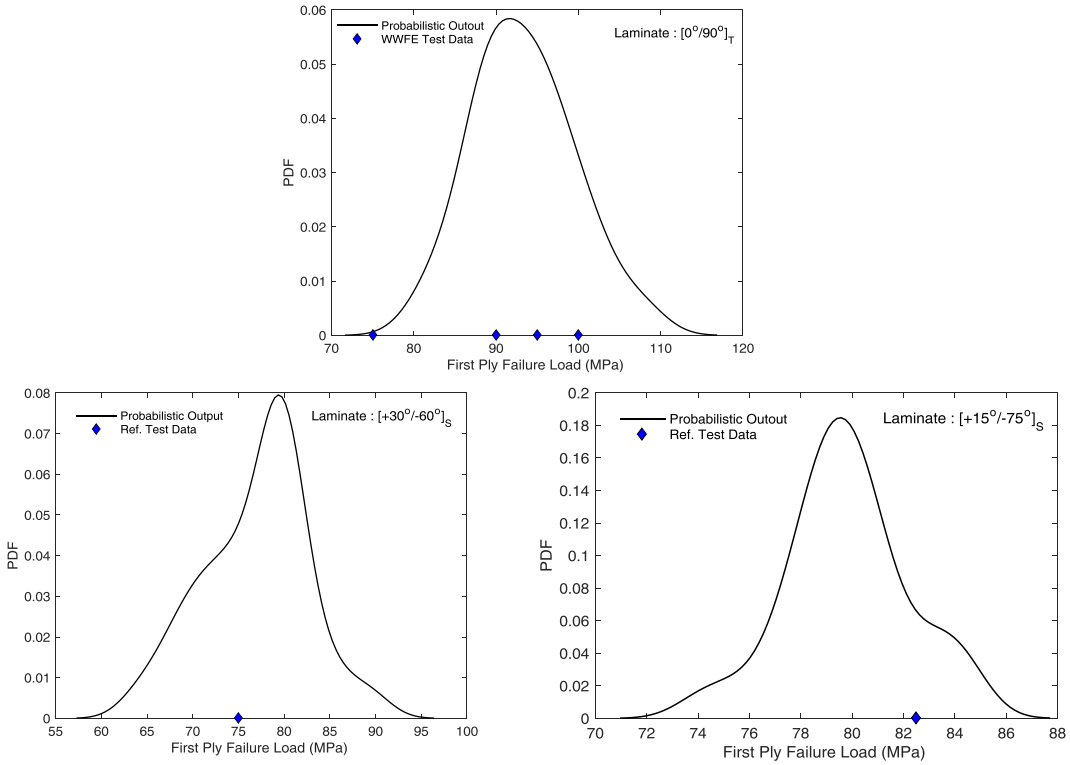

Figure 3.28: Probabilistic FPF of cross-ply laminate (top row) and angle ply laminates (bottom row)

The probabilistic FPF analysis of a qusai-isotropic laminate $[0^o/\pm 45/90^o]_T$ is shown in Figure 3.29. The material is AS4/epoxy with 60% fibre volume fraction. The results from Tsai-Wu [43] and Multicontinuum [51] (MCT) failure theories are also given in this figure. The results from Tsai-Wu and MCT were deterministic. The probabilistic mean falls near the test data and MCT. The Tasi-Wu prediction is far from the test data and micromechanics based predictions from M-SaF and MCT.

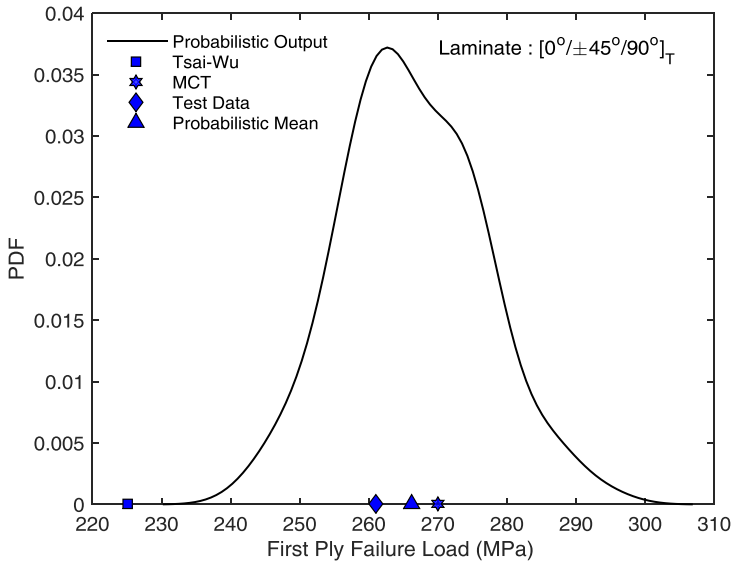

Figure 3.29: Probabilistic FPF of quasi-isotropic laminate

3.7 Conclusion

In this paper, a methodology for the failure of composite laminates based on micromechanics, i.e. Micromechanics based approach for Static Failure (M-SaF), is used to evaluate first ply failure. This method is based upon behavior of the constituents, i.e. the fiber, matrix, and interface. The model determines the failure of composites by considering failure of constituents in a micromechanical analysis. The M-SaF FPF results matches well with well known Tsai-Wu failure theory. Also, the Bayesian Inference framework was used to calibrate the M-SaF model parameters from available test data. This calibration produced posterior distribution of constituent strength properties. By using Metropolis-Hastings MCMC simulation, samples of M-SaF model parameters θ are drawn efficiently from prior distribution. The first order statistics of posterior found to be very close to the available values from literature. The joint posterior probability density function of θ was then used for FPF probabilistic analysis of a variety of laminates. The base material for all considered laminates was e-glass and epoxy. But, this will be extended to carbon fiber laminates in future. Additional test data will improve the accuracy and the bonds of the calibrated parameters. The presented coupled approach facilitates to identify the probability density functions of the constituent properties. This allows structural designers to incorporate uncertainty in analysis with confidence and can

benefit reliability based composite structural design and optimization by allowing contracted the factor of safety due to improved knowledge on uncertainties in the constituent material properties. The next step in this research is to extend presented coupled micromechanics based probabilistic framework to estimate the fatigue life of composites. Deterministic values of the constituent stiffness properties are used in the present work but these will be calibrated with the Bayesian inference method along with constituent strength properties in future work. Finally, there is clearly a need for more reporting of statistical test data by experimental practitioners to support further development of probabilistic failure models.

Chapter 4 Damage Initiation and Growth in Composite Laminates of Wind Turbine Blades

This paper was presented in the 10th Canada-Japan Conference Vancouver Canada and has been accepted for publication in the scientific proceedings of the Design, Manufacturing and Applications of Composites (2014): pp 17-28
[ISBN: 978-1-60595-169-0, Publisher: DEStech Publications Inc.]

This chapter is a subsequent step for the composite structures analysis using micromechanics. The principal focus of this chapter is to predict the last ply failure (LPF) of composites. As LPF requires progressive running damage scheme, so scope was limited to use mean values of the constituents.

ABSTRACT

The physical properties of composite materials, such as high strength-to-density and stiffness-to-density ratios, are key properties for wind turbine blade structure. These materials are however vulnerable to damage during service. The static failure of composites occurs in two stages: 1) onset of damage and 2) damage evolution that leads to final failure. The response of damaged composites depends upon a mixture of mechanisms that take place at the micro level, i.e., in the fiber and the matrix. Consequently a model is proposed for predicting ultimate strength of composite laminates based on the constituent's properties; the fiber, the matrix, and the interface. For onset of damage, the Stassi Equivalent stress model $\sigma_{eq,m}$ is used for the matrix. This model take cares of different tensile and compressive strengths of the matrix. For the fiber, the failure criterion for onset of fiber breakage is related to fiber strength. Once failure occurs, gradual degradation of material properties is used, i.e., $D_m = 1 - exp\left[\gamma\left\{1 - \frac{\sigma_{eq,m}}{T_i}\right\}\right]$. The analysis is carried out on a three dimensional representative unit cell of the composite. The ultimate strength predictions were in reasonably good agreement with the test data for E-glass/epoxy laminates used in wind turbine blades.

4.1 Introduction

The size of wind turbines is increasing to capture more energy and this trend will continue into the future [14]. Several multi-MW prototype wind turbines exist for offshore applications [15, 16]. The power of a wind turbine scales as square of the rotor diameter and the mass of the blade geometrically scales as the cube of rotor diameter. The cost of the blade would then also scale as cube of rotor diameter but advanced structural concepts reduce its scaling exponent to ~2.5 [17]. Considering these scaling laws one might predict that in the end material costs might govern and avert further scaling. Wind turbine blades have two important design constraints. First, blades should be stiff enough to resist excessive defection and avoid striking the tower. Second, the blades should be strong enough to sustain a number of variable load cycles during its lifetime of 20 years according to IEC 61400-1 Ed 3 [19]. A polymer-based composite material is a good choice for large structures such as wind turbine blades. The high strength-to-density ratio, high stiffness-to-density ratio, good fracture toughness, fatigue performance and suitability for use in fast production of large structures makes composites a good choice for their use in structural application. The fibres are embedded in polymer matrix which not only holds fibres at their place but also takes some axial load in proportion to relative stiffness [98].

A lot of effort has been put into understanding failure of composite materials in order to better use these materials in structural applications. Significant success has been made particularly in the aerospace industry. Most of the work done had focused on failure of composite materials at the ply or even laminate level. At ply level, most of the failure theories treat the ply as a one homogenous system. But, in reality, composites are made up of distinct materials that have different mechanical and thermal properties. The work by Azzi and Tsai [1] focused on the analysis of thin plies and proposed interaction based formulation. Later, Tsai and Wu [43] provide interaction based quadratic failure criterion for laminates and they used stresses as failure contributors. This failure criterion is the most widely used in industry today due to its easy to application in practice. The different failure modes, fibre failure or matrix failure, were identified by the failure criterion given by Hashin and Rotem [9]. Hart-Smith used isotropic failure criteria to cover orthotropic

cases. He also used strain to characterize the failure rather than stress. Puck [45] used Mohr-Coulomb effective stresses to calculate the fracture.

Most of the existing failure criteria for fibre reinforced composites are at laminate level and treat the fibre-matrix system as a whole making it difficult to predict whether failure occurs in the fibre or matrix or at the fiber-matrix interface. These theories are referred to as macro level theories. These macro level theories apply failure criteria on homogenized stiffness and strength properties. This homogenization not only smears the fibre and matrix properties but also requires interaction parameters which can only be determined from combined stress tests [3]. Thus, in order to understand the detailed damage mechanism of composites used in a wind turbine blade, an improved method is required that provides information about failure at the constituent level.

This research proposes the micromechanics based methodology for the failure of polymer-based composites that are used in wind turbine blades. This methodology is termed the Micro Level approach for Static Failure (M-SaF). The M-SaF is formulated using a representative unit cell (RUC) of composite laminate of a structure [48, 99]. The methodology is based on the properties of the constituents, i.e. the fiber, the matrix and the interface. The fibres are not in a regular pattern in the laminate, however, it is appropriate to build idealized fiber array with fibres arranged in some specific pattern. Then ply level properties are simulated using M-SaF using RUC. We used Square (SQR) and Hexagonal (HEX) RUC in this study. The macro level stresses at laminate level are calculated using the Finite Element Method (FEM). The ply level macro stresses are then computed using FEM or Classical Laminate Theory (CLT). Micro level stresses are computed using ply level macro stresses and with RUC. Failure criterion is then applied separately to each constituent to see which constituent is critical under various loading conditions. The following sections explain the theory behind this approach.

This is organized as follows. In section 4.2, the definition of unit cell is explained. A comprehensive relation for micro stress calculation using stress amplification factor is outlined in section 4.3. Section 4.4 details the failure criterion for each constituent. Section 4.5 provides a scheme for progressive damage in composites. Results are presented in section 4.6, followed by conclusions in section 4.7.

4.2 Theory

4.2.1 Representative Unit Cell (RUC) Models

The wind turbine blade structure is made up of polymer-based composite laminates, which are in turn made up of plies stacked in a certain sequence. These plies are made up of fibre and matrix constituents. All these levels are divided into two main groups: macro level and micro level as shown in the Figure 4.1. Customarily, one moves right or left in these levels via localization and homogenization. A homogenization procedure provides the response of a structure given the properties of the structure's constituents. Conversely, localization method provides the response of the constituents given the response of the structure.

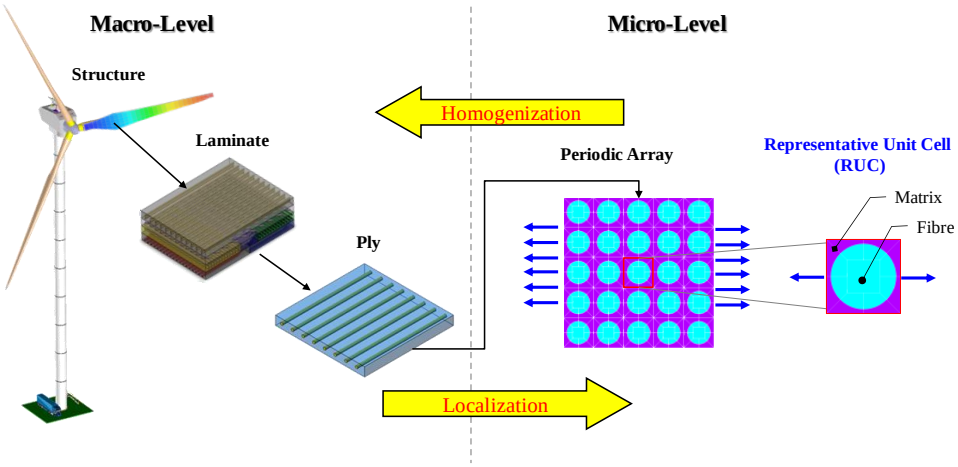

Figure 4.1: Macro and Micro Levels

The fibres are randomly arranged in the real unidirectional (UD) ply. The far left side of the Figure 4.2 shows a cross section of a continuous UD ply [25]. There is no obvious regular pattern in which the fibres are arranged. A true representation of the fibre arrangement is shown in the middle of the Figure 4.2. To aid computation, and idealized fibre arrangement is used, as shown in the far right side of the Figure 4.2. In this study, an idealized square (SQR) RUC model is used for probabilistic analysis as shown at the bottom of Figure 4.2. Although it is possible with suitable boundary conditions to represent a hexagonal arrangement with square unit cell. Other choices for the RUC, such

as triangular RUC, could be exploring in the future. The modelling and mesh generation of RUC were performed in the finite element code ANSYS Multiphysics [31].

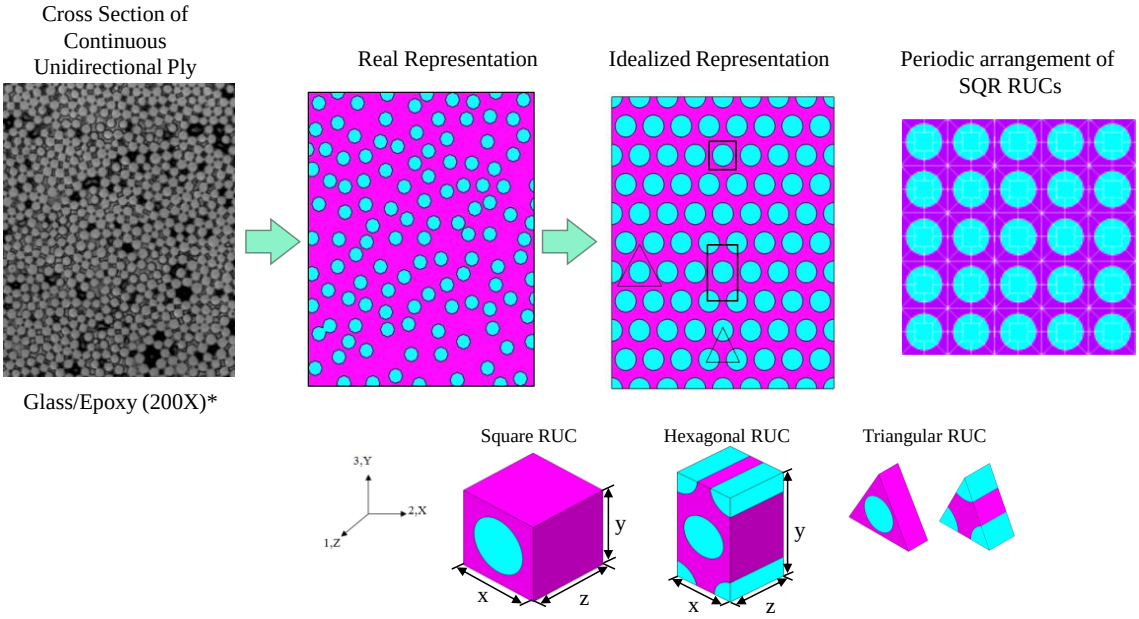

Figure 4.2: Representative Unit Cell Models

4.2.2 Ply Stiffness Computational Procedure

The stiffness properties of a unidirectional (UD) ply were calculated from the constituent's properties; fibre and resin (or matrix) properties, and with certain fibre volume fraction v_f. In the stiffness properties prediction procedure, it is assumed that in an undamaged state both constituents are perfectly bonded everywhere along the length of the fibre/resin interface. For a fully reversible linear material domain, the relationship between stress and strain is given in Equation 4.1:

$$\sigma = C\varepsilon \qquad \text{Equation 4.1}$$

Where σ and ε are the stress and strain components and C is the elastic stiffness tensor. The composite material is orthotropic in nature [3, 25]. For the plane stress case, the stiffness matrix C is invertible to obtain a compliance matrix S. Their product must produce unity matrix, i.e., $[S] = [C]^{-1}$. By definition, ply stiffness properties can be computed from the elements of the $[S]$ matrix [25].

4.3 Micro Stresses Calculation Procedure and Stress Amplification Factor (SAF)

The stresses in the matrix and fibre are related to macro stresses at ply level by Stress Amplification Factors (SAF). Another name for these matrices found in literature as Stress Magnification Factor [3, 6]. The SAF was determined by the finite element method (FEM) using ANSYS. The SAF depends on RUC (fibre and matrix combination) and the fibre volume fraction. It is necessary to apply proper boundary conditions (BC) to obtain the SAF. These BC include: (i) nodes at the boundaries of RUC will have the same displacements and (ii) the free faces must remains flat as proposed by [6, 29]. For all stresses in a Cartesian coordinate system XYZ (or 123), the macro stresses $\bar{\sigma}$ and resultant micro stresses σ are related as given in Equation 4.2:

$$\begin{bmatrix}\sigma_1\\ \sigma_2\\ \sigma_3\\ \sigma_4\\ \sigma_5\\ \sigma_6\end{bmatrix}^{(j)} = \begin{bmatrix}A_{11} & A_{12} & A_{13} & A_{14} & A_{15} & A_{16}\\ A_{22} & A_{21} & A_{23} & A_{24} & A_{25} & A_{26}\\ A_{31} & A_{32} & A_{33} & A_{34} & A_{35} & A_{36}\\ A_{41} & A_{42} & A_{43} & A_{44} & A_{45} & A_{46}\\ A_{51} & A_{52} & A_{53} & A_{54} & A_{55} & A_{56}\\ A_{61} & A_{62} & A_{63} & A_{64} & A_{65} & A_{66}\end{bmatrix}^{(j)} \begin{bmatrix}\bar{\sigma}_1\\ \bar{\sigma}_2\\ \bar{\sigma}_3\\ \bar{\sigma}_4\\ \bar{\sigma}_5\\ \bar{\sigma}_6\end{bmatrix} \qquad \text{Equation 4.2}$$

4.4 Failure Criterion for Constituents

The failure prediction of composite plies or laminates will be made using micro stresses in each constituent, i.e., the fibre, the matrix and the interface. There is different failure criterion for each constituent. As the matrix is isotropic in nature, a Stassi Equivalent stress model [65] was used for the matrix. This model includes different tensile and compressive strengths of a material as:

$$\sigma_{eq,m} = \frac{(\beta-1)I_{1,m} \pm \sqrt{(\beta-1)^2 I_{1,m}^2 + \beta\sigma_{vm,m}^2}}{2\beta} \qquad \text{Equation 4.3}$$

Where $\sigma_{eq,m}$ is the equivalent stress in matrix, β is the ratio of compressive to tensile strength, i.e., $\beta = {}^{C}/_{T}$, I_1 is the first stress invariant, i.e., $I_1 = \sigma_1 + \sigma_2 + \sigma_3$, $\sigma_1, \sigma_2, \sigma_3$ are the three normal stresses, σ_{vm} is the Von-Misses stress, and the subscript $'m'$ denotes the matrix.

The Maximum Stress Criteria [25] was used for fibre failure for simplicity. This is expressed in Equation 4.4:

$$\sigma_{eq,f} = \sigma_{xx,f} \qquad \text{Equation 4.4}$$

Where $\sigma_{eq,f}$ is the micro stress in the fibre and $\sigma_{xx,f}$ could be either be X_f, which fibre longitudinal tensile strength, or X_f' , which fibre longitudinal compressive strength.

The interface between matrix and fibre plays a role in ply strengths, such as transverse tensile and shear strength [67]. Perfect bonding between matrix & fiber is considered here however and, thus the interface will not enter in the current analysis.

4.5 Progressive Damage Scheme

The physical properties of composite materials including high strength, stiffness, and stiffness-to-density ratios are the key properties for wind turbine blade structures. Regardless of these attractive properties, these materials are fragile and vulnerable to damage from a number of sources, both during initial processing and in service [100]. As the damage cannot be avoided completely, the blade structure should be designed to function safely despite the presence of flaws. The failure of composites occurs at two stages: 1) onset of damage and 2) damage evolution. Here the Stassi Equivalent stress model (Equation 4.3) is used to predict onset of damage. The failure index is then calculated as given in Equation 4.5 [63]. Where T_i is the yield strength of the matrix.

$$k_m = \frac{\sigma_{eq,m}}{T_i} \qquad \text{Equation 4.5}$$

There are three conditions that are associated with k_m; 1) if $k_m < 1$, then material is in linear elastic range, 2) if $k_m = 1$, then this is damage onset stage, 3) for $k_m \geq 1 \; and \; k_m < T_f/T_i$, then damage accumulates in the matrix and it causes stiffness reduction, T_f is final tensile strength of the matrix. In case of the fibre, the failure criterion for onset of fibre breakage is expressed in Equation 4.6 [101]:

$$\left|\frac{\sigma_{11}^{f}}{X_{T}^{f}}\right| = 1 \; if \sigma_{11}^{f} > 0 \; or \left|\frac{\sigma_{11}^{f}}{X_{C}^{f}}\right| = 1 \; if \; \sigma_{11}^{f} < 0 \qquad \text{Equation 4.6}$$

Where X^f is the failure strength of fiber, and subscripts T and C denote tension and compression, respectively. σ_{11}^{f} is the maximum stress in the fibre.

The failure criterion adopted for matrix and fiber assumed that a composite starts to fail when either fiber or matrix fails. Once failure occurs, the material may undergo some degree of property degradation in the damaged area. This property degradation process could be either gradual or instantaneous [102]. Gradual degradation of material properties was considered in this research as this more realistic representation of the actual process and, for this, the degradation scheme proposed by Huang et al [63] was used. The damage in the matrix considered as isotropic and damage is being accumulated inside matrix till failure. This SAF based micromechanics approach requires to use reduced or degraded matrix modulus only for matrix dominated failure than traditional methods like Tsai-Wu where different factors required at ply level for transverse and shear moduli. The damage factor, D_m, is related to failure index, k_m, in Equation 4.7 or Equation 4.8 respectively as:

$$D_m = 1 - exp[\gamma(1 - k_m)] \qquad \text{Equation 4.7}$$

$$D_m = 1 - exp\left[\gamma(1 - \frac{\sigma_{eq,m}}{T_i})\right] \qquad \text{Equation 4.8}$$

Where $\sigma_{eq,m}$ is the maximum stress in the matrix and its value is between T_i and T_f. The parameter, γ, describes the shape of the nonlinear part of stress-strain curve and will be available from test data. Final failure occurs when D_m reaches unity. The overall procedure of M-SaF with progressive damage modelling is given in Figure 4.3.

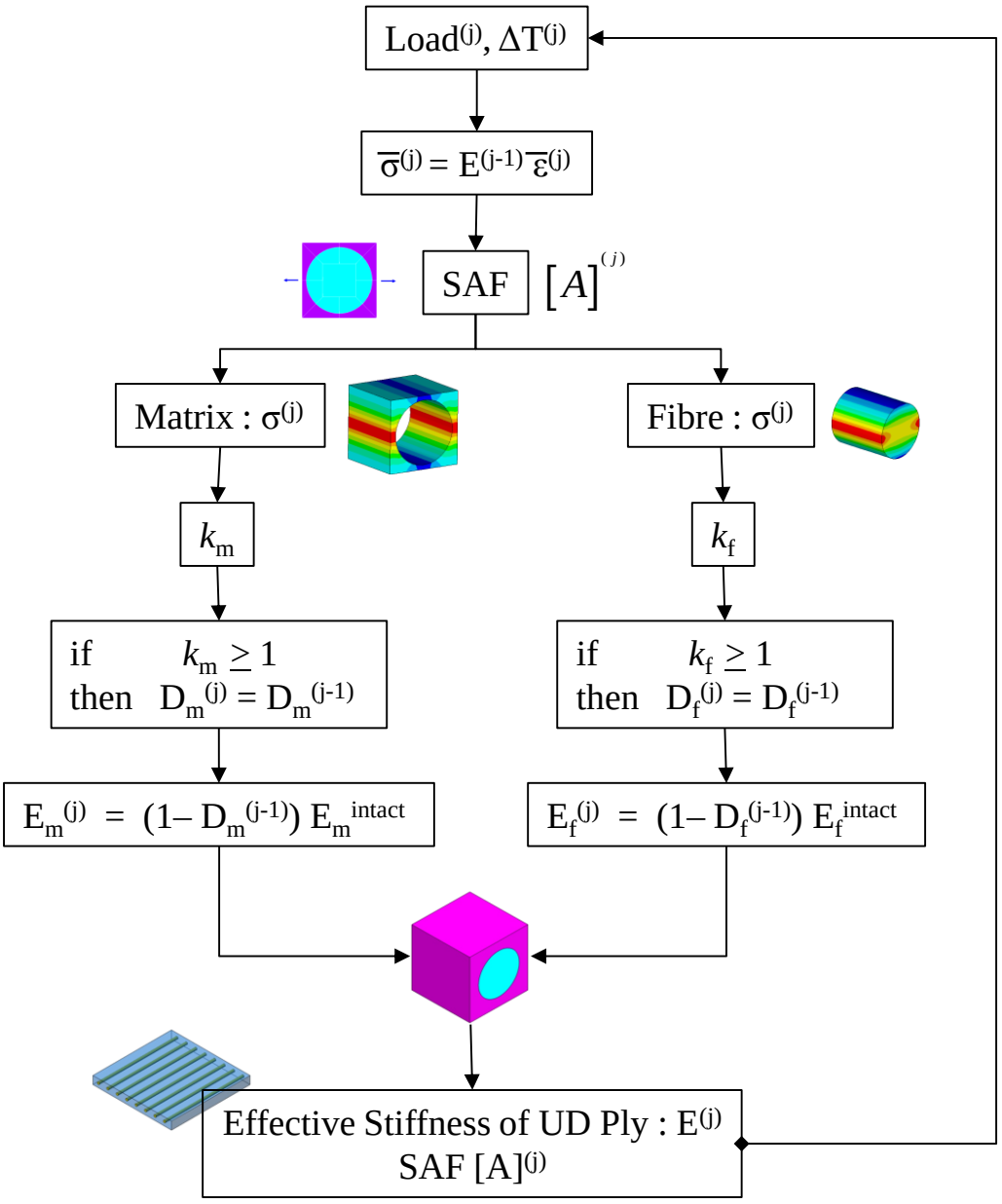

Figure 4.3: Progressive Damage Scheme

4.6 Results and Discussion

4.6.1 Comparison of Shear Stress distribution in Multi-Cell & Unit Cell Model

The periodic boundary conditions (BCs) devised by Xia [29] are applied to a SQR and HEX unit cell FEM model which insures that the composite has the same deformation mode and there is no separation between unit cells. The responses of the multi-cell array

and the unit cell model were compared for different loading conditions with proper periodic boundary conditions. As an example, the comparison of the multi-cell model and the unit cell model under shear load is shown in Figure 4.4. It is clear from the Figure 4 that the stress distributions in the multi-cell model and the unit cell are identical, which verifies the boundary conditions used for the unit cell models.

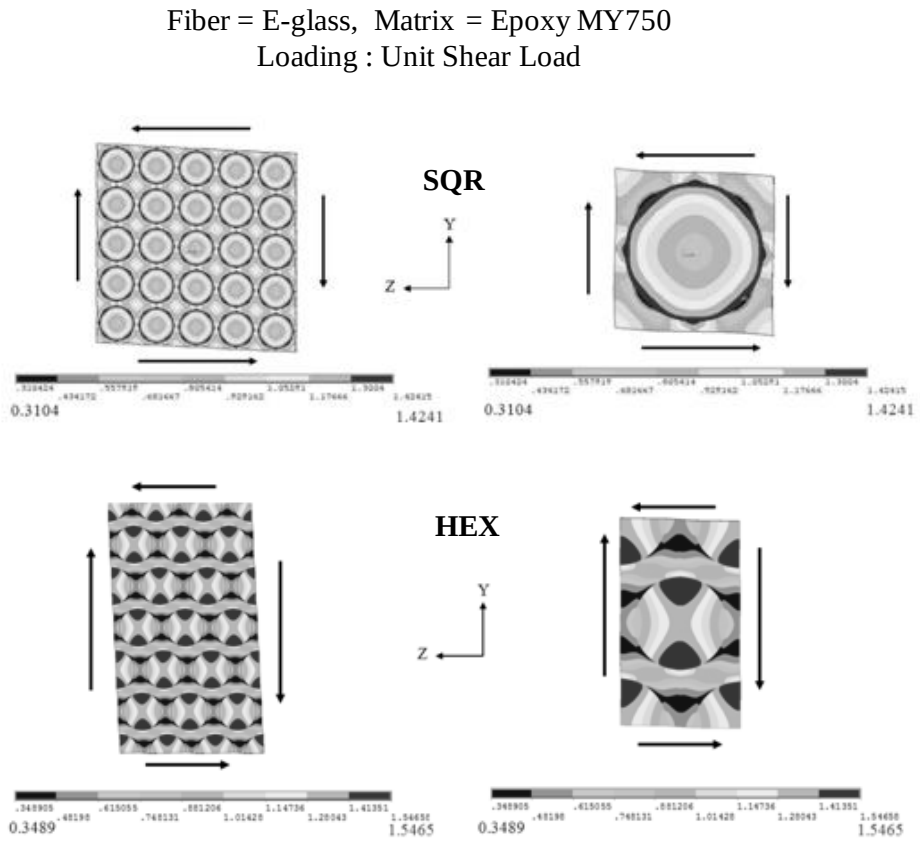

Figure 4.4: Shear Stress in Multi & Unit Cell Model

4.6.2 UD Ply Stiffness Properties

With M-SaF methodology, the stiffness properties of the E-glass/epoxy UD ply were calculated using the SQR and HEX RUC and 60% fiber volume fraction. The E-glass fibre and MY750 epoxy was used for this analysis. These properties were calculated in linear elastic region. The predictions were compared with test data [7] and were found to be in good agreement, as shown in Figure 4.5.

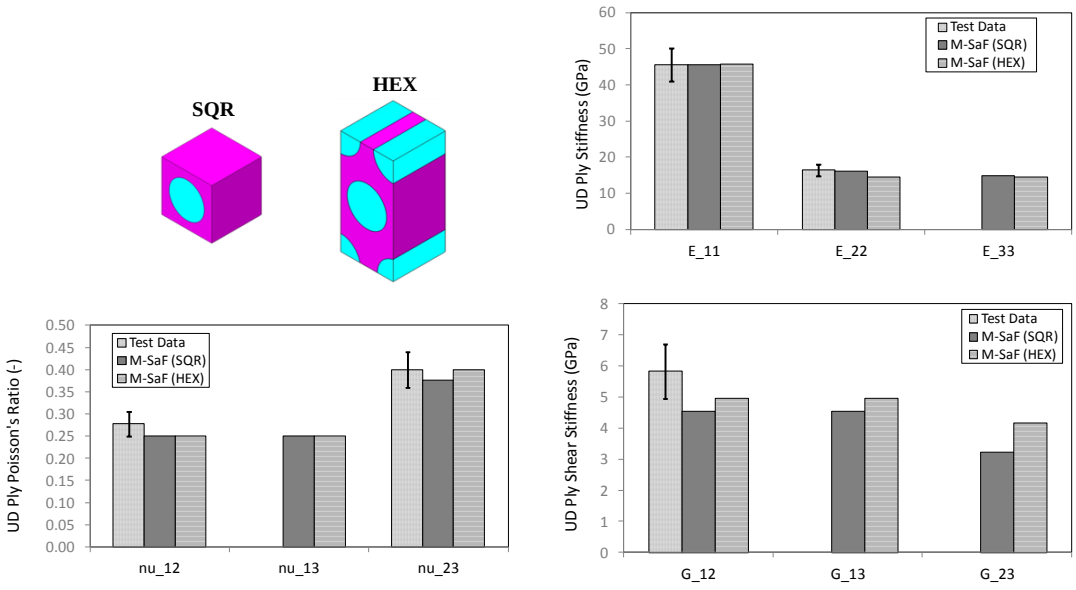

Figure 4.5: Comparison of Stiffness Properties from M-SaF with Test Data

4.6.3 Stress versus Strain Curves of Composite Laminates

In this section, stress-strain curves of composite laminates determined by M-SaF are presented. These laminates are made up from different material systems and having various layups (including cross-ply laminates and quasi-isotropic laminates). These test cases were taken from the World Wide Failure Exercise [WWFE] [103]. The first test case is an E-glass/epoxy MY750 cross-ply laminate $[0/90]_s$ subject to uniaxial tensile loading. The stress-strain curve ($\sigma_x \; vs \; \varepsilon_x$) exhibits bilinear behavior. The predictions from M-SaF were compared with the test data [103] and found in good agreement. The simulation from M-SaF also indicates that the damage initiation, damage propagation, and final failure occurred at various locations on stress-strain curve. Results from MCT [51] and Tsai-Wu failure criterion were also reported as shown in Figure 4.6. The implication of using current M-SaF based failure predictions is loss of multi-linearity in the stress-strain curve, even though the bi-linear behaviour was captured due to distinct material behaviour of constituents. Also, the sub-plot in Figure 4.6 shows the D_m and D_f. The slopes for both constituent damages will go from positive to near zero which corresponds to final constituent's material strength. Also, M-SaF evaluates damage at specific locations in matrix and fiber, so RUC mesh sensitivity is not playing much role.

This will be critical when damage will be evaluated at all locations inside RUC and this will explore in future work.

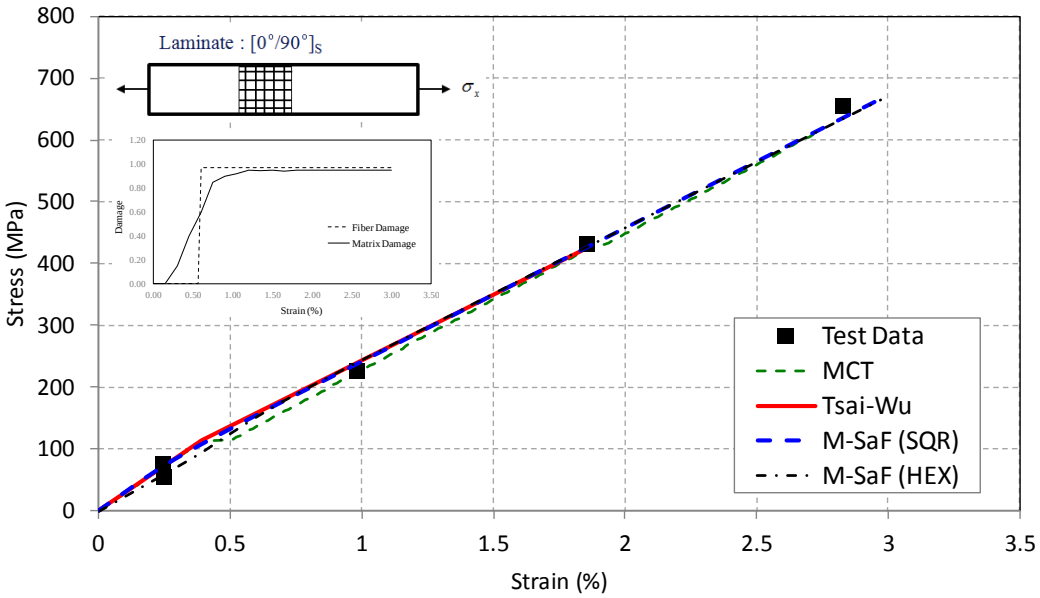

Figure 4.6: Stress–Strain curve of Cross Ply Laminate

The second test case was a quasi-isotropic laminate $[0/\pm 45/90]_s$ made up from AS4 fibers and 3501-6 epoxy matrix system with 60% fiber volume fraction. The stress/strain test data of this laminate under tensile load is given in Figure 4.7 along with predictions from M-SaF using Square and Hexagonal unit cells. Simulations from MCT and Tsai-Wu were also plotted. The simulation results from M-SaF were strain controlled and obtained in 50 load steps. Matrix failure in the 90^0 plies initiated at 225 MPa and final failure took place at 700 MPa where fiber breakage occurs. One observation can be taken from this simulation is that AS4/3501-6 $[0/\pm 45/90]_s$ laminate exhibits multi-linear stress/strain behavior to final failure but apparently it looks like bi-linear. This is due to epoxy non-linearity and epoxy cracking contributes towards laminate stress-strain curve.

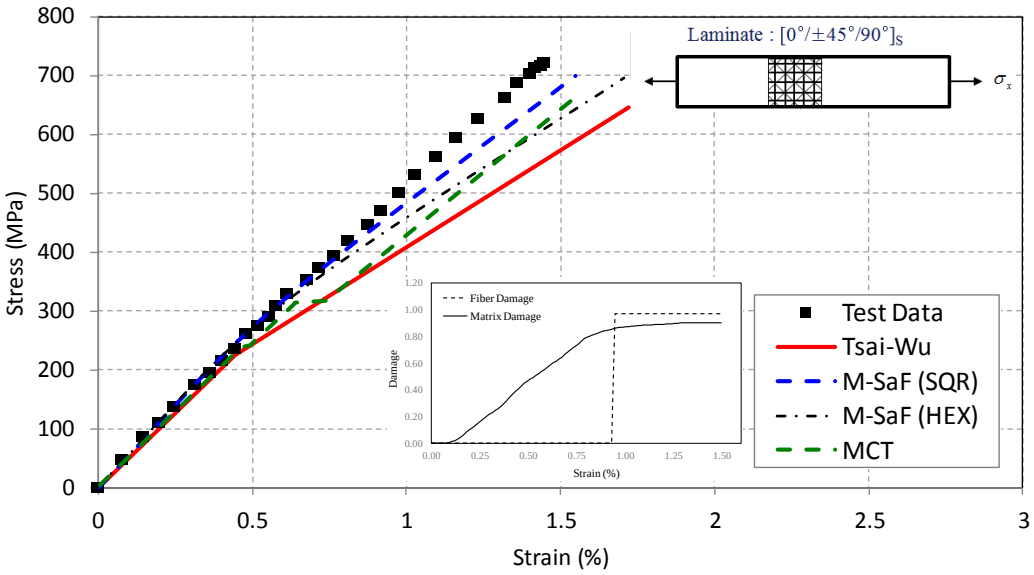

Figure 4.7: Stress–Strain curve of AS4/3501-6 $[0/+45/90]_s$ laminate

4.6.4 Failure Envelope of Composite Laminates

The failure envelope of the E-glass/epoxy composite under combined loading system, i.e. σ_x versus σ_y were plotted. The test data [104] was superimposed on the same graph for comparison, Figure 4.8. The failure envelopes computed by the Tsai-Wu failure criterion [25] and Multi Continum Theory (MCT) [51] are also reported together for comparison. In the failure envelope, fiber, matrix, and interfacial failure modes appear distinctly and determine the biaxial failure loads. The M-SaF is in good agreement with the test data in quadrant I and in quadrant IV. In these quadrants, the failure is matrix dominated. Also, M-SaF matches well with test data at the coordinates axes with excellent accuracy, i.e. parallel and transverse to fibers, fiber and matrix dominated failure modes respectively. The lack of variation in the M-SaF quadrant 1 failure envelope is a result of the assumption that the matrix strength controls failure in the transverse direction. Likewise, the vertical straight line at the right-edge of the M-SaF failure envelope predictions is fiber dominant. However, the Tsai-Wu failure criterion predicts greater ply strength under biaxial compression. The rectangular failure envelope predicted by MCT is similar to one that would be produced by a simple maximum stress failure criterion.

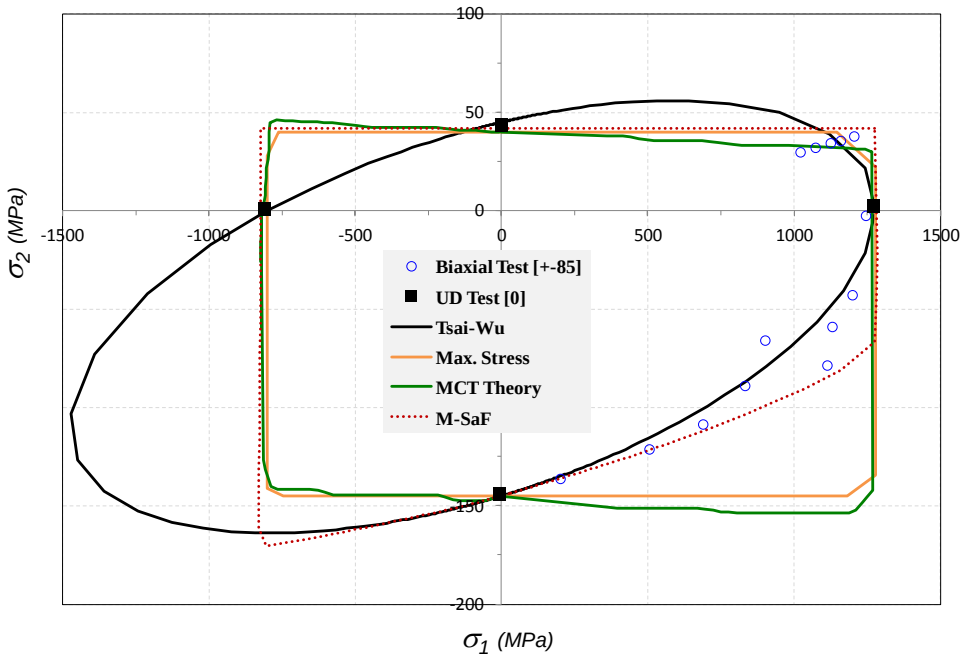

Figure 4.8: Failure envelope of E-glass/Epoxy in $\boldsymbol{\sigma_1 - \sigma_2}$ stress space

4.7 Conclusion

In this paper, a methodology for the failure analysis of composite laminates in wind turbine blades based on Micromechanics, i.e. the M-SaF (Micro Level approach for Static Failure analysis) is used to evaluate the static strength. This approach is based upon behavior of the constituents, i.e. the fiber, matrix, and interface. The model determines the failure of composites by considering failure of constituents in a micromechanical analysis. Good agreement between test data and prediction of failure envelope was observed. M-SaF clearly indicates the failure mode of the composites and the stress level in each constituent upon failure. This makes it more flexible approach to optimize a composite strength by choosing proper constituent materials as well as fiber reinforcement/laminate lay-ups. One of the features of M-SaF is that it provides stiffness properties of the UD ply that can be compared directly with test data and found to be in good agreement. The concept of using basic constituent properties in the wind turbine blade design will help to choose a variety of material combinations. This will not only lead to accelerate the design cycle but also reduce a considerable cost of testing.

Chapter 5 Fatigue life prediction of Laminated Composites using a multi-scale M-LaF and Bayesian Inference

This paper was accepted in Composite Structures Journal in February 2016.

Mustafa, Ghulam, Afzal Suleman, and Curran Crawford. " Fatigue life prediction of Laminated Composites using a multi-scale M-LaF and Bayesian Inference." Composite Structures (2016) (doi:10.1016/j.compstruct.2016.02.024)

This chapter is last in a series of analysis for composite structures. The concept of Bayesian inference was used to predict probabilistic fatigue life of composite laminates.

ABSTRACT

This paper presents a probabilistic model for fatigue life estimation of composite laminates using a high fidelity multi-scale approach called M-LaF (Micromechanics based approach for Fatigue Life Failure). To this end, square and hexagonal representative unit cells are introduced to calculate constituent stresses using a bridging matrix between macro and micro stresses referred to as the stress amplification factor matrix. The M-LaF is based on the constituent level input data that makes it possible to predict fatigue life of a variety of laminates with any possible fiber volume fraction. The M-LaF model parameters are calibrated as posterior distribution using the Bayesian Inference methodology. A reference test data from literature was used for parameter calibration. The calculated posterior statistics were then used to calculate probabilistic fatigue life estimates of sample laminates. The predicted S-N curves are in good agreement with the test data for a range of composite laminas as well as laminates with different fiber volume fractions and under diverse stress ratios. As an illustration, the above approach was applied to a wind turbine blade to show the effect of multi-axial loading on the fatigue life of composite laminates.

5.1 Introduction

Fatigue failure mechanisms in composite materials are different than in metals. In general, fatigue in a material is caused by a non-conservative deformation process where the creation of new surface area causes the energy loss that leads to failure. In metals, the initiation of a single crack and its intermittent propagation until catastrophic failure governs the fatigue life of the structure. On the other hand, fatigue in composite materials is due to multiple damage mechanisms. There are many factors that govern the damage growth in composite materials such as relative stiffness of the fiber and matrix, ply stacking sequence, load direction, and loading rate [105].

The fatigue life of composites can be evaluated using methods that include S-N curves, energy based approaches, stiffness based fatigue models, and strength degradation models. Hashin and Rotem [106] presented a simple fatigue failure criterion expressed in terms of S-N curves obtained by uniaxial cyclic testing of unidirectional specimens. Here, the criterion is proposed for unidirectional laminates only. Information about stress interaction between laminas in non-unidirectional laminates and its effects on failure was lacking. Also, this macroscopic failure criterion did not focus on the developing damage during cyclic loading. The critical element concept of Reifsnider and Stinchcomb [107] represents a non-linear fatigue life prediction methodology for layered composites which accounts for fatigue damage initiation and growth as well as final failure. This methodology assumes that a representative volume can be chosen such that the stress state in that volume is typical in the laminate, and failure of this element causes final failure. To predict fatigue life using the critical element concept, S-N relations of unidirectional composites are still needed. The fatigue life prediction methodology developed by N. Himmel [108] requires prior experimental information on the relevant fatigue damage and failure processes. Here the critical element model was used as a starting point to simulate the fatigue behavior of composites.

Energy-based criteria incorporate both stresses and strains; the multiplication of these components represents energy. In this approach, the damage is related to input energy which cannot give any information about the failure mechanism [109, 110]. This energy-based method is only applicable for unidirectional composites, and it is difficult to extend it to multidirectional laminates because calculation of strain energy from stress/strain

redistribution in fatigue would be difficult. Additionally, this approach is not appropriate for handling fatigue under variable loading. Natarajan et al. [111] proposed a strain energy density based fatigue model. That model performs well for tension-tension and bending fatigue experiments, but did not investigate the influence of combined loadings such as tension-torsion fatigue.

Composite laminate condition can be assessed by its stiffness condition. This will also help to gage fatigue resistance or can be useful in lifetime predictions. The fatigue modulus degradation approach was given by Hwang in which fatigue life was calculated using strain failure criteria [112]. The concept of fatigue modulus is different than elastic modulus; the stiffness is degraded once initial damage occurs. This degradation in the stiffness can be noted by reduction in the dynamic modulus (or secant modulus). The dynamic modulus is the slope of the extremities of a stress/strain hysteresis loop. The damage evolution function and dynamic modulus is based on some assumption or experimental results which limits its usage. Also, some difficulties have been found in predicting the cumulative damage under stress dependent strain. In the residual stiffness model given by Whitworth [113, 114] an equivalent cycles approach for variable amplitude loading was used. This methodology relies on the limiting assumption that the response of a structure is independent of load history. Additional studies by Hahn and Kim [115], Hashin [116], and Yang et al. [117] are among the other researchers that have considered the degradation of the fatigue or dynamic modulus as indicators of fatigue damage.

In strength degradation models [118, 119, 120], life is predicted by calculating the effect of each load cycle on residual strength, until the load exceeds the remaining strength. The expected advantage of this approach is that the sequence effects of random loads can be implicitly included. The successful application of the strength-based method requires a description of the post-fatigue strength, which entails considerable experimental effort. Akshantala [118] assessed the fatigue life of Carbon Fiber Reinforced Plastic (CFRP) laminates by employing a micromechanics approach. He employed fracture mechanics analysis of micro cracking for fatigue in composites. Conventional fracture mechanics analysis of fatigue crack growth normally uses a Paris law that relates crack growth rate with applied stress intensity factor. However, in micro

cracking, there is no observation of crack growth, but it is feasible to measure the rate of increase in crack density per cycle, which is the most computationally expensive part of the method.

Jen and Lee [121] proposed a modified version of the well known Tsai Hill failure criterion for plane stress fatigue. This strength-based model does not account for damage accumulation and does not consider specific damage mechanisms. This requires prior knowledge of fatigue strengths as function of number of cycles, which can only be determined experimentally. Recently, Sarfaraz et al. [122] developed a semi empirical hybrid formulation for composite materials under constant amplitude fatigue. However, they achieved improved model accuracy in both Low Cycle Fatigue (LCF) and High Cycle Fatigue (HCF) regimes, but still required power law fitting functions or parameters. All these criteria are macroscopic and work at the ply level but do not directly take into account the constituents' failure modes. Also, a large number of mechanical properties are required to particularly apply these models for structural analysis.

Despite the fact that so many efforts have been made into predicting fatigue life of laminated composite materials, so far there is not a well-established and widely accepted approach for life prediction of these materials. Micromechanics is getting attention in industry more recently as it requires fewer tests, thus saving time and accelerates product development. There are various models proposed to predict the behaviour of composite materials based on properties of composite components, such as the rule of mixture (ROM), modified role of mixture (MROM), and method of cells (MOC). These micromechanics based methods provide response insight into the constituents and help to better understand the fatigue mechanisms in composites. The successful implementation of this approach requires characteristics of the constituents beforehand which are not easy to obtain. Some researchers back-calculated constituent properties from lamina properties using a simple rule of mixture [3]. Others calibrated material properties in a deterministic fashion with the aid of genetic algorithms and gradient-based techniques [54, 55]. These calibrated values are the mean parameters and did not reflect any uncertainty due to the materials' natural variability. In contrast to deterministic approaches, a Bayesian approach can provide conditional probability and calibrates parameters with test data [56,

57]. Bayesian methods are presently becoming popular in science and engineering as a means to calculate probabilistic inference [58]. In these methods, expert opinion or previous information is reflected in prior distributions which are basically a wide range of possible realistic values of the parameters to be calibrated. These values are updated using a likelihood formulation with test data to determine posterior distributions.

The objective of this work is to estimate the probabilistic fatigue life of laminated composites using novel combination of a micromechanics based model for Fatigue Life Failure (M-LaF) with a Bayesian inference approach. The aim is to develop a unified framework for the representation and quantification of uncertainty present in the fiber and matrix properties with the use of the Bayesian inference approach in order to calculate probabilistic composite fatigue failure. The proposed framework is applied to glass-fiber reinforced composite laminates. The paper is organized as follows. In section 5.2, the M-LaF framework is described; with an emphasis on explanation of the fatigue failure criterion is presented. A comprehensive presentation of the Bayesian inference technique is given section 5.3. Section 5.4 details the computational implementation of M-LaF with Bayesian Inference approach. Results with discussions are presented in section 5.5. In section 5.6, the application to the structural design of a wind turbine blade is presented to show the effect of multi-axial loading on the fatigue life. Finally, conclusions and future work are summarized in section 5.7.

5.2 M-LaF Methodology

5.2.1 Representative Unit Cell (RUC) Models

Composite structures, such as wind turbine blades and aircraft components are made up of polymer-based composite laminates, which are in turn made up of plies stacked in an appropriate sequence and orientation according to the detailed design. These plies are made up of fibre and matrix constituent materials. All these levels are divided into two main groups, the macro and micro levels as shown in the Figure 5.1 [11]. Customarily, one moves right or left in these levels via localization and homogenization. A homogenization procedure provides the response of a structure given the properties of the structure's constituents. Conversely, the localization method provides the response of the constituents given the response of the structure.

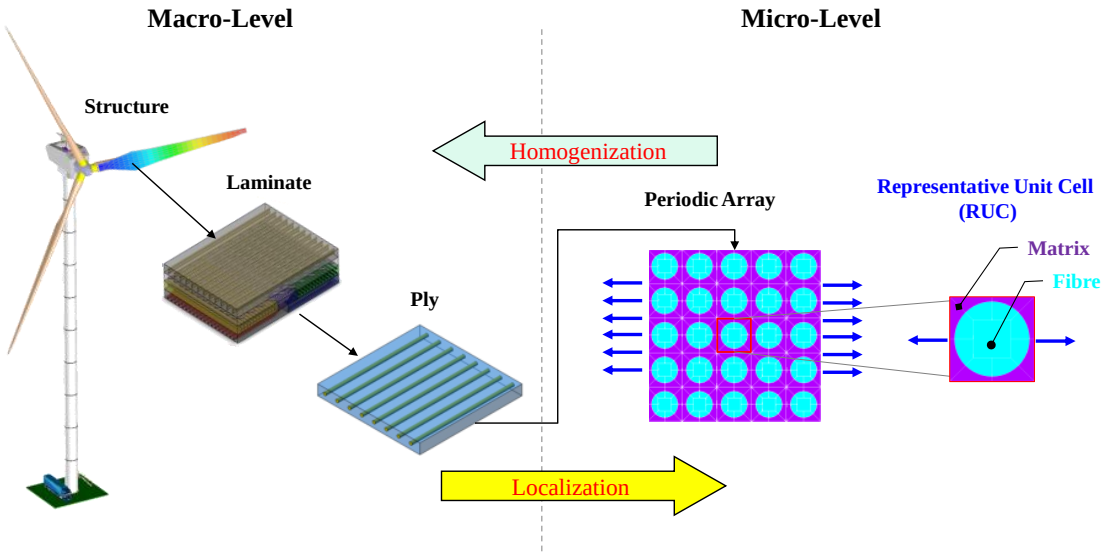

Figure 5.1: Macro and Micro Levels [11]

The fibres are randomly arranged in the matrix of a unidirectional (UD) ply; the current work focuses on laminates from unidirectional plies. The far left side of Figure 5.2 [11] shows a cross section of a continuous UD ply [25]. There is no noticeable regular pattern in which the fibres are arranged. A proper representation of the fibre arrangement is shown in the middle of Figure 5.2. To assist in the computation, an idealized fibre arrangement is used, as shown in the far right side of the Figure 5.2. In this study, two idealized RUC models are used: square (SQR) and hexagonal (HEX), as shown at the bottom of Figure 5.2. Other choices for the RUC, such as triangular RUC, could be explored in the future. The modelling and mesh generation of RUC were performed within ANSYS finite element environment [31].

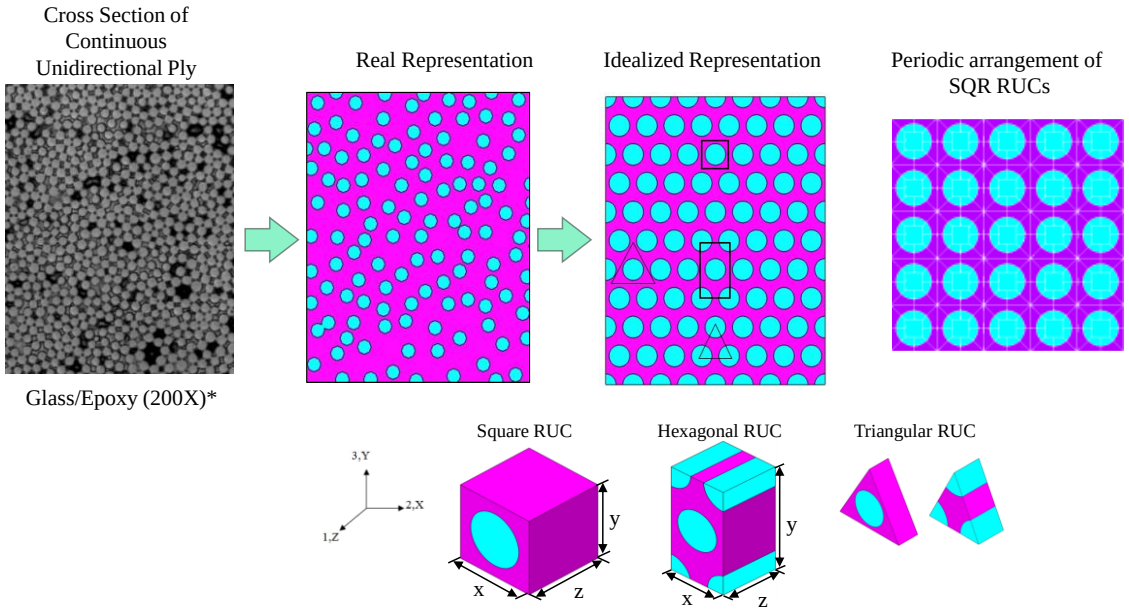

Figure 5.2: Representative Unit Cell Models [11]

5.2.2 Boundary Conditions on RUC

The primary element between the macroscopic and the microscopic scale analyses is the homogenization approach which acts as a bridge between these two levels. It consists of two steps: 1) calculating local stresses and strains in the constituents; 2) using homogenization to obtain global stresses/strains for elastic property calculations. The successful implementation of homogenization assumes that the RUC has global repetition or periodicity. There are a variety of homogenization approaches to predict the composite material behaviour [20, 27]. The homogenization technique given by Sun and Vaidya [27] is the most widely used because of its relatively low computational cost and can be implemented by applying proper boundary conditions (BCs) that are periodic. The displacement field boundary condition on the boundary Γ of domain Ω of the unit cell is given in Equation 5.1 as stated by Suquet [30]:

$$u_i(x_1, x_2, x_3) = \bar{\varepsilon}_{ik} x_k + u_i^*(x_1, x_2, x_3) \qquad \text{Equation 5.1}$$

where $\bar{\varepsilon}_{ik}$ is the global average strain of the periodic structure and x_k represents a linear distributed displacement field. u_i^* is a periodic part of the displacement from one RUC to another on the boundary surface and, unfortunately, it cannot be directly applied to the

boundaries since it is unknown. For a RUC with parallel opposite surfaces (such as SQR and HEX) the displacements on a parallel opposite boundaries Γ^{j+} and Γ^{j-} are expressed in Equation 5.2 and Equation 5.3:

$$u_i^{j+} = \bar{\varepsilon}_{ik} x_k^{j+} + u_i^* \qquad \text{Equation 5.2}$$

$$u_i^{j-} = \bar{\varepsilon}_{ik} x_k^{j-} + u_i^* \qquad \text{Equation 5.3}$$

where u_i^* is the same on the two parallel boundaries due to periodicity, therefore, the difference between the Equation 5.2 and Equation 5.3 is given as:

$$u_i^{j+} - u_i^{j-} = \bar{\varepsilon}_{ik}(x_k^{j+} - x_k^{j-}) = \bar{\varepsilon}_{ik} \Delta x_k^j \qquad \text{Equation 5.4}$$

where Δx_k^j is constant with the known $\bar{\varepsilon}_{ik}$ making the right hand side of the equation constant. These displacements constraint equations were implemented in the ANSYS finite element code [31]. Additional constraints must be enforced in order to avoid rigid body motion of the unit cell. For example, a displacement constraint applied at arbitrary point $(\hat{x}_1, \hat{x}_2, \hat{x}_3)$ of the RUC is:

$$u_i(\hat{x}_1, \hat{x}_2, \hat{x}_3) = 0 \qquad \text{Equation 5.5}$$

The composite ply is considered as a homogenous orthotropic material with effective stiffness properties. These material properties are, in fact, ‘average’ material properties of the composite. The average stress and strain quantities ensure equivalence between strain energy from the homogenous RUC with that from heterogeneous one. In order to determine the stiffness matrix, different displacement boundary conditions are applied on the RUC with appropriate periodicity as determined by Equation 5.1. The graphical explanation of these BCs is given in Figure 5.3 [11].

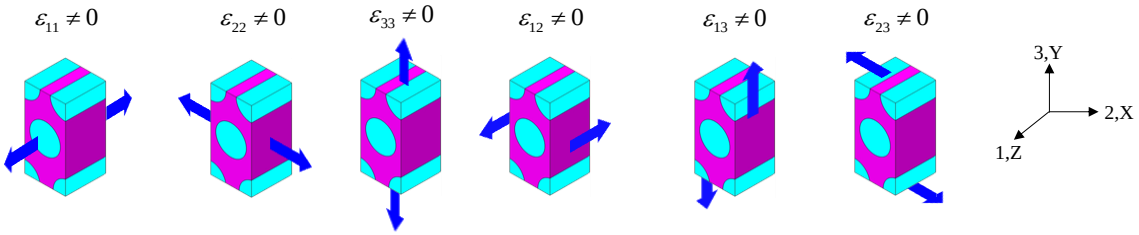

Figure 5.3: Boundary Conditions for Calculation of Effective Material Properties of UD [11]

For example, in the case of $\varepsilon_{13} \neq 0$, the constrained equations applied on HEX RUC are given in Equation 5.6. The Von-Mises stress distribution on the RUC under the BCs is given in Figure 5.4. Two important points should be noted from the RUC stress distribution. First, stresses at the same location on opposite sides are the same confirming the traction continuity condition. The second is that the boundary faces are no longer planes.

$$\begin{vmatrix} u_x^{1+} - u_x^{1-} = 0 \\ u_y^{1+} - u_y^{1-} = 0 \\ u_z^{1+} - u_z^{1-} = 0 \end{vmatrix} \begin{vmatrix} u_x^{2+} - u_x^{2-} = 0 \\ u_y^{2+} - u_y^{2-} = \varepsilon_{12} d_{nk} \\ u_z^{2+} - u_z^{2-} = 0 \end{vmatrix} \begin{vmatrix} u_x^{3+} - u_x^{3-} = 0 \\ u_y^{3+} - u_y^{3-} = 0 \\ u_z^{3+} - u_z^{3-} = \varepsilon_{12} d_{mn} \end{vmatrix} \quad \text{Equation 5.6}$$

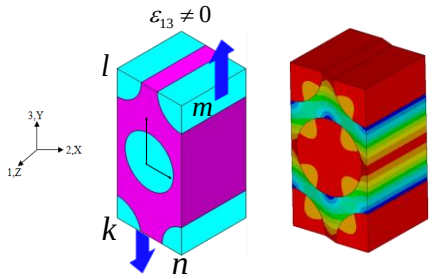

Figure 5.4: Shear boundary conditions on HEX RUC

5.2.3 Stress Amplification Factor (SAF) Matrix

The macro stresses under mechanical and thermal loads are related to the micro stresses below the elastic limit with the following relation [3, 6, 59, 60]:

$$\{\sigma\} = [A^M]\{\bar{\sigma}\} + [A^T]\Delta T \quad \text{Equation 5.7}$$

where matrices $[A^M]$ and $[A^T]$ denote Stress Amplification Factors (SAFs) for macro mechanical stresses and for the macro temperature increment, respectively. This work considers only mechanical stresses, so the last term on the right hand side of Equation 5.7 is excluded. Based on Equation 5.7, the micro stresses in fiber and matrix are related to the macro stresses as:

$$\{\sigma\}^f = [A]^f\{\bar{\sigma}\}$$
$$\{\sigma\}^m = [A]^m\{\bar{\sigma}\} \qquad \text{Equation 5.8}$$

where $[A]^f$ and $[A]^m$ represent SAF for fiber phase and matrix phase respectively under mechanical loading. These matrices are determined by the finite element method for a particular fiber volume fraction and specific fiber-matrix mixture. It is necessary to apply proper boundary conditions (BC) to obtain the SAF. These BC include: (i) nodes at the boundaries of RUC having the same displacements and (ii) the free faces must remains flat as proposed by [6, 29]. The SAFs are 6 x 6 matrix. For all stresses in a Cartesian coordinate system XYZ (or 123), Equation 5.8 can be expanded into Equation 5.9 [59, 60]. The superscript j represents either the fiber or the matrix phase.

$$\begin{bmatrix}\sigma_1\\ \sigma_2\\ \sigma_3\\ \sigma_4\\ \sigma_5\\ \sigma_6\end{bmatrix}^{(j)} = \begin{bmatrix}A_{11} & A_{12} & A_{13} & A_{14} & A_{15} & A_{16}\\ A_{22} & A_{21} & A_{23} & A_{24} & A_{25} & A_{26}\\ A_{31} & A_{32} & A_{33} & A_{34} & A_{35} & A_{36}\\ A_{41} & A_{42} & A_{43} & A_{44} & A_{45} & A_{46}\\ A_{51} & A_{52} & A_{53} & A_{54} & A_{55} & A_{56}\\ A_{61} & A_{62} & A_{63} & A_{64} & A_{65} & A_{66}\end{bmatrix}^{(j)} \begin{bmatrix}\bar{\sigma}_1\\ \bar{\sigma}_2\\ \bar{\sigma}_3\\ \bar{\sigma}_4\\ \bar{\sigma}_5\\ \bar{\sigma}_6\end{bmatrix} \qquad \text{Equation 5.9}$$

The elements of SAF are determined by applying unit macro mechanical loads of vector $\{\bar{\sigma}\}$ one at a time. For example, a glass or carbon fiber presents a higher modulus of elasticity than the epoxy matrix. This stiffness disparity will reflect once the composite material experience the load and show dissimilar stresses due to stress concentration. The illustration of this is shown in Figure 5.5 which shows stress distribution in a SQR and HEX RUCs under applied unit load $\bar{\sigma}_2 = 1$. The stress $\bar{\sigma}_2$ is called macro stress. As can be seen from the Figure 5.5 that the stresses within the RUCs are no longer unitary. The

stress distribution in the RUC is called a micro stresses. From Figure 5.5, the maximum stress concentration, both in the SQR and HEX RUC, occurs at the fiber-matrix interface in the direction of the applied macro load, whereas the stress concentration is at its lowest value in the matrix region near interface which is perpendicular to the applied macro load

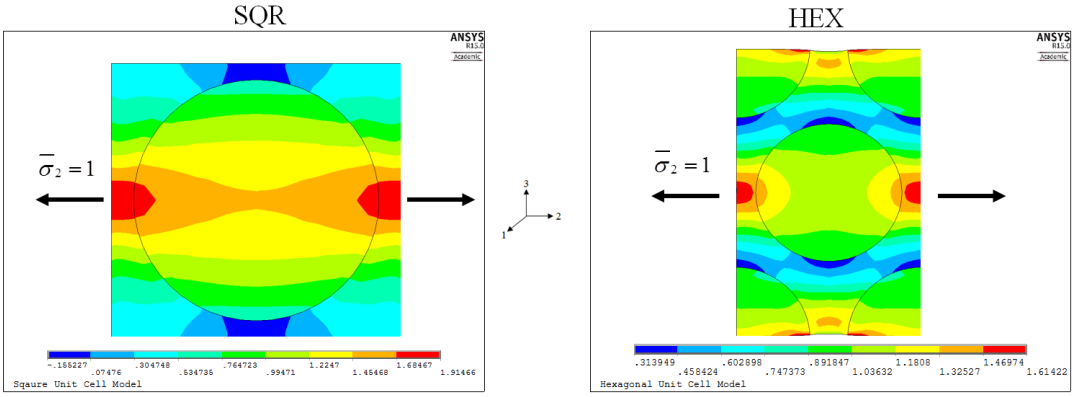

Figure 5.5: Stress distribution in RUC subjected to a transverse unit load

Once the stress amplification factors are calculated in RUC, then actual stresses in the structure such as a wind turbine blade is amplified with these SAFs to calculate actual micro stresses before failure criteria is applied and compared with the critical values as shown in Figure 5.6. The time varying in-plane loads in composite laminates, for example in case of a wind turbine blade, are calculated using the finite element method under particular loading conditions. Then on-axis ply stresses are calculated from the in-plane loads either using finite element method or Classical Laminate Theory (CLT) [2, 3, 43]. These on-axis ply stresses are then multiplied with SAFs to get time varying micro stresses.

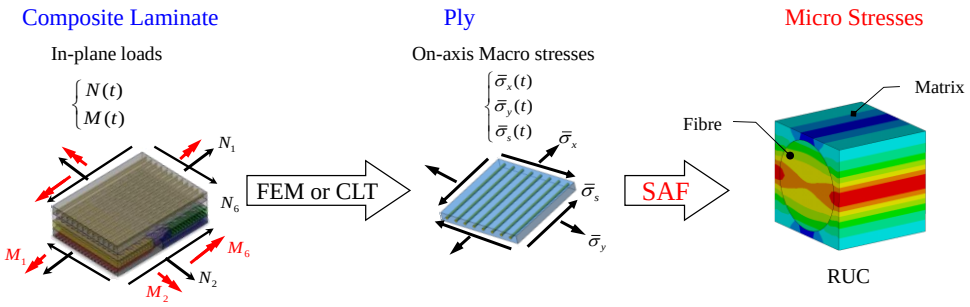

Figure 5.6: Time varying micro stresses from macro to micro level

5.2.4 Fatigue Models for Composite Material Criterions

Three constituent regions exist in composite material: the fiber, the matrix and the fiber-matrix interface. All posses distinct material behaviours and behave differently under the same load [3], so it is rational to apply appropriate failure criteria to each constituent individually. In M-LaF, three different models are employed to treat each constituent of the ply differently. The concept of equivalent micro stress was used in order to account for multi-axial stresses in each constituent. For the matrix material, a modified Von-Misses failure criterion, presented in Equation 5.10, proposed by Ragava et al [62] was used in this work. Even though the matrix behaves isotropically, it has different tensile and compressive strengths. The modified version of Von-Misses criterion considers this aspect of the material:

$$\sigma_{eq}^{m} = \frac{(\beta - 1)I_1^m + \sqrt{(\beta - 1)^2 I_1^{m^2} + 4\beta\sigma_{VM}^{m^2}}}{2\beta} \qquad \text{Equation 5.10}$$

where β is a ratio of compressive matrix strength C^m and tensile matrix strength T^m, first stress invariant: $I_1^m = \sigma_1^m + \sigma_2^m + \sigma_3^m$, Von-Mises Stress $\sigma_{VM}^m = \sqrt{\frac{1}{2}[(\sigma_1^m - \sigma_2^m)^2 + (\sigma_2^m - \sigma_3^m)^2 + (\sigma_3^m - \sigma_1^m)^2 + 3(\sigma_4^{m2} + \sigma_5^{m2} + \sigma_6^{m2})]}$ with $\sigma_1^m, \sigma_2^m, \sigma_3^m$ are normal micro stresses and $\sigma_4^m, \sigma_5^m, \sigma_6^m$ are shear micro stresses in matrix.

Many researchers [60, 63, 66] used a Maximum Stress Criteria [25] for fibre failure for simplicity and as fibres undertake load mostly in their longitudinal direction. This model is adopted in this work and is expressed in Equation 5.11. The micro longitudinal stress σ_1^f is used as equivalent stress in fibre region.

$$\sigma_{eq}^{f} = \sigma_1^f \qquad \text{Equation 5.11}$$

Perfect bonding between the matrix and the fiber is assumed here for typical well matched fibres/matrix systems. Thus the interface will not enter in the current analysis but could be added in the future work.

As the constituent micro stresses are changing with time, the equivalent micro stresses are varying with time as well. This leads to considering the mean stress effects due to fluctuating nature of stresses. This is accounted for the overall M-LaF methodology via considering a Constant Life Diagram (CLD). A CLD is a plot of alternating stress versus mean stress and is a design tool which represents the stress states corresponding to a number of cycles to failure. The CLD is formulated by combining S-N curves at different stress ratios. The stress ratio is defined by Equation 5.12.

$$R = \frac{\sigma_{min}}{\sigma_{max}} = \frac{\sigma_{mean} - \sigma_{amp}}{\sigma_{mean} + \sigma_{amp}} \qquad \text{Equation 5.12}$$

where σ_{min}, σ_{max}, σ_{mean} , and σ_{amp} represents minimum stress, maximum stress, mean stress and stress amplitude respectively for the time varying stress history. Figure 5.7 shows typical S-N diagrams for fatigue data at different stress ratios R. The definitions of amplitude and mean stresses for pure sinusoidal cyclic loading are illustrated on the same figure as well. The data from S-N curves at stress ratio R = -1, 0, and 0.5 are plotted on a Constant Life Diagram. Lines corresponding to these stress ratios are also shown, with the vertical axis corresponds to R = - 1 line for fully reversed loading.

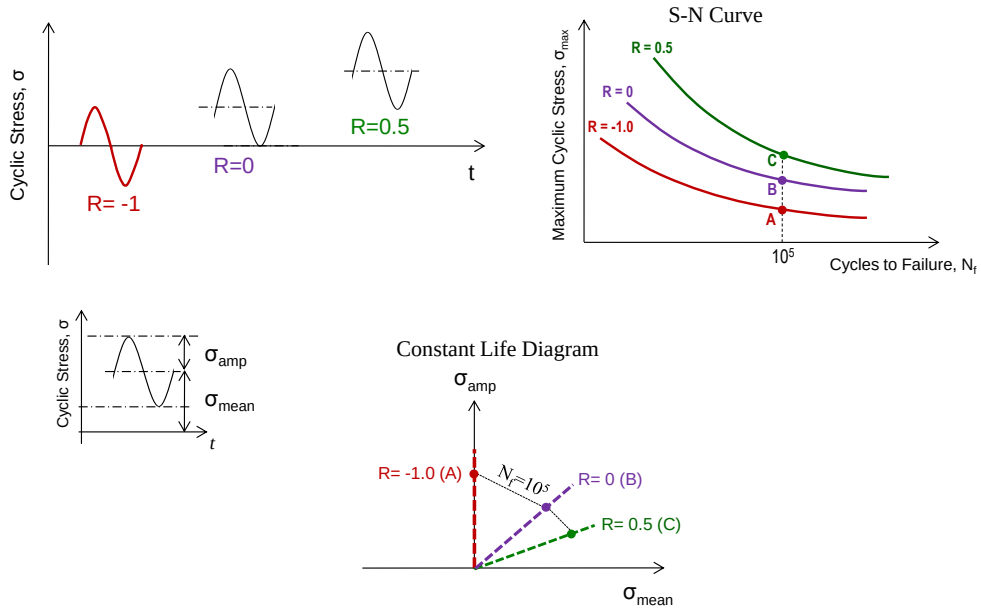

Figure 5.7: SN Curve and Constant Life Diagram

Based on the mean and amplitude micro stresses in the constituents, the constituent effective stress is obtained using Modified Goodman CLD expressed as:

$$\sigma_{eff}^{i} = \frac{\sigma_{eq}^{amp} T}{\frac{T+C}{2} - \left|\sigma_{eq}^{mean} - \frac{T-C}{2}\right|} \quad \text{Equation 5.13}$$

where i refers to fiber and matrix; T and C represent static tensile and compressive strengths of each constituent, respectively. Then with the use of Basquin's equation , represented by Equation 5.14, the number of cycles to failure, N_f, can be calculated.

$$\log\left(\sigma_{eff}^{i}\right) = A\, log\left(N_f\right) + B \quad \text{Equation 5.14}$$

where A and B are the constituent SN curve parameters.

Due to the random nature of fatigue loads on the structure, the nature of the fatigue damage in composites is very complicated and involves a mixture of matrix and fibre damage [123]. The damage is accumulated during each cycle. One of the oldest methods for cumulative damage was proposed by Miner [124] and is called Miner's Linear Damage Acculturation Rule. According to this rule, a damage fraction D_i is defined as the fraction of life used up by an event (or cycle) or a series of events (or cycles), i.e. damage is the ratio of number of cycles of operations, n_i, to the number of cycles to failure, N_i^f, at that load level. Then the total damage factor D (it is equal to unity in correspondence of fatigued life) is calculated as:

$$D = \frac{n_1}{N_1^f} + \frac{n_2}{N_2^f} + \frac{n_3}{N_3^f} + \cdots + \frac{n_k}{N_k^f} \quad \text{Equation 5.15}$$

$$D = \sum_{i=1}^{k} \frac{n_i}{N_k^f} = \sum_{i=1}^{k} D_i \quad \text{Equation 5.16}$$

5.2.5 Fatigue Life Prediction of Composite Laminates

The methodology for fatigue life calculation of entire composite laminates is given in the Figure 5.8. The in-plane loads, N and M, on each laminate are first calculated from the loads and environmental conditions using a macro scale finite element model. These in-plane loads are time varying. Then, using either directly the FEM results or Classical Laminate Theory (CLT), the on-axis ply stresses are determined in each ply of the laminate. In computation of the micro stresses, the M-LaF approach was used with the RUC. These time varying micro stresses, and so the equivalent stress σ_{eq} in the matrix and the fiber, are then converted into blocks of certain numbers of cycles corresponding to constant amplitude and mean values using the Rain Flow Counting (RFC) algorithm. Then, with the aid of a S-N curve and Constant Life Diagram (CLD), a fatigue analysis is carried out. The CLD used in M-LaF is a Modified Goodman diagram that describes cycles-to-failure as a function of mean stress $\sigma_{eq,mean}$ and alternate stress $\sigma_{eq,alternate}$ along lines of constant R-values. Finally, fatigue life is estimated using the damage accumulation law.

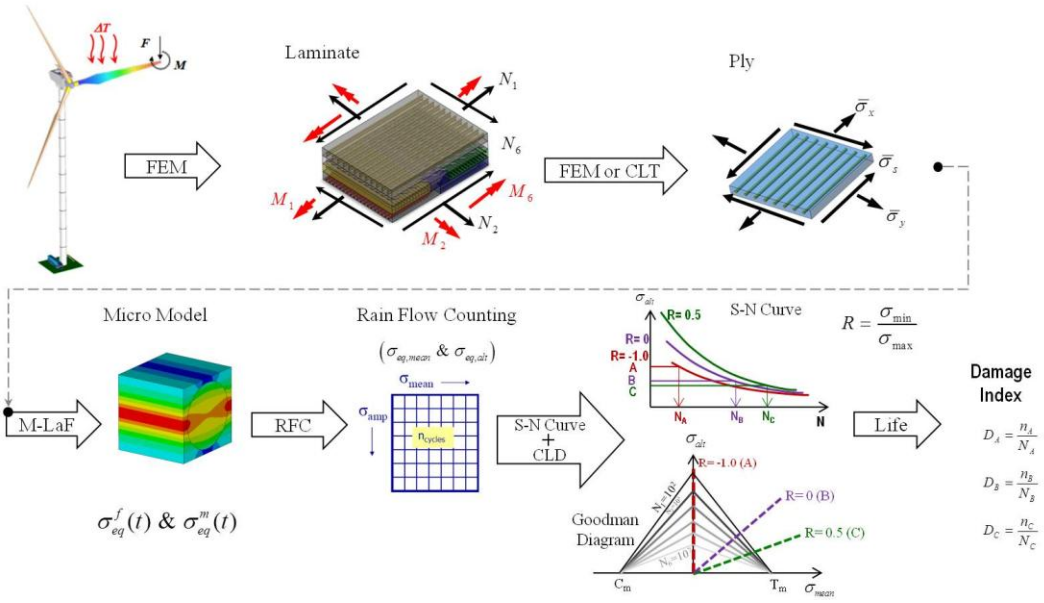

Figure 5.8: Flow diagram for fatigue life prediction of composite laminates

5.3 Bayesian Inference Methodology for Parameter Uncertainty Quantification

5.3.1 Bayes' Rule

In this section, the Bayesian inference methodology is explained with a view to calibrating the mechanical model parameters using available test data. Bayes' formula estimates the degree of belief in the hypothesis based on the evidence by using a conditional probability [56]:

$$P(X \cap Y) = P(X|Y)P(Y) = P(Y|X)P(X) \quad \text{Equation 5.17}$$

where the term $P(X|Y)$ is a conditional probability of X when Y is given. In the scenario of estimating the M-LaF model parameters, the conditional probability of model parameter θ when the test statistics are available can be written as:

$$p(\theta|y_{test}) = \frac{p(y_{test}|\theta)p(\theta)}{\int p(y_{test}|\theta)p(\theta)d\theta} \quad \text{Equation 5.18}$$

Bayes' theorem in Equation 5.18 is extended from a probability distribution to a probability density function (PDF) as this is more appropriate in the present work and can be re-written as:

$$f(\theta|y_{test}) = \frac{L(\theta)f(\theta)}{f(y_{test})} \quad \text{Equation 5.19}$$

where $f(\theta|y_{test})$ is the posterior PDF representing the updated knowledge about the model parameters θ, $f(\theta)$ is the prior distribution (assumed) of the model parameters θ before the test data is observed, $L(\theta) = f(y_{test}|\theta)$ represents the likelihood which is a conditional probability of observing the test data given the parameter θ, and the term $f(y_{test}) = \int L(\theta)f(\theta)d\theta$ is the normalizing constant that makes Equation 5.19 a PDF to ensure that area under the posterior PDF is equal to unity.

5.3.2 Mathematical Model

The computational mathematical model $M(x, \theta)$ represents the set of procedures to simulate the values of the $y_{model}(x, \theta)$. For example, in the case of M-LaF, the elements of y_{model} are the fatigue life of composite material constituents. The predictive model with known variables x and unknown parameters θ is written as:

$$y_{model}(x, \theta) = M(x, \theta) \quad \text{Equation 5.20}$$

In the case of M-LaF, the set of variables x are time varying on-axis ply stresses, the RUC model, stiffness properties of the fiber and the matrix materials; θ represents the vector of parameters. It includes tensile and compressive strength properties of the fiber and the matrix, T^i, C^i, and constituent S-N curve parameters, A^i, B^i. The superscript i refers to either the fiber or matrix material. As the mathematical model y_{model} provides the approximate solution of physical phenomenon, the true outcome of the test data y_{test} accounts for various sources of uncertainty:

$$y_{test} = y_{model}(x, \theta) + \epsilon_m \quad \text{Equation 5.21}$$

where ϵ_m denote the error and could arise from measurement error and/or numerical error; this term is sometime referred to as the model discrepancy term [76, 77]. In order to predict the mean of y_{model} the mean of ϵ_m, i.e. μ_{ϵ_m}, is set to zero for unbiased model analysis which assumes the measurement process is well calibrated [78, 79] which is typically should be for composite testing.

5.3.3 Likelihood Function

The first building block of the Bayesian approach is to formulate the likelihood function of the observed test data y_{test}. The likelihood defines the value of θ that makes the dataset y_{test} most probable. The higher the likelihood value is, the more likely it is to have obtained the best estimates of the parameters. Given the observed value y of y_{test}, the likelihood of θ for one test data point is defined by [75, 80]:

$$L(\theta) = f(y_{test}|\theta) \quad \text{Equation 5.22}$$

For statistically independent and identical (iid) error ϵ_m which is typically Gaussian distributed with mean $\mu_{\epsilon_m} = 0$ and variance $\sigma^2_{\epsilon_m}$, i.e., $N(\mu_{\epsilon_m} = 0, \sigma^2_{\epsilon_m})$, the likelihood function follows the form:

$$L(\theta) = f(y_{test}|\theta) = \prod_{i=1}^{n} f\left(\left\{y^{(i)}\right\}|\theta_i\right)$$
$$L(\theta) = f(y_{test}|\theta) = \prod_{i=1}^{n}\left[\frac{1}{\sqrt{2\pi}\sigma^2_{\epsilon_m}} exp\left\{-\frac{1}{2\sigma^2_{\epsilon_m}}\left(y^{(i)}_{test} - y^{(i)}_{model}(x,\theta_i)\right)^2\right\}\right] \quad \text{Equation 5.23}$$

Rearranging, Equation 5.23 becomes:

$$L(\theta) = f(y_{test}|\theta) = \left(2\pi\sigma_{\epsilon_m}\right)^{-n/2} exp\left\{-\frac{1}{2\sigma^2_{\epsilon_m}}\sum_{i=1}^{n}\left(y^{(i)}_{test} - y^{(i)}_{model}(x,\theta_i)\right)^2\right\} \quad \text{Equation 5.24}$$

where $y^{(i)}_{test}$ is vector of test data and $y^{(i)}_{model}(x,\theta_i)$ is a vector of mathematical computational model results (computed with M-LaF in this work).

5.3.4 Prior Distribution of Parameters

The prior PDF $f(\theta)$ represents the previous knowledge of the parameter values θ that is independent of the test data. Many researchers have addressed the issue of specifying the priors [81, 82, 83]. There are broadly two categories for prior: conjugate prior and non-conjugate prior [84]. A prior is said to be conjugate to a class of likelihood functions if the resulting posterior distributions are in the same family as the prior distribution; otherwise, it is non-conjugate prior [80]. Suppose we have a Bayesian model with a likelihood $p(y|\theta)$ and a prior $p(\theta)$. If we multiply the likelihood with a prior, we get the posterior $p(\theta|y)$. If the posterior distribution is of the same family as the prior, then there exists a conjugacy. In this situation, the prior is conjugate to the likelihood. There are two typical prior distributions commonly used for material property parameters: one is uniform prior and the other is a Gaussian prior. Both flat (uniform) and Gaussian priors will be examined in this work. If little or no information is available, it is appropriate to choose a non-informative prior [85].

5.3.5 Estimating Posterior Distribution of Parameters

The prior distribution of the unknowns when combined with the likelihood function following the Bayes' theorem gives the posterior distribution $f(\theta|y_{test})$ without the denominator proportionality constant $f(y_{test})$ as:

$$f(\theta|y_{test}) \propto L(\theta)f(\theta)$$
$$f(\theta|y_{test}) \propto \left(2\pi\sigma_{\epsilon_m}\right)^{-n/2} exp\left\{-\frac{1}{2\sigma_{\epsilon_m}^2}\sum_{i=1}^{n}\left(y_{test}^{(i)} - y_{model}^{(i)}(x,\theta_i)\right)^2\right\}.f(\theta) \quad \text{Equation 5.25}$$

Equation 5.25 represents the posterior distribution of a parameter once the test data is observed. For a complex computational mathematical model like M-LaF, analytical solution of posterior distribution is not possible. Therefore, a numerical method to approximately calculate the posterior inference of parameters is employed. For this purpose, a Markov Chain Monte Carlo (MCMC) [84] technique, in this work the Metropolis-Hastings (M-H) algorithm, is used to calibrate the parameters and quantify their uncertainty. The M-H algorithm (Metropolis et al.[89]; Hastings et al.[90]) works as follows:

For j = 1 to N (where N is number of iterations of the algorithm)

1: Set the initial value of the parameter θ, such that $p(\theta) \neq 0$

2: Calculate posterior $f\left(\theta^j|y_{test}\right)$ using Equation 5.25. This step involves running the mechanical model, i.e. M-LaF.

3: Randomly generate a sample parameter input (or realization), θ^*, from prior distribution and calculate $p(\theta^*)$

4: Run y_{model} based on θ^*. Then calculate Likelihood 0.

using Equation 5.24 and finally calculate Posterior $f(\theta^*|y_{test})$ using Equation 5.25

5: Calculate Acceptance Ratio (A_{ratio})

$$A_{ratio} = min\left\{1, \frac{f(\theta^*|y_{test})}{f(\theta^{(j-1)}|y_{test})}\right\} \quad \text{Equation 5.26}$$

6: Generate a random value u from a uniform distribution with bounds 0 and 1, i.e. $U(0,1)$

7: Compare A_{ratio} with u

$$\begin{aligned} &If \quad u \leq A_{ratio} \\ &\text{then} \quad \theta^{j} = \theta^{*} \\ &\text{else} \quad \theta^{j} = \theta^{j-1} \\ &\text{end if} \end{aligned} \qquad \text{Equation 5.27}$$

8: Increment j and go back to Step # 1. This repetition continues until a sufficient number of samples obtained so that the posterior distribution stops evolving or in other words Markov chain converges.

The Markov chain takes some iteration at the beginning of the MCMC run to converge to a stationary position. These iterations are called burn-in iterations and are usually discarded from generated samples in order to compose the final posterior PDF and to calculate statistical moments of the posterior.

5.4 Computational Implementation

The workflow for M-LaF model parameter estimation using the Bayesian inference approach is shown in Figure 5.9. The inputs to and outputs from the M-LaF are given in Figure 5.8. In order to calculate the fatigue life of composite materials, the strength properties of the fiber and matrix materials T^f, C^f, T^m, C^m and constituent S-N curve parameters A^f, B^f, A^m, B^m are required. This comprises a vector of unknown parameters which have to be calibrated using the Bayesian inference approach. The test data used for calibration is taken from the OptiDAT data base [8], World Wide Failure Exersice (WWFE) [53], and from other literature results [106, 125]. The model $y_{model}(x, \theta)$ is M-LaF where x are the known inputs and θ are the unknown parameters. The Bayesian approach uses the test data y_{test} on the model outputs to update the PDF for the parameters. This is done by applying Bayes' theorem: $f(\theta|y_{test}) = L(\theta)f(\theta)/f(y_{test})$, where $f(\theta|y_{test})$ is the posterior distribution, $f(\theta)$ is the prior distribution a, $L(\theta)$ is the likelihood and $f(y_{test})$ is a normalization constant. The prior is combined with the likelihood to provide a posterior distribution. The posterior will be narrower and more sharply peaked than the prior, indicating that parameter θ is calibrated and the parameter uncertainty is reduced and properly calibrated to the available test data. The posterior can then be used to compute probabilistic predictions of lifetime fatigue behaviour for general

composite layups of the same calibrated material base constituents, but arbitrary layup schedules.

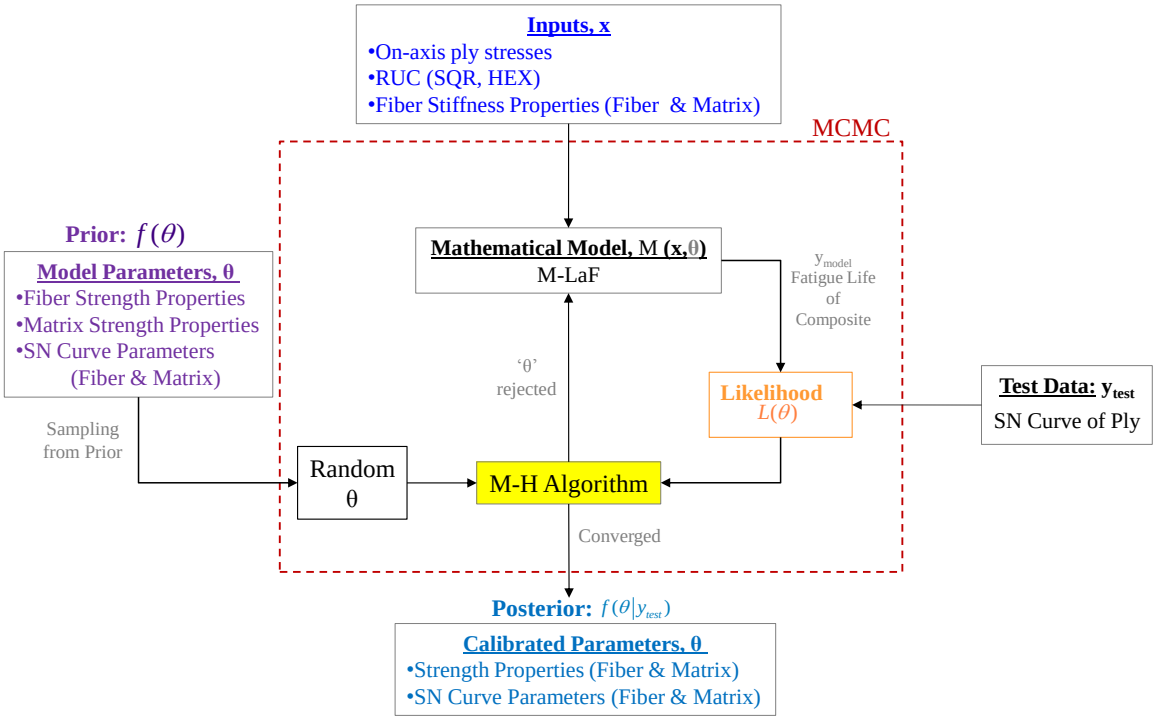

Figure 5.9: Workflow for Model Parameters Estimation using Bayesian Inference

5.5 Results and Discussion

5.5.1 Calibration of Model Parameters

The Bayesian inference scheme with the M-LaF method was employed to calibrate the model parameters and quantify the uncertainties of constituent strength material parameters. The test data used for this was from the OptiDaT data base [126] and the World Wide Failure Exercise (WWFE) [53]. The ply material used is constructed of the e-glass/epoxy material system. The ultimate longitudinal tensile strength, X, of a ply was used in calibrating the longitudinal tensile strength of fiber X^f or T^f. It is asserted that fibers are the main load bearing constituent in this loading condition. The ultimate transverse tensile strength Y of a ply was used in calibrating the tensile strength of the matrix T^m. It is believed that the matrix is the main load bearing constituent in this load

condition. The prior distribution of X^f is taken as uniform U[1200, 2800] MPa and T^m is also assumed uniform U[20, 150] MPa. The distributions of these parameters are calibrated using MCMC sampling with the Metropolis-Hastings algorithm. A random value was sampled from the parameter prior distribution in each of MCMC iteration. The likelihood function was then calculated from observing test data and the outputs from M-SaF. This step requires running finite element analyses on the RUC. MCMC simulations were carried out for five thousand samples from each prior distribution.

The results of calibrated parameters $(X^f$ and $T^m)$ from the coupled framework described in section 5.4 are shown in Figure 5.10. The top row of Figure 5.10 shows results for X^f and the bottom row is for T^m. The trace plots of both parameters were given as well and emerge to be well mixed. The posterior mean of X^f was used in order to calculate T^m distribution. The first 500 samples were discarded as burn-in samples and were not considered in calculating the statistics of the parameters. In the second column of Figure 5.10, the posterior distribution of parameters can be seen. The posterior mean value is plotted as a blue triangular symbol. The circular red dot shows the fiber longitudinal tensile strength provided by the WWFE [7]. The square black dot is the value of X^f used by Huang [52] in order to predict test data. It can be seen clearly that the posterior mean is closer to the WWFE value, however the WWFE just provides a single point value. Evidently the value used by Huang was far from WWFE and the posterior mean. A similar pattern can be found for parameter T^m. In this case, the posterior mean is closer to the WWFE provided value. The calibration accuracy could be further improved by utilizing more test data. From the trace plots, the calibrated posterior parameters do exhibit good convergence. Similar procedures were implemented to calibrate the other M-LaF model parameters. The calibrated posterior of parameters: matrix compressive strength C^m and fiber longitudinal compressive strength $X^{f'}$ or C^f are given in Figure 5.11. These distributions show the narrower band of parameter values from prior distributions.

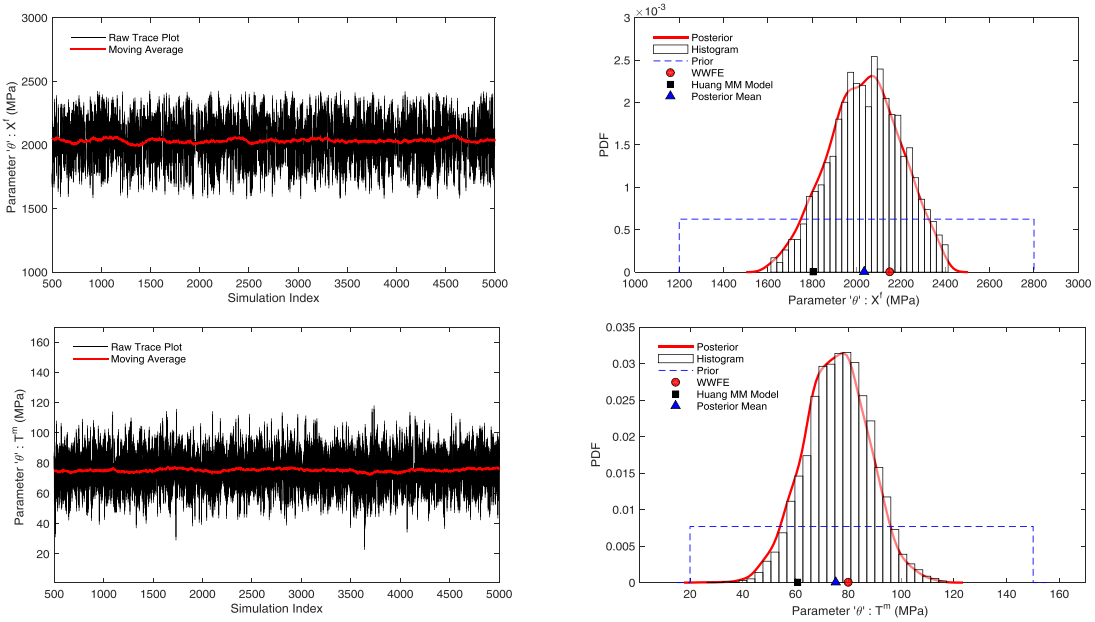

Figure 5.10: The posterior distribution of X^f (top row)and T^m (bottom row)

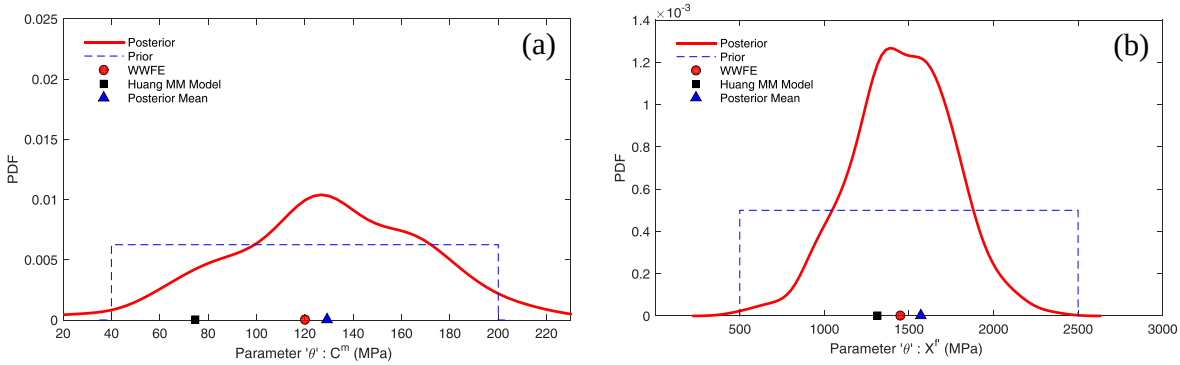

Figure 5.11 : Posterior distribution: (a) matrix compressive strength (C^m); fiber longitudinal compressive strength ($X^{f'}$)

A similar procedure was adopted to calibrate constituent S-N curve parameters A^f, B^f, A^m, B^m. The fiber parameters were calibrated based on a unidirectional ply with fiber angle $[0^o]$. The test data used from [8] had a stress ratio 0.1 and there exists three to five data points at each load level. Similarly, the matrix parameters were calibrated from $[90^o]$ lamina fatigue test data from [125]. The resulting statistics were: A^f (mean = -0.075, C.oV. = 0.0965), B^f (mean = 3.43, C.oV. = 0.048), A^m (mean = -0.087, C.oV. = 0.071), and B^m (mean = 1.955, C.oV. = 0.063).

5.5.2 Fatigue Life Prediction of Unidirectional Composite Lamina

The M-LaF methodology with calibrated parameters was applied to E-glass/epoxy laminates subjected to various stress ratios R, and the results were compared with the test data of various researchers [106, 125, 127]. These unidirectional laminates were tested as flat specimens under cyclic off-axis loadings. A fiber volume fraction of $V_f = 0.6$ have been used. Figure 5.12 shows the comparison between the predicted and test data [106] S-N curves for angled ply laminates subjected to tension-tension (T-T) fatigue with stress ratio $R = 0.1$. There is reasonably good agreement between the predicted values and the test data. The 95% confidence intervals on the mean fatigue curve are also added to the plots represented with dotted blue lines. Most of test data falls under the lower and upper bonds. In the case of a ply angle $[5^o]$ some of the test data falls outside the interval bounds. This may be because of a conservative estimation of fiber equivalent stress σ_{eff}^{f}. This σ_{eff}^{f} value was just considered in the longitudinal direction of the fiber. This can further be improved by considering stresses in all directions.

As the M-LaF handles fiber and matrix constituent separately during the analysis, there is some deviation of predictions from the test data in case of fiber dominated composites, for example, S-N curves of 5^o and 10^o laminates in Figure 5.12. As can be seen in this figure that the test data falls outside of 95% lower and upper bonds for these composites. This will lead to higher safety factor and ultimately adds weight to the structure where these laminates will be used. The predictions might be improved considering random fiber distribution at computational cost, but there exits scatter in these test data too. Another implication of assuming fibres packed in regular manner is not predicting well strain hardening behaviour due to assumed elastic/perfectly plastic behaviour as assumed for the matrix. On the other side, this behaviour is quite noticeable for randomly distributed fibers in stress-strain curve. This is obviously beyond the scope of the present paper but it's worth mentioning to readers.

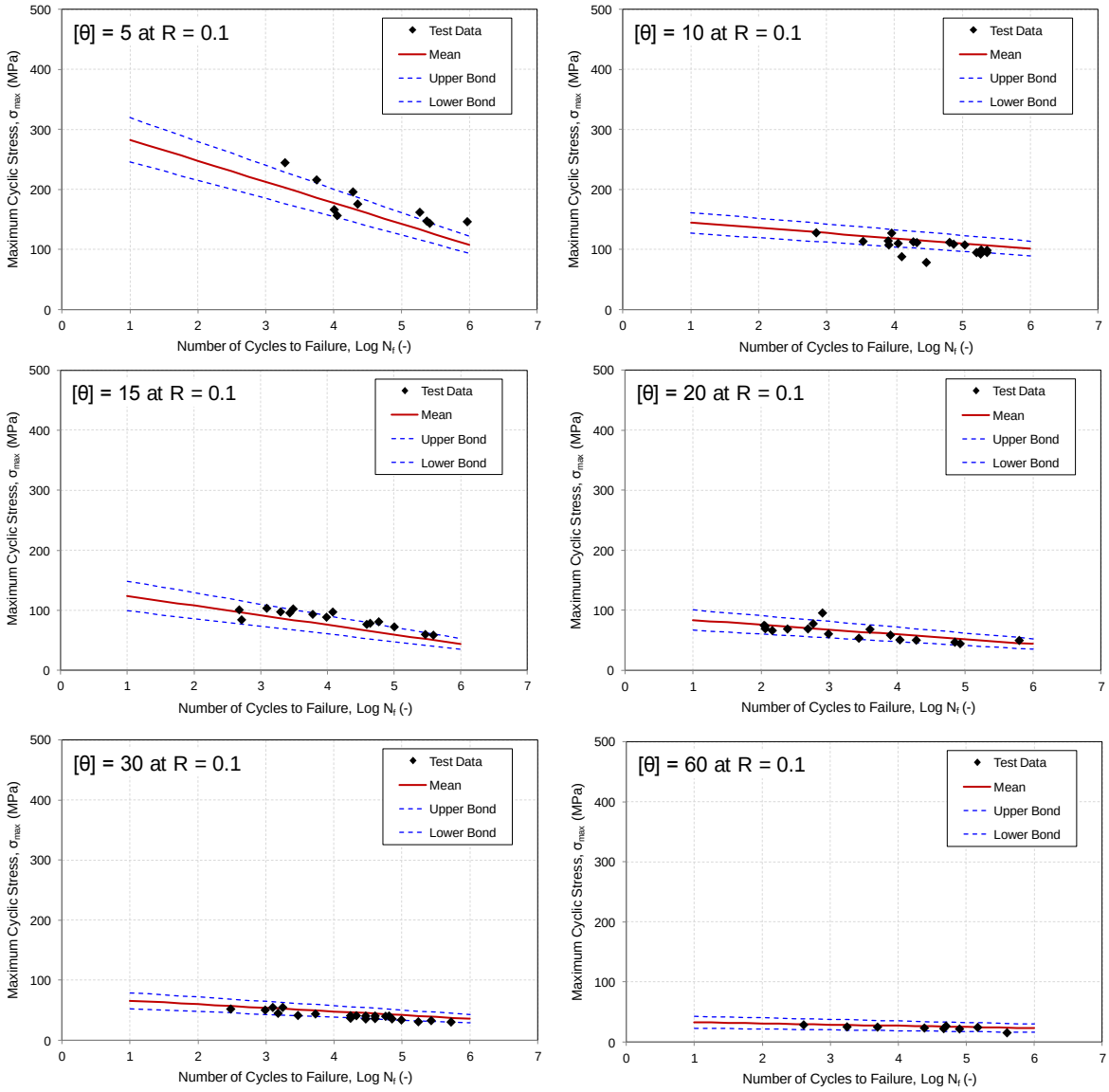

Figure 5.12: Predicted and experimental S-N curves under T-T fatigue of lamina from 5^o to 60^o

5.5.3 Fatigue Life Prediction of Multidirectional Composite Laminates

In order to validate M-LaF for fatigue in multidirectional composites, data for three kinds of specimens of E-glass/epoxy laminates were tested at Hanyang University (South Korea) [127]. The resin system used in this study was Hexion RIM 135 (L135i) epoxy and Hexion RIMH 134 hardener. The E-glass/Epoxy laminates were: BX $[\pm 45^0]_S$ and TX $[0^0{}_2/\pm 45^0]_S$. The fiber volume fractions were measured according to ASTM D 3171 and were 55% in this experiment. The static properties of the laminates were characterized using ASTM D 3039 with displacement control mode of 1 mm/min. The fatigue tests

were performed following ASTM D 3479 guidelines. All fatigue tests were performed at a stress ratio of 0.1. These fatigue tests were conducted under load control mode with a test frequency of 1 Hz. The load levels for the fatigue tests were from 50 to 80% of static strength. Figure 5.13 shows the test data for the BX and TX laminates along with the predictions from M-LaF. The square (SQR) unit cell model was employed to predict the fatigue behavior of these laminates. Figure 5.13 shows that predictions made by M-LaF using the SQR unit cell model are in good agreement with the test data. Here the mean values of the parameters were used for life prediction. For BX, the predicted failure mode in the laminate is matrix dominant, which matches the real behavior of this laminate. In the case of TX, the initial fatigue failure is $[\pm 45^0]$, which is matrix dominant. The final fatigue failure is $[0^0]$, i.e. fiber breakage. This shows that the M-LaF predicts not only matrix dominant laminate failure but also predicts fiber dominant laminate behavior.

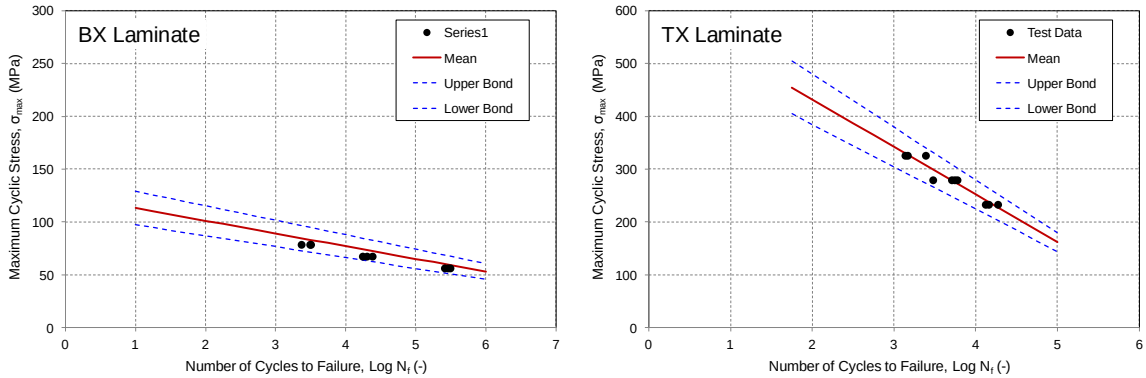

Figure 5.13: Fatigue life prediction of the Composite Laminates under T-T Cyclic Loading

5.6 Application to Wind Turbine Blades

A case study was carried out to highlight the application of the proposed M-LaF based fatigue life prediction methodology to a composite wind turbine blade structure. A wind turbine blade can be analyzed as a typical beam-like structure as described by state-of-the-art design codes [19, 35]. In these design codes, fatigue life calculations are limited to only the action of the normal stress component in the beam axis direction. The M-LaF life-prediction methodology is used to show the effect of normal and shear stress components in determining the fatigue life of a typical wind turbine blade. The 35 m GFRP blade is made of a shell and box spar type structure. There are flanges and

stiffeners as well. The shell and spars are assumed to carry only shear stresses, and the flanges and stiffeners are assumed to carry only axial stresses. The detailed finite-element model, material properties and design load case (power production at rated wind speed) definitions are reported in reference [128]. The blade consists of different types of laminates made of E-glass/Epoxy: biaxial [$\pm 45^0$] and triaxial [$0^0_2/\pm 45^0$]. The triaxial fabric is used in the shell structure along with a PVC core. Biaxial fabric and a PVC core is used in the shear webs. The rotor blade is also assumed to be a thin-walled beam structure. Thus the resultant tangential stresses in the shell through the thickness are very small compared to the axial stresses and are neglected. However, the shear stress is of comparable magnitude to the axial stress in areas such as the shear webs and leading/trailing edges of the blade. The resulting stresses in the transition section of the blade under a typical power production condition are presented based on the results given in the reference [128] and are shown in Figure 5.14. As these elements of the blade are placed in the confined region, edge effects do not occur and, therefore, the Classical Laminate Theory (CLT) is appropriate to calculate on-axis macro ply stresses. For the purpose of comparison, the stress ratio R is kept constant at -1. With R = -1, there is no mean stress effect that will make the conclusion straightforward. Also, sinusoidal cycling load is considered for ease of calculations.

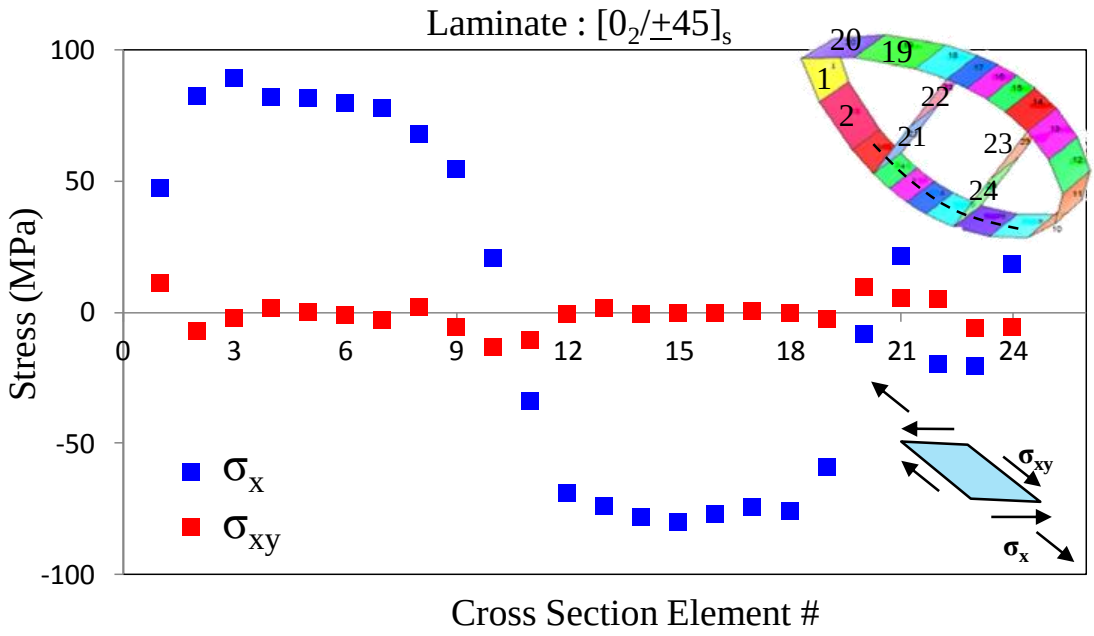

Figure 5.14: In-plane Stress State at the section of a 35m blade [128]

The M-LaF based life prediction with and without the contribution of the in-plane shear stress component demonstrates this stress component is important in reducing fatigue life. The mean fatigue life curves of biaxial and triaxial laminates from previous section used here for the blade analysis. The fatigue life was calculated based on the variation of stresses that are generated during power production [128]. The overestimation of the fatigue life prediction under different stress states is shown in Figure 5.15 which shows the S-N curve with maximum stress amplitude versus log of number of cycles to failure for constant amplitude cyclic loading at R = -1. The number of cycles is drastically reduced when in-plane shear stress is considered. This shows that life is overestimated when only the axial stress component N1 is taken in the fatigue life analysis. It is interesting to note from these fatigue calculations, as shown in Figure 5.15, that the shear stress component N_6 is about 60% the magnitude of the axial (longitudinal) normal stress component N_1 (this value is at shear web), but the fatigue life is overestimated by a factor of 20 at some load level like 250 MPa.

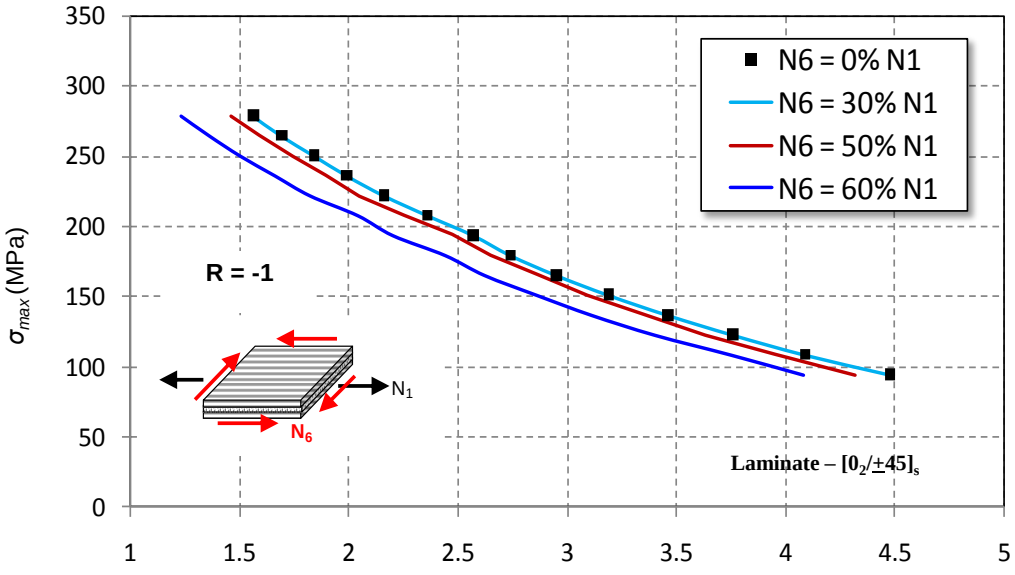

Figure 5.15: Fatigue Life with and without shear stress

5.7 Conclusion

In this paper, a methodology for the failure of composite materials based on micromechanics M-LaF was used to evaluate fatigue behaviour. The M-LaF model is based on the constituent properties and these properties were calibrated using a Bayesian inference approach. The combination of these two approaches made it possible to perform probabilistic fatigue analysis. The proposed methodology was validated against a range of unidirectional laminas and a variety of composite laminates. The predicted S-N curves were in good agreement with the test data. As an illustration, the proposed approach was applied to a structural application of a wind turbine laminate blade structure and a special case was considered to evaluate the fatigue life under different levels of shear stress compared to normal stress. In this practical example, the life was reduced by up to 20 times with respect to situations where only the axial normal stress component was used in simulations. As an initial step, this verification was performed under constant amplitude cyclic loading and at room temperature. It is proposed to extend to variable amplitude loading and diverse environmental situations that includes high/low temperature and moisture. This constituent based probabilistic fatigue analysis approach makes it possible to predict fatigue of a variety of composites with any fiber volume fractions which is appropriate for a range of applications that includes but not limited to proper material selection, structural layup optimization, different kinds of parametric studies, and probabilistic design.

Chapter 6 Conclusions and Future Work

The research presented in this dissertation as a collection of various papers provides a logical progression toward a novel way to incorporate high fidelity micromechanics with stochastic techniques for the design of composite materials under static and fatigue loading.

In summary, the followings are the key significant contributions in this research work.

6.1 Probabilistic Micromechanical Analysis of Composite Material Stiffness Properties

Chapter 2 investigated a coupled approach for stiffness property prediction of composite materials used in wind turbine blades using advanced micromechanics and reliability-based methodologies. The homogenization approach was used with a unit cell to estimate composite material stiffness properties. The predicted results were compared with SROM and MROM along with the test data and found to be in good agreement with test data and MROM. The work was then extended to perform the probabilistic analysis with Monte Carlo Simulation to incorporate uncertainties in the constituent's properties. Latin Hypercube Sampling was employed to cover most of the input variable design space. From the probabilistic analysis, it was found that the equivalent properties of UD followed the Gaussian distribution and these properties were affected by variations in fiber and matrix properties. The Spearman Rank Order sensitivity analysis gave insights into important constituent's properties and found that the modulus of fiber and matrix has more influence on composite properties. In addition, correlations were calculated between UD properties which were then used in blade analysis. This probabilistic micromechanical approach for composite materials provides a useful tool for performing preliminary material design for finalizing material for structural application. From a practical point of view, the method was then applied to a 5MW wind turbine blade structural analysis. A section of the blade was considered for demonstration purposes. The stochastic finite element analysis was performed in ANSYS/Multiphysics using a user subroutine in order to simulate probabilistic response of wing box section. Two

analyses were simulated with and without correlations between UD properties. There was no significant difference between PDFs but ignoring correlations suppressed the sensitivities of input variables on the response of wing box. Also, it was found that longitudinal modulus and in-plane shear modulus of the composite are the most critical material properties that influence deflection of the blade box. Besides this, sensitivity analysis screens out unimportant input variables which can be treated as deterministic in the further analysis. Furthermore, sensitivity analysis highlights the key material properties that most influence the response of the structure and this will eliminate/reduce unnecessary time consuming and expensive full testing campaign.

6.2 Probabilistic First Ply Failure Prediction of Composite Laminates using a multi-scale M-SaF and Bayesian Inference Approaches

In the chapter 3, a methodology for the failure of composite laminates based on micromechanics, i.e. Micromechanics based approach for Static Failure (M-SaF), is used to evaluate first ply failure. This method is based upon behavior of the constituents, i.e. the fiber, matrix, and interface. The model determines the failure of composites by considering failure of constituents in a micromechanical analysis. The M-SaF FPF results matches well with well known Tsai-Wu failure theory. Also, the Bayesian Inference framework was used to calibrate the M-SaF model parameters from available test data. This calibration produced posterior distribution of constituent strength properties. By using Metropolis-Hastings MCMC simulation, samples of M-SaF model parameters θ are drawn efficiently from prior distribution. The first order statistics of posterior found to be very close to the available values from literature. The joint posterior probability density function of θ was then used for FPF probabilistic analysis of a variety of laminates. The base material for all considered laminates was e-glass and epoxy. But, this will be extended to carbon fiber laminates in future. Additional test data will improve the accuracy and the bonds of the calibrated parameters. The presented coupled approach facilitates to identify the probability density functions of the constituent properties. This allows structural designers to incorporate uncertainty in analysis with confidence and can benefit reliability based composite structural design and optimization by allowing contracted the factor of safety due to improved knowledge on uncertainties in the constituent material properties. The next step in this research is to extend presented

coupled micromechanics based probabilistic framework to estimate the fatigue life of composites. Deterministic values of the constituent stiffness properties are used in the present work but these will be calibrated with the Bayesian inference method along with constituent strength properties in future work. Finally, there is clearly a need for more reporting of statistical test data by experimental practitioners to support further development of probabilistic failure models.

6.3 Damage Initiation and Growth in Composite Laminates

Chapter 4 demonstrated a methodology for the failure analysis of composite laminates in wind turbine blades based on Micromechanics, i.e. the M-SaF (Micro Level approach for Static Failure analysis) is used to evaluate the static strength. This approach is based upon behavior of the constituents, i.e. the fiber, matrix, and interface. The model determines the failure of composites by considering failure of constituents in a micromechanical analysis. Good agreement between test data and prediction of failure envelope was observed. M-SaF clearly indicates the failure mode of the composites and the stress level in each constituent upon failure. This makes it more flexible approach to optimize a composite strength by choosing proper constituent materials as well as fiber reinforcement/laminate lay-ups. One of the features of M-SaF is that it provides stiffness properties of the UD ply that can be compared directly with test data and found to be in good agreement. The concept of using basic constituent properties in the wind turbine blade design will help to choose a variety of material combinations. This will not only lead to accelerate the design cycle but also reduce a considerable cost of testing.

6.4 Fatigue life prediction of Laminated Composites using a multi-scale M-LaF and Bayesian Inference

Chapter 5 focused on a methodology for the failure of composite materials based on micromechanics M-LaF was used to evaluate fatigue behaviour. The M-LaF model is based on the constituent properties and these properties were calibrated using a Bayesian inference approach. The combination of these two approaches made it possible to perform probabilistic fatigue analysis. The proposed methodology was validated against a range of unidirectional laminas and a variety of composite laminates. The predicted S-N curves were in good agreement with the test data. As an illustration, the proposed

approach was applied to a structural application of a wind turbine laminate blade structure and a special case was considered to evaluate the fatigue life under different levels of shear stress compared to normal stress. In this practical example, the life was reduced by up to 20 times with respect to situations where only the axial normal stress component was used in simulations. As an initial step, this verification was performed under constant amplitude cyclic loading and at room temperature. It is proposed to extend to variable amplitude loading and diverse environmental situations that includes high/low temperature and moisture. This constituent based probabilistic fatigue analysis approach makes it possible to predict fatigue of a variety of composites with any fiber volume fractions which is appropriate for a range of applications that includes but not limited to proper material selection, structural layup optimization, different kinds of parametric studies, and probabilistic design.

6.5 Future possibilities of current research work

Future work to continue this line of research could include the following topics. First, the computational framework of M-SaF and M-LaF needs to be extended to include environmental (thermal and moisture) effects on the behavior of polymer composites. Second, modelling and integration of manufacturing defects at the unit cell level on the performance of composites should be added. In addition, implementation of composite manufacturing process parameters with micromechanics will be a useful tool for preliminary design stages. Third, the stochastic nature of randomly distributed fibers can be used with other stochastically calibrated input parameters for structural design. This will also include the effects of fiber location and different diameter distribution [129, 130] on parameter calibration under Bayesian framework. Forth, although a constant ply thickness was considered thus far, M-SaF/M-LaF can be broadened by considering the variations in the ply thickness as well as at the ply drop-off region. Fifth, the current M-LaF was validated against a variety of composite fatigue life test data under contact amplitude loading. However, composite structures experience random fatigue loading. Therefore, variable amplitude loading (sequence effects like high-low or low-high loading) should be investigated in more detail along with a non-linear damage accumulation fatigue model for composite laminates. Also, results for a particular

application from various unit cell models should be compared with each other using an extended Bayesian methodology. This will help to identify the best unit cell for structural application. In addition to this, unit cells of other composite types like woven composites or non-crimp fabrics composites will be used under proposed computational framework. Furthermore, currant framework considers un-correlated input priors but the approach is certainly be extended to consider correlations between priors as this is common in frequentist statistical approach.

Lastly, the present work could form the base module of more advanced design tools for composite structural design optimization with M-Saf/M-Laf and MDO (Multidisciplinary Design Optimization). For example, a number of applications could benefit from an integrated MDO approach, including wind turbine blades, unmanned air vehicles, pressure vessels, storage tanks, etc.

Bibliography

[1] Azzi, V. and S. Tsai, Anisotropic strength of composites, in Experimental Mechanics. 1965, Springer. p. 283-288.

[2] Tsai, S.W., Theory of composites design. 1992: Think composites Dayton.

[3] Tsai, S.W., Strength & life of composites. 2008: Stanford University.

[4] Sihn, S. and J.W. Park, MAE: an integrated design tool for failure and life prediction of composites. Journal of Composite Materials, 2008. 42(18): p. 1967-1988.

[5] Caporale, A., R. Luciano, and E. Sacco, Micromechanical analysis of interfacial debonding in unidirectional fiber-reinforced composites. Computers & structures, 2006. 84(31): p. 2200-2211.

[6] Soutis, C. and P.W. Beaumont, Multi-scale modelling of composite material systems: the art of predictive damage modelling. 2005: Woodhead Cambridge.

[7] Soden, P., M. Hinton, and A. Kaddour, Lamina properties, lay-up configurations and loading conditions for a range of fibre-reinforced composite laminates, in Composites Science and Technology. 1998, Elsevier. p. 1011-1022.

[8] Nijssen, R., Optidat-database reference document. The Knowledge Centre Wind turbine Materials and Constructions, Delft university of Technology, 2005.

[9] Hashin, Z. and A. Rotem, A fatigue failure criterion for fiber reinforced materials, in Journal of Composite Materials. 1973, SAGE Publications. p. 448-464.

[10] El Kadi, H. and F. Ellyin, Effect of stress ratio on the fatigue of unidirectional glass fibre/epoxy composite laminae. Composites, 1994. 25(10): p. 917-924.

[11] Mustafa, G., A. Suleman, and C. Crawford, Probabilistic micromechanical analysis of composite material stiffness properties for a wind turbine blade. Composite Structures, 2015. 131: p. 905-916.

[12] Ghualam Mustafa, Afzal Suleman, and C. Crawford, Design, Manufacturing and Applications of Composites Tenth Workshop 2014: Proceedings of the Tenth Joint Canada-Japan Workshop on Composites, August 2014, Vancouver, Canada. 2015, pp 17-28: DEStech Publications, Incorporated.

[13] Mustafa, G., C. Crawford, and A. Suleman, Fatigue life prediction of laminated composites using a multi-scale M-LaF and Bayesian inference. Composite Structures, 2016.

[14] Veers, P.S. and T. Ashwill, Trends in the Design, Manufacture and Evaluation of Wind Turbine Blades, in Wind Energy. 2003. p. 245-259.

[15] Henderson, A.R. and C. Morgan, Offshore Wind Energy in Europe— A Review of the State-of-the-Art, in Wind Energy. 2003, John Wiley & Sons, Ltd. p. 35-52.

[16] B Hillmer, T.B., Aerodynamic and Structural Design of MultiMW Wind Turbine Blades beyond 5MW, in Journal of Physics: Conference Series. 2007.

[17] Fingersh, L.J., M.M. Hand, and A.S. Laxson, Wind turbine design cost and scaling model. 2006: National Renewable Energy Laboratory Golden, CO.

[18] Kam, T., S. Tsai, and K. Chu, Fatigue reliability analysis of composite laminates under spectrum stress. International Journal of Solids and Structures, 1997. 34(12): p. 1441-1461.

[19] International Electrotechnical Commission, IEC 61400-1 3rd edn 2005-08 Wind turbines - Part 1: Design requirements. 2005.

[20] Hashin, Z. and B.W. Rosen, The elastic moduli of fiber-reinforced materials. Journal of applied mechanics, 1964. 31(2): p. 223-232.

[21] Liu, G., A step-by-step method of rule-of-mixture of fiber-and particle-reinforced composite materials. Composite Structures, 1997. 40(3): p. 313-322.

[22] Halpin, J.C., Effects of Environmental Factors on Composite Materials. 1969, DTIC Document.

[23] Dong, J.-w. and M.-l. Feng, Asymptotic expansion homogenization for simulating progressive damage of 3D braided composites. Composite Structures, 2010. 92(4): p. 873-882.

[24] Kamiński, M. and M. Kleiber, Perturbation based stochastic finite element method for homogenization of two-phase elastic composites. Computers & structures, 2000. 78(6): p. 811-826.

[25] Tsai, S.W., Theory of Composite Design 1992, Dayton, Ohio

[26] Hashin, Z., Analysis of composite materials—a survey. Journal of applied mechanics, 1983. 50(3): p. 481-505.

[27] Sun, C. and R. Vaidya, Prediction of composite properties from a representative volume element. Composites Science and Technology, 1996. 56(2): p. 171-179.

[28] Kouznetsova, V., W. Brekelmans, and F. Baaijens, An approach to micro-macro modeling of heterogeneous materials. Computational Mechanics, 2001. 27(1): p. 37-48.

[29] Xia, Z., Y. Zhang, and F. Ellyin, A unified periodical boundary conditions for representative volume elements of composites and applications, in International Journal of Solids and Structures. 2003, Elsevier. p. 1907-1921.

[30] Suquet, P., Elements of homogenization theory for inelastic solid mechanics. Homogenization techniques for composite media, 1987: p. 1994-275.

[31] ANSYS, Ansys Multiphysics Release 14.0. 2013.

[32] Ayyub, B.M. and A. Haldar, Practical structural reliability techniques. Journal of Structural Engineering, 1984. 110(8): p. 1707-1724.

[33] Driels, M.R. and Y.S. Shin, Determining the number of iterations for Monte Carlo simulations of weapon effectiveness. 2004, DTIC Document.

[34] Burton, T., et al., Wind Energy Handbook. 2011: John Wiley & Sons.

[35] LlOYD, G., Rules and regulations, IV-Non-marine technology, Part 1-Wind Energy. 1993.

[36] Jonkman, J.M., et al., Definition of a 5-MW reference wind turbine for offshore system development. 2009: National Renewable Energy Laboratory Golden, CO.

[37] Somers, D., The S816, S817, and S818 Airfoils. NREL Contractor Report NREL/SR-500-36333, 2004.

[38] Gurit, Gurit PVC Structural Foam Core. 2014.

[39] Jonkman, J.M. and M. Buhl, FAST User's Guide. National Renewable Energy Laboratory. 2005, NREL/EL-500-29798.

[40] Engelhardt, M., On simple estimation of the parameters of the Weibull or extreme-value distribution. Technometrics, 1975. 17(3): p. 369-374.

[41] Al-Fawzan, M.A., Methods for estimating the parameters of the Weibull distribution. King Abdulaziz city for science and technology Saudi Arabia, 2000.

[42] Hinton, M. and P. Soden, Predicting failure in composite laminates: the background to the exercise. Composites Science and Technology, 1998. 58(7): p. 1001-1010.

[43] Tsai, S.W. and E.M. Wu, A general theory of strength for anisotropic materials, in Journal of Composite Materials. 1971, SAGE Publications. p. 58-80.

[44] Hart-Smith, L., Predictions of a generalized maximum-shear-stress failure criterion for certain fibrous composite laminates. Composites Science and Technology, 1998. 58(7): p. 1179-1208.

[45] Puck, A. and H. Schürmann, Failure analysis of FRP laminates by means of physically based phenomenological models. Composites Science and Technology, 1998. 58(7): p. 1045-1067.

[46] Li, S. and A. Wongsto, Unit cells for micromechanical analyses of particle-reinforced composites. Mechanics of materials, 2004. 36(7): p. 543-572.

[47] Aboudi, J., Micromechanical analysis of the strength of unidirectional fiber composites. Composites Science and Technology, 1988. 33(2): p. 79-96.

[48] Paley, M. and J. Aboudi, Micromechanical analysis of composites by the generalized cells model. Mechanics of materials, 1992. 14(2): p. 127-139.

[49] Kwon, Y. and J. Berner, Micromechanics model for damage and failure analyses of laminated fibrous composites. Engineering Fracture Mechanics, 1995. 52(2): p. 231-242.

[50] González, C. and J. LLorca, Mechanical behavior of unidirectional fiber-reinforced polymers under transverse compression: microscopic mechanisms and modeling. Composites Science and Technology, 2007. 67(13): p. 2795-2806.

[51] Mayes, J.S. and A.C. Hansen, A comparison of multicontinuum theory based failure simulation with experimental results, in Composites Science and Technology. 2004. p. 517-527.

[52] Huang, Z.-M., A bridging model prediction of the ultimate strength of composite laminates subjected to biaxial loads. Composites Science and Technology, 2004. 64(3): p. 395-448.

[53] Hinton, M.J., A.S. Kaddour, and P.D. Soden, Failure criteria in fibre reinforced polymer composites: the world-wide failure exercise. 2004: Elsevier.

[54] Oskay, C. and J. Fish, On calibration and validation of eigendeformation-based multiscale models for failure analysis of heterogeneous systems. Computational Mechanics, 2008. 42(2): p. 181-195.

[55] Emery, T., et al., A generalised approach to the calibration of orthotropic materials for thermoelastic stress analysis. Composites Science and Technology, 2008. 68(3): p. 743-752.

[56] Bayes, M. and M. Price, An essay towards solving a problem in the doctrine of chances. by the late rev. mr. bayes, frs communicated by mr. price, in a letter to john canton, amfrs. Philosophical Transactions (1683-1775), 1763: p. 370-418.

[57] Reilly, P.M. and H. Patino-Lea1, A Bayesian study of the error-in-variables model. Technometrics, 1981. 23(3): p. 221-231.

[58] Malakoff, D., Bayes offers a 'new'way to make sense of numbers. Science, 1999. 286(5444): p. 1460-1464.

[59] Junior, P.C.P., F.L. de Silva Bussamra, and F.K. Arakaki, Finite element procedure for stress amplification factor recovering in a representative volume of composite materials. Journal of Aerospace Technology and Management, 2011. 3(3): p. 239-250.

[60] Jin, K.-K., et al., Distribution of micro stresses and interfacial tractions in unidirectional composites. Journal of Composite Materials, 2008.

[61] Tay, T., et al., Progressive failure analysis of composites. Journal of Composite Materials, 2008.

[62] Raghava, R., R.M. Caddell, and G.S. Yeh, The macroscopic yield behaviour of polymers. Journal of Materials Science, 1973. 8(2): p. 225-232.

[63] Huang, Y., C. Jin, and S.k. Ha, Strength prediction of triaxially loaded composites using a progressive damage model Journal of Composite Materials, 2012.

[64] Xu, L., C.Z. Jin, and S.K. Ha, Ultimate strength prediction of braided textile composites using a multi-scale approach. Journal of Composite Materials, 2014: p. 0021998314521062.

[65] Stassi-D'Alia, F., Flow and fracture of materials according to a new limiting condition of yelding, in Meccanica. 1967, Springer. p. 178-195.

[66] Ghulam Mustafa, A.S., Curran Crawford. Damage Initiation and Growth in Composite Laminates of Wind Turbine Blades. in Design, Manufacturing and Applications of Composites Tenth Workshop 2014. 2014: DEStech Publications, Inc, 2015.

[67] Zhao, F. and N. Takeda, Effect of interfacial adhesion and statistical fiber strength on tensile strength of unidirectional glass fiber/epoxy composites. Part I: experiment results. Composites Part A: Applied Science and Manufacturing, 2000. 31(11): p. 1203-1214.

[68] Le Maître, O.P. and O.M. Knio, Spectral methods for uncertainty quantification: with applications to computational fluid dynamics. 2010: Springer Science & Business Media.

[69] Moffat, R.J., Describing the uncertainties in experimental results. Experimental thermal and fluid science, 1988. 1(1): p. 3-17.

[70] Benjamin, J.R. and C.A. Cornell, Probability, statistics, and decision for civil engineers. 2014: Courier Corporation.

[71] Faber, M.H., On the treatment of uncertainties and probabilities in engineering decision analysis. Journal of Offshore Mechanics and Arctic Engineering, 2005. 127(3): p. 243-248.

[72] Paté-Cornell, M.E., Uncertainties in risk analysis: Six levels of treatment. Reliability Engineering & System Safety, 1996. 54(2): p. 95-111.

[73] Cheung, S.H., et al., Bayesian uncertainty analysis with applications to turbulence modeling. Reliability Engineering & System Safety, 2011. 96(9): p. 1137-1149.

[74] Sorenson, H.W., Parameter estimation: principles and problems. Vol. 9. 1980: M. Dekker.

[75] Kaipio, J. and E. Somersalo, Statistical and computational inverse problems. Vol. 160. 2006: Springer Science & Business Media.

[76] Kennedy, M.C. and A. O'Hagan, Bayesian calibration of computer models. Journal of the Royal Statistical Society: Series B (Statistical Methodology), 2001. 63(3): p. 425-464.

[77] Santner, T.J., B.J. Williams, and W. Notz, The design and analysis of computer experiments. 2003: Springer Science & Business Media.

[78] Park, I. and R.V. Grandhi, A Bayesian statistical method for quantifying model form uncertainty and two model combination methods. Reliability Engineering & System Safety, 2014. 129: p. 46-56.

[79] Bayarri, M.J., et al., A framework for validation of computer models. Technometrics, 2007. 49(2).

[80] Yuen, K.-V., Bayesian methods for structural dynamics and civil engineering. 2010: John Wiley & Sons.

[81] Paulo, R., Default priors for Gaussian processes. Annals of Statistics, 2005: p. 556-582.

[82] Bornkamp, B., Functional uniform priors for nonlinear modeling. Biometrics, 2012. 68(3): p. 893-901.

[83] Khan, U.T. and C. Valeo. Predicting Dissolved Oxygen Concentration in Urban Watersheds: A Comparison of Fuzzy Number Based and Bayesian Data-Driven Approaches. in The International Conference on Marine and Freshwater Environments (iMFE 2014). 2014.

[84] Gelman, A., et al., Bayesian data analysis. Vol. 2. 2014: Taylor & Francis.

[85] Box, G.E. and G.C. Tiao, Bayesian inference in statistical analysis. Vol. 40. 2011: John Wiley & Sons.

[86] Sudret, B., Uncertainty propagation and sensitivity analysis in mechanical models--Contributions to structural reliability and stochastic spectral methods. 2007.

[87] Ditlevsen, O. and H.O. Madsen, Structural reliability methods. Vol. 178. 1996: Wiley New York.

[88] Liang, F., C. Liu, and R. Carroll, Advanced Markov chain Monte Carlo methods: learning from past samples. Vol. 714. 2011: John Wiley & Sons.

[89] Metropolis, N., et al., Equation of state calculations by fast computing machines. The journal of chemical physics, 1953. 21(6): p. 1087-1092.

[90] Hastings, W.K., Monte Carlo sampling methods using Markov chains and their applications. Biometrika, 1970. 57(1): p. 97-109.

[91] Silverman, B.W., Density estimation for statistics and data analysis. Vol. 26. 1986: CRC press.

[92] Mustafa, G., A Micromechanical approach for the predoction of fatigue life of composite lamiantes, in Mechanical Engineering. 2011, Hanyang University: Ansan. p. 40.

[93] Theodore P. Philippidis, T.T.A., Vaggelis A. Passipoularidis, Alexandros E. Antoniou, Static and Fatigue Tests on ISO Standard [±45] Coupons. 2004.

[94] Cormier, L., S. Joncas, and R.P. Nijssen, Effects of low temperature on the mechanical properties of glass fibre–epoxy composites: static tension, compression, R= 0.1 and R=− 1 fatigue of±45° laminates. Wind Energy, 2015.

[95] Nelson, P.R., M. Coffin, and K.A. Copeland, Introductory statistics for engineering experimentation. 2003: Academic Press.

[96] Natrella, M., NIST/SEMATECH e-handbook of statistical methods. 2010.

[97] Lin, W.-P. and H.-T. Hu, Parametric study on the failure of fiber-reinforced composite laminates under biaxial tensile load. Journal of Composite Materials, 2002. 36(12): p. 1481-1503.

[98] Jackson, K.J. and M.D. Zuteck, Innovative design approaches for large wind turbine blades, in Wind Energy. 2005, John Wiley & Sons, Ltd. p. 141-171.

[99] Lee, K., S. Moorthy, and S. Ghosh, Multiple scale computational model for damage in composite materials. Computer methods in applied mechanics and engineering, 1999. 172(1): p. 175-201.

[100] Manwell, J.F., J.G. McGowan, and A.L. Rogers, Wind Energy Explained: Theory, Design and Application. 2010: Wiley Online Library.

[101] Kwon, Y. and J. Berner, Micromechanics model for damage and failure analyses of laminated fibrous composites, in Engineering Fracture Mechanics. 1995, Elsevier. p. 231-242.

[102] Hahn, H. and S. Tsai, On the behavior of composite laminates after initial failures, in Journal of Composite Materials. 1974, SAGE Publications. p. 288-305.

[103] Soden, P.D., M.J. Hinton, and A.S. Kaddour, Biaxial test results for strength and deformation of a range of E-glass and carbon fibre reinforced composite laminates: failure exercise benchmark data. Composites Science and Technology, 2002. 62(12–13): p. 1489-1514.

[104] Soden, P., M. Hinton, and A. Kaddour, Biaxial test results for strength and deformation of a range of E-glass and carbon fibre reinforced composite laminates: failure exercise benchmark data, in Composites Science and Technology. 2002, Elsevier. p. 1489-1514.

[105] Reifsnider, K., Fatigue behavior of composite materials. International Journal of Fracture, 1980. 16(6): p. 563-583.

[106] Hashin, Z. and A. Rotem, A fatigue failure criterion for fiber reinforced materials. Journal of Composite Materials, 1973. 7(4): p. 448-464.

[107] Reifsnider, K.L. and W. Stinchcomb, A critical element model of the residual strength and life of fatigue-loaded composite coupons. Composite materials: fatigue and fracture, ASTM STP, 1986. 907: p. 298-313.

[108] Himmel, N., Fatigue life prediction of laminated polymer matrix composites. International journal of fatigue, 2002. 24(2): p. 349-360.

[109] Shokrieh, M. and F. Taheri-Behrooz, A unified fatigue life model based on energy method. Composite Structures, 2006. 75(1): p. 444-450.

[110] Varvani-Farahani, A., H. Haftchenari, and M. Panbechi, An energy-based fatigue damage parameter for off-axis unidirectional FRP composites. Composite Structures, 2007. 79(3): p. 381-389.

[111] Natarajan, V., H.V. Gangarao, and V. Shekar, Fatigue response of fabric-reinforced polymeric composites. Journal of Composite Materials, 2005. 39(17): p. 1541-1559.

[112] Hwang, W. and K.S. Han, Fatigue of composites—fatigue modulus concept and life prediction. Journal of Composite Materials, 1986. 20(2): p. 154-165.

[113] Whitworth, H., Modeling stiffness reduction of graphite/epoxy composite laminates. Journal of Composite Materials, 1987. 21(4): p. 362-372.

[114] Whitworth, H., Cumulative damage in composites. Journal of engineering materials and technology, 1990. 112(3): p. 358-361.

[115] Hahn, H.T. and R.Y. Kim, Fatigue behavior of composite laminate. Journal of Composite Materials, 1976. 10(2): p. 156-180.

[116] Hashin, Z., Analysis of stiffness reduction of cracked cross-ply laminates. Engineering Fracture Mechanics, 1986. 25(5): p. 771-778.

[117] Yang, J., et al., A stiffness degradation model for graphite/epoxy laminates. Journal of Composite Materials, 1990. 24(7): p. 753-769.

[118] Akshantala, N.V. and R. Talreja, A micromechanics based model for predicting fatigue life of composite laminates. Materials Science and Engineering: A, 2000. 285(1): p. 303-313.

[119] Liu, Y. and S. Mahadevan, A unified multiaxial fatigue damage model for isotropic and anisotropic materials. International journal of fatigue, 2007. 29(2): p. 347-359.

[120] Philippidis, T. and A. Vassilopoulos, Fatigue strength prediction under multiaxial stress. Journal of Composite Materials, 1999. 33(17): p. 1578-1599.

[121] Jen, M.-H.R. and C.-H. Lee, Strength and life in thermoplastic composite laminates under static and fatigue loads. Part II: Formulation. International journal of fatigue, 1998. 20(9): p. 617-629.

[122] Sarfaraz, R., A.P. Vassilopoulos, and T. Keller, A hybrid S–N formulation for fatigue life modeling of composite materials and structures. Composites Part A: Applied Science and Manufacturing, 2012. 43(3): p. 445-453.

[123] Degrieck, J. and W. Van Paepegem, Fatigue damage modeling of fibre-reinforced composite materials: review. Applied Mechanics Reviews, 2001. 54(4): p. 279-300.

[124] Miner, M.A., Cumulative damage in fatigue. Journal of applied mechanics, 1945. 12(3): p. 159-164.

[125] El Kadi, H. and F. Ellyin, Effect of stress ratio on the fatigue of unidirectional glass/epoxy composite laminates. Composites, 1994. 10: p. 1-8.

[126] Nijssen, R., Optidat-database reference document-'. The Knowledge Centre Wind turbine Materials and Constructions, Delft university of Technology, 2005.

[127] Mustafa, G., A micromechanical approach for the prediction of fatigue life in composite laminates, in MSc Thesis 2011: Ansan, Hanyang University

[128] Wedel-Heinen, J., J. Tadich, and C. Brokopf, Implementation of OPTIMAT in technical standards. OB_TG6_R002 rev, 2006. 7.

[129] Mohammadi, M.S., et al., Toward better understanding of the effect of fiber distribution on effective elastic properties of unidirectional composite yarns. Computers & structures, 2016. 163: p. 29-40.

[130] Li, H., B. Zhang, and G. Bai, Effects of constructing different unit cells on predicting composite viscoelastic properties. Composite Structures, 2015. 125: p. 459-466.